Computer Aided Engineering in the Foot Orthosis Development Process

by

Samuel Jewell Lochner

A thesis
presented to the University of Waterloo
in fulfillment of the
thesis requirement for the degree of
Doctor of Philosophy
in
Mechanical Engineering

Waterloo, Ontario, Canada, 2013

AUTHOR'S DECLARATION

I hereby declare that I am the sole author of this thesis. This is a true copy of the thesis, including any required final revisions, as accepted by my examiners.

I understand that my thesis may be made electronically available to the public.

Abstract

An orthosis, or orthotic device is used to straighten or correct the posture of part of the body. A foot orthosis (FO) is the subject of study for this dissertation. A FO is situated between the foot and the midsole of the shoe and replaces the insole. Foot orthoses (FOs) are intended to prevent or aid in the recovery of injury by acting to redistribute pressure experienced by the plantar surface of the foot as well as cause adjustments to the relative positions of the foot's bones during standing and gait.

Traditional methods for developing a FO require extensive skilled manual labour and are highly dependent on subjective input. Modern FO development methods have sought to address these issues through the use of computer driven technological advancements. Foot scanners record geometry, computer aided design (CAD) software is used to develop the FO geometry, and automated manufacturing tools are used to either fabricate the FO or fabricate a mould about which the FO can be formed.

A variety of modern solutions have successfully automated the process, however, it remains highly subjective. Skilled manual labour has merely been replaced with equally subjective skilled computer labour. In particular, adjustments to the foot are made with basic deformation functions to the static surface foot models generated by modern digitizers. To improve upon this, a model that describes the mechanics and properties of the various tissues of the foot is required. Such a model will also be useful for validating and optimizing FO designs prior to fabrication through simulation of weight-bearing conditions.

Given the deformable characteristics of the tissues of the foot, the finite element (FE) modeling method is appropriate. The FE foot model has become a common medical and engineering tool in recent years. Its application, however, has primarily been limited to research as few clinical applications warrant the development cost. High cost stems from the MRI or CT scan and the skilled labour required to assemble the model for FE analysis. Consequently, the FE modeling approach has previously been out of reach for the application of FO development.

The solution proposed and implemented was to map a detailed generic FE foot model to an inexpensive surface scan obtained from a modern digitizer. The mapping accurately predicted anatomical geometry and resulted in simulation models that can be used in the FO development process first to carry out postural adjustments prescribed by a practitioner and second in a validation step where a FO design can be tested prior to fabrication. In addition to simulation tools, novel

complementary tools were developed for designing and fabricating FOs. The simulation, design, and fabrication tools were incorporated into a novel, seven step FO development process. The proposed process is beneficial to FO development as it reduces the required subjective input from practitioners and lab technicians and allows for the validation of potential FO designs prior to fabrication. Future work is required to improve computational efficiency of the FE foot models and to fully automate the process to make it commercially viable. In addition to FOs, the proposed approach also presents opportunities for improving other orthoses and prostheses for the human body.

Acknowledgements

I would like to thank Professors Sanjeev Bedi and Jan Huissoon for guiding me through both my masters degree and this PhD. Their unwavering encouragement and keen wisdom have made this accomplishment possible as they shaped my development academically, professionally, and personally.

I give my thanks to the other members of my committee, Naveen Chandrashekar, Stephen Mann, Kaan Inal, and Jean-Christophe Cuilliere, for taking the time to review my work and their support along the way. I would also like to thank Professors John McPhee and Jonathan Kofman for their input and for providing access to lab equipment.

Tezera Ketema of Podo-Pal, the industry partner for the project, provided his invaluable knowledge, introduced me to many industry experts in the field including Ray Bauman of Foot Foundation and Ray Rasoulli of Varifit, provided funding, and has been a friend through this time. The funding organization, Ontario Centres of Excellence, worked with the industry partner to fund this project. I thank the organization and more specifically, Steve Colbert and Jessie Maggard for their hard work and support.

I am grateful to all of the students who have accompanied me through this degree as both colleagues and friends.

Finally, I am forever thankful to my family and friends for their unconditional support. It is both for them and because of them that I am able to finish this step in my life and move on to the next.

Table of Contents

AUTHOR'S DECLARATION ii
Abstract iii
Acknowledgements v
Table of Contents vi
List of Figures ix
List of Tables xiv
Chapter 1 Introduction 1
1.1 Foot Anatomy and Mechanics 1
1.1.1 Some Common Terms for Describing Relative Positions and Movements 1
1.1.2 Foot Anatomy 3
1.1.3 Joints of the Foot 6
1.1.4 Joint Angles and Positions 6
1.1.5 Primary Mechanisms of the Foot 9
1.1.6 Foot Motion During Gait 11
1.2 The FO and its Development 12
1.2.1 Pressure Redistribution 12
1.2.2 Postural Correction 13
1.2.3 FO Development 13
1.3 The Proposed Solution 22
1.4 Contributions of the Dissertation 23
1.5 Outline of the Dissertation 24
Chapter 2 Foot Modeling 26
2.1 Introduction 26
2.2 Methods 29
2.2.1 Foot Geometry Development 29
2.2.2 Joint Articulation Modeling 33
2.2.3 Interactions 39
2.2.4 Loads, Boundary Conditions, and Steps 39
2.2.5 Patient Specific Soft Tissue Material Properties, Meshing, and Convergence 41
2.2.6 Model Simplifications 45
2.2.7 Experimental Setup 46

2.3 Results and Discussion 47
2.4 Summary 50
Chapter 3 Development of a Patient-Specific Anatomical Foot Model and Finite Element Foot Model from Structured Light Scan Data 52
3.1 Introduction 52
3.2 Anatomical Foot Model Morphing 53
3.2.1 Generic and Specific Anatomical Foot Model Development 54
3.2.2 Orienting and Positioning 56
3.2.3 Morphing The Anatomical Model 57
3.2.4 Affine Transformations 57
3.2.5 Free Form Deformation 58
3.2.6 Algorithm 59
3.3 Anatomical Morphing Results and Discussion 60
3.4 FE Foot Model Morphing 66
3.4.1 FE Model Morphing Methods 66
3.4.2 FE Model Morphing Results and Discussion 68
3.5 Summary 73
Chapter 4 FO Design and Fabrication 75
4.1 Introduction 75
4.2 Proposed System 76
4.2.1 Manual Anatomical Landmark Selection 77
4.2.2 Foot Alignment 78
4.2.3 Boundary Geometry 79
4.2.4 Surface Design 80
4.2.5 Fabrication 87
4.3 Summary 90
Chapter 5 The Proposed Foot Orthosis Development Process 91
5.1 Demonstration of the Proposed Method 91
5.2 Comparison with a Common Modern Scanning Method 97
5.3 Discussion 99
5.4 Summary 100
Chapter 6 Conclusion 102

6.1 Conclusions 102
6.2 Improvements and Advancements 103
6.3 Other Applications 105
Bibliography 107

List of Figures

Figure 1.1: Common reference frame used for representing the human foot 2
Figure 1.2: Movement and positioning of the foot: a) eversion/inversion, b) adduction/abduction, c) dorsiflexion/plantarflexion, d) pronated (valgus)/supinated (varus) (adapted from [1]) 3
Figure 1.3: The foot connects with the lower leg at the talus, tibia, and fibula interface (adapted from [1]) 4
Figure 1.4: Dorsal view of the bones of the rearfoot, midfoot, and forefoot (adapted from [1]) 5
Figure 1.5: Plantar view of the first ray of the foot 5
Figure 1.6: Joint angles: a) tibial stance angle, b) subtalar joint angle, c) midtarsal joint angle (adapted from [6]) 7
Figure 1.7: Rearfoot and forefoot angles with the midtarsal joint locked and the subtalar joint in neutral position (adapted from [6]) 8
Figure 1.8: Arches of the foot: a) lateral arch, b) transverse arch, c) medial arch (adapted from [1]) . 10
Figure 1.9: Lever and windlass mechanisms of the foot (adapted from [1]) 11
Figure 1.10: Heel strike, mid stance, and push off in the stance phase of gait 12
Figure 1.11: Capturing foot geometry: a) suppine plaster casting, b) foam impression, c) resulting positive cast 16
Figure 1.12: Modifying the positive plaster cast: a) adding plaster with a spatula, b) cast with added plaster, c) cast after smoothing out plaster addition (adapted from [6]) 17
Figure 1.13: Creating the FO shell by vacuum forming materials to the positive cast 18
Figure 1.14: Capturing the foot's geometry: a) optically as the foot rests on a flat glass plate (Sharp Shape uses a variation on this scanner type to capture the non-weight-bearing geometry with the patient suppine), b) the Varifit device records the position of an array of pins (Ideas uses a variation on this where the impression of the foot made in a foam box is digitized) 20
Figure 1.15: *FO geometry developing*: a) development of the actual FO, b) development of a mould about which the FO's materials are to be vacuum formed 20
Figure 1.16: FO fabrication: a) vacuum forming the FO to a reconfigurable mould in the form of an array of pins (Varifit), b) CNC machining either the actual FO model or a mould for vacuum forming the FO 21
Figure 2.1: Publications found per time period 28
Figure 2.2: MRI scanning the foot with a fixture for both housing a dedicated coil and restraining the foot 30

Figure 2.3: Cross sections of the foot and masking the bones with MIMICS 30
Figure 2.4: Reconstructed Bone volumes viewed in MIMICS 31
Figure 2.5: Skin and bone volumes after masking and reconstruction and the three cardinal planes.. 32
Figure 2.6: Anatomical surface model development: a) Skin and bones surfaced and converted to IGES, b) soft tissue volume created by a Boolean subtraction of the bones from the skin 32
Figure 2.7: Locating ligaments and fascia: a) guided by the anatomy educational software Ankle Foot Interactive, b) located on the foot model 33
Figure 2.8: Assembly of the ground, FO, and foot model: a) view with soft tissue visible, b) view with tendons, fascia, and bones visible 33
Figure 2.9: Talocrural joint hinge axis development on the talus: a) transverse view, b) sagital view 35
Figure 2.10: Subtalar joint hinge axis development on the talus: a) transverse view, b) sagital view. 35
Figure 2.11: Calcaneocuboid joint hinge axis development on the cuboid: a) transverse view, b) sagital view 36
Figure 2.12: Navicular joint centre of rotation developed on the talus: a) transverse view, b) sagital view 36
Figure 2.13: Metatarsocuneiform joint centre of rotation developed on the medial cuneiform and first metatarsal: a) transverse view, b) sagital view 37
Figure 2.14: First metatarsophalangeal centre of rotation developed on the first metatarsal: a) transverse view, b) sagital view 37
Figure 2.15: Talocrural hinge joint (red), subtalar hinge joint (green), calcaneocuboid hinge joint (blue), tarsonavicular pin joint (blue), intertarsal pin joints (green), and metatarsophalangeal pin joints (red): a) transverse view, b) sagital view 38
Figure 2.16: Boundary conditions and loads for the contacting and loading steps 40
Figure 2.17: The foot model while in the initial, contacted, and loaded positions 41
Figure 2.18: Force Displacement sensor applied to plantar heel soft tissue 42
Figure 2.19: Force Displacement data from 4 experiments and the converged simulation 42
Figure 2.20: Plantar tissue testing simulation setup 43
Figure 2.21: Assembly of the meshed parts: a) soft tissue visible, b) soft tissue not visible 45
Figure 2.22: a) Machined FO surface, b) F-Scan sensor under trimmed and taped to the FO surface to minimize kinking 46
Figure 2.23: Plantar pressure: a) experimental on flat ground, b) simulated on flat ground, c) experimental on the FO, d) simulated on the FO 48

Figure 2.24: Plantar pressure error between experimental and simulated loading: a) on flat ground, b) on the FO 49
Figure 3.1: Diagram of morphing procedure 54
Figure 3.2: Anatomical landmarks 55
Figure 3.3: Sample model orientation 57
Figure 3.4: An example of a 13,7,7 lattice: a) side view, b) perspective view 59
Figure 3.5: Original bones (blue) overlaid with morphed bones (yellow) for six experiments 61
Figure 3.6: Topology deviation maps between generic and specific models for experiment AC (colour scale in mm): a) skin models, b) bone models 62
Figure 3.7: Topology deviation map between generic and specific fifth metatarsal models for experiment AC 62
Figure 3.8: Topology deviation maps between generic and specific models for experiment AB: a) calcaneus models, b) talus models 63
Figure 3.9: Topology deviation map between generic and specific fibula models for experiment AB 64
Figure 3.10: a) an example of poor intermediate phalange accuracy due to the lack of a local landmark, b) morphing the exceptionally long first toe of subject B resulted in shearing of the toe joints axes 65
Figure 3.11: Prone, non-weight-bearing position during scanning foot with landmarks 67
Figure 3.12: Plantar pressure for subject 1: a) experimental, b) simulated, c) simulated (after scaling) 69
Figure 3.13: Plantar pressure for subject 2: a) experimental, b) simulated (after scaling) 70
Figure 3.14: Plantar pressure for subject 3: a) experimental, b) simulated (after scaling) 71
Figure 3.15: Plantar pressure error between experimental and simulated for: a) subject 1, b) subject 2, c) subject 3 72
Figure 3.16: Mesh of a single part foot model 73
Figure 4.1: A 3D model of a foot composed of approximately 8000 vertices and 16000 triangles. The XY plane represents the ground plane 76
Figure 4.2: a) Common deformities make automatic landmark detection from a 3D model challenging, b) Landmarks to be manually selected by user shown first on a digital image of the plantar surface of the foot and then on the corresponding 3D model 78

Figure 4.3: An example of the Brannock and second toe method performing poorly. The large size of the foot results in an overly medial Brannock central axis while the deformed second toe and posterior lateral exostosis undesirably influence the central axis 79
Figure 4.4: BoundaryXY determined from a standard shoe last..... 80
Figure 4.5: First the posterior FO surface is designed, then the anterior FO surface, and finally the model is completed by adding the transition FO surface 81
Figure 4.6: Traditional manual techniques add plaster to the plaster cast of the foot. A FO built about the modified cast will allow for tissue expansion during weight-bearing..... 82
Figure 4.7: A series of points are found along BoundaryXY posterior to the ball curve and an arc is created for each point..... 83
Figure 4.8: Designing the arc. Note that the extension of the FO beyond the edge of the foot is exaggerated for clarity 83
Figure 4.9: An end angle of 0 is advisable for the arch region of the foot..... 84
Figure 4.10: Curves and points used to construct the posterior FO surface..... 85
Figure 4.11: Curves used to construct the anterior FO surface..... 86
Figure 4.12: a) Curves used to construct the transition FO surface, b) finished FO surface. The splotchy pattern corresponds with a close match between the FO and foot surfaces 86
Figure 4.13: Additional pressure adjustments: a) manual control point repositioning, b) blended control point adjustment from a point, c) blended control point adjustment from a line and a cavity created for a heel plug..... 87
Figure 4.14: Conceptual model of additive manufactured part: a) including support material, b) after material is injected into the cavities and the support material has been dissolved 89
Figure 4.15: 3D model of the FO to be sent to the FDM software 89
Figure 4.16: Printed FO 90
Figure 5.1: Conventional methods and the proposed method..... 91
Figure 5.2 Points where boundary conditions are applied to achieve postural adjustments 93
Figure 5.3 Posterior view of the foot with Y (green) and Z (blue) axes: a) before postural adjustment, b) after postural adjustment 94
Figure 5.4 Medial view of the foot with X axes (red): a) before postural adjustment, b) after postural adjustment..... 95
Figure 5.5 FO: a) initial surface design, b) body design with uniform thickness for FEA use..... 96

Figure 5.6: Plantar pressure distributions: a) initial FO, b) FO with 2mm drop along lateral arch and fifth metatarsal head, c) FO with 4mm drop along lateral arch and fifth metatarsal head 97
Figure 5.7: Plantar pressure distributions: a) on an FO developed with the proposed method, b) on an FO developed with a typical conventional method 98

List of Tables

Table 3.1: Anatomical landmarks and corresponding short forms 55
Table 3.2: Skin Landmark Error (SLE), Bone Landmark Error (BLE), Skin Surface Error (SSE), Bone Surface Error (BSE), and average errors for the 6 experiments (in mm) 61
Table 3.3: Loads and ratio of loads for the three subjects 67

Chapter 1
Introduction

The foot orthosis (FO) supports the foot during standing and gait and is used to redistribute the pressures experienced by the plantar tissues of the foot and to achieve postural adjustments to the foot. The base FO geometry is a near duplicate of the plantar foot surface while deviations from this base geometry are used to achieve more specific pressure and postural adjustments. The traditional FO development method is centered about plaster casting and vacuum forming techniques while more modern methods incorporate computer enabled technologies into the process.

Advancing the FO development process with computer aided engineering is the subject of study of this dissertation. A summary of the proposed advancements will be provided later in the chapter. However, to provide a comprehensive understanding of the proposed advancements, this chapter will first begin with a description of foot anatomy and mechanics followed by descriptions of traditional and modern FO development methods and their various short comings. The chapter will be concluded with a list of the contributions and an outline of the dissertation.

1.1 Foot Anatomy and Mechanics

In this section some common terms are explained for describing the foot and its movement followed by descriptions of foot anatomy and mechanics. Much of this chapter draws on the knowledge base surrounding FO treatment.

1.1.1 Some Common Terms for Describing Relative Positions and Movements

Figure 1.1 illustrates the common reference frame used when representing the human foot. The three cardinal planes (sagital, transverse, and frontal) and corresponding perpendicular directions (medial, lateral, superior, inferior, anterior, posterior) will be used to describe the features and functions of the foot. Proximal and distal are two terms commonly used to describe the relative position of an anatomical feature to the centre of the body. For example, the proximal head of the tibia (largest bone in the lower leg) refers to the end of the bone closet to the trunk.

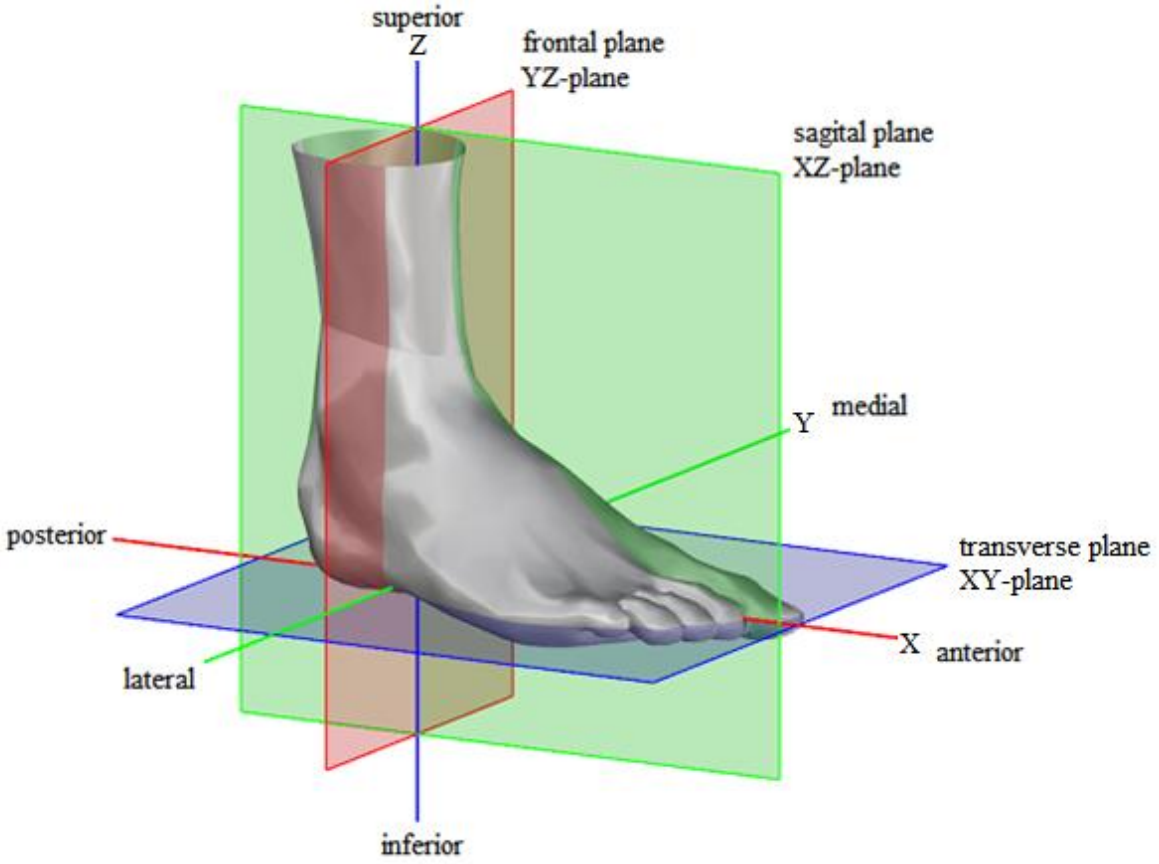

Figure 1.1: Common reference frame used for representing the human foot

Movement of the foot can be described as occurring in the sagital, transverse, and frontal planes. Abduction and adduction occur in the transverse plane, dorsiflexion and plantarflexion occur in the sagital plane, and eversion and inversion occur in the frontal plane (Figure 1.2). Summing the articulations in the various joints results in the overall motions of the foot. For instance, dorsiflexion occurring in the joints of the rearfoot, midfoot, and forefoot add up to the total dorsiflexion of the foot. Two common tri-planar articulations are referred to as supination and pronation. Supination consists of plantarflexion, adduction, and inversion. Pronation consists of dorsiflexion, abduction, and eversion. Varus and valgus are terms used to describe inward and outward angulation of a distal segment respectively (Figure 1.2).

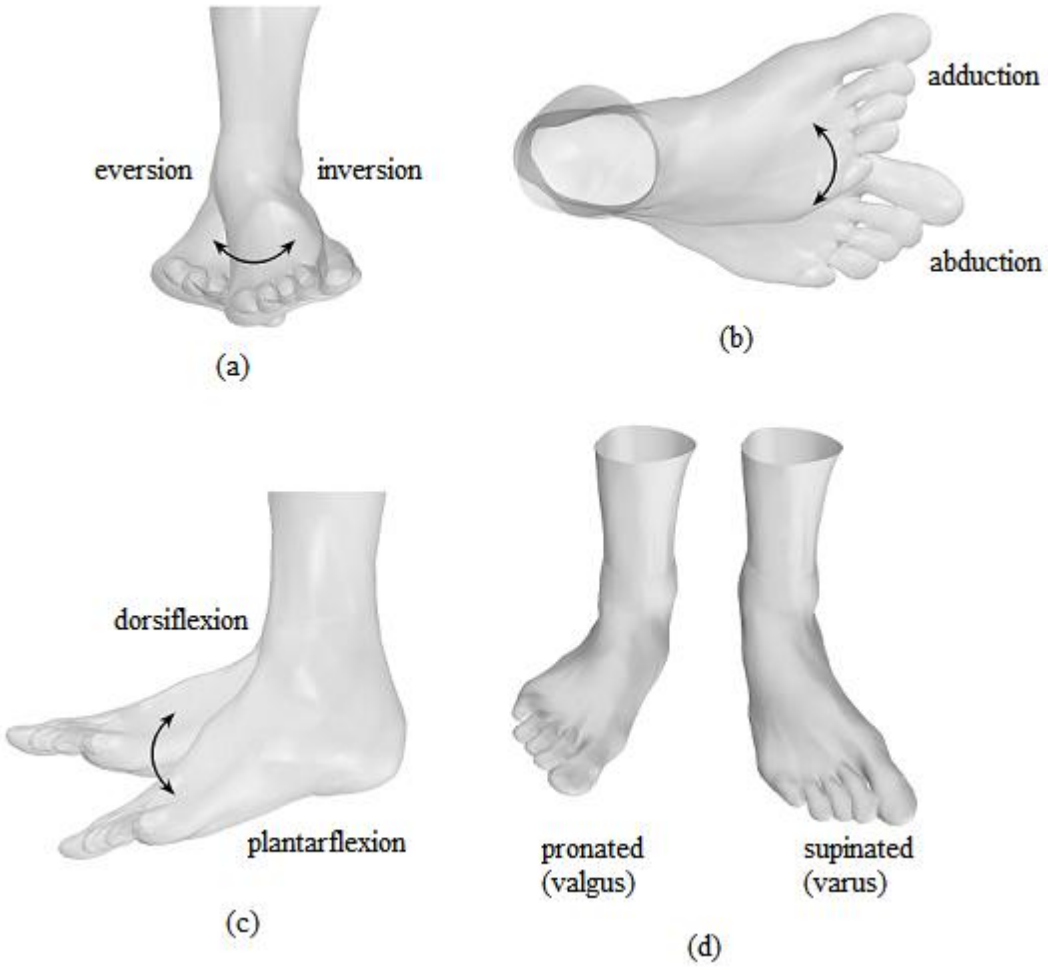

Figure 1.2: Movement and positioning of the foot: a) eversion/inversion, b) adduction/abduction, c) dorsiflexion/plantarflexion, d) pronated (valgus)/supinated (varus) (adapted from [1])

1.1.2 Foot Anatomy

The human foot is connected to the body via the articulating surfaces provided by the tibia and fibula (Figure 1.3). It is often divided into three sections: the hindfoot, the midfoot, and the forefoot (Figure 1.3, Figure 1.4).

Hindfoot -The talus connects the foot to the lower leg. The calcaneus (heel bone) provides a connection between the talus and the ground.

Midfoot - Anterior to the talus is the navicular, which resides on the medial side of the foot. Anterior to the calcaneus is the cuboid, which resides on the lateral side of the foot. The three cuneiforms (lateral, intermediate, and medial) reside anterior to the navicular.

Forefoot - The forefoot consists of the 5 metatarsals and the 14 phalanges: the hallux or first toe has only 2 phalanges while the remaining toes have 3 phalanges each referred to as the proximal, middle, and distal. Finally, two sesamoid bones sit beneath the first metatarsal phalangeal joint (Figure 1.5).

Figure 1.3: The foot connects with the lower leg at the talus, tibia, and fibula interface (adapted from [1])

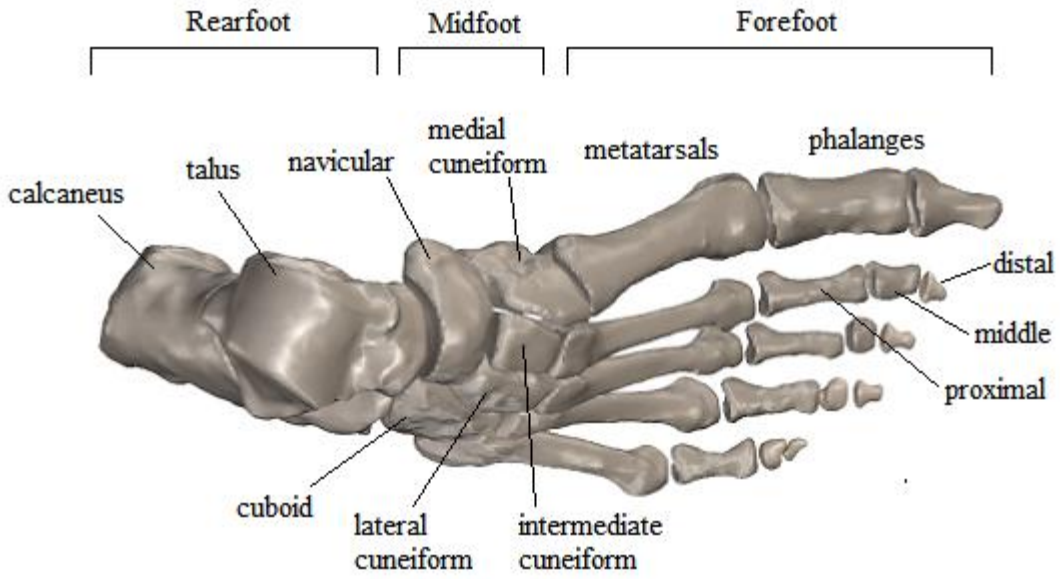

Figure 1.4: Dorsal view of the bones of the rearfoot, midfoot, and forefoot (adapted from [1])

Figure 1.5: Plantar view of the first ray of the foot

In addition to bones, the foot's musculoskeletal anatomy includes many muscles, tendons, ligaments, cartilages, and fascia. The muscles act on the foot via tendons both intrinsically and extrinsically with muscle bodies located in the lower leg. Cartilage allows for smooth movement between adjacent bones while ligaments provide support and limit range in motion. The plantar fascia runs along the plantar surface of the foot and its function is described later. Non-pathological human feet are similar in the number and relative location of the various musculoskeletal tissues. However, the geometry and properties of these tissues as well as neutral joint positions can vary significantly between individuals.

1.1.3 Joints of the Foot

Each joint of the foot consists of two or more adjacent bones that articulate via contacting cartilaginous surfaces. The motion of each joint is restricted by ligaments and actuated by muscles via tendons. A basic description of the joints of the foot follows, while a more detailed description can be found in chapter 2.

The talocrural joint (ankle joint) can be approximated as a hinge joint and occurs at the interface between the talus, tibia, and fibula. The talocalcaneal joint (subtalar joint) is another hinge joint and occurs at the interface between the talus and calcaneus. It is the subtalar joint that is predominantly responsible for pronation and supination of the foot. The calcaneocuboid joint refers to the calcaneus and cuboid interface. The talonavicular joint is a ball joint and refers to the interface between the talus and navicular. The navicular and cuboid have been seen to articulate as a unit [1] as they articulate with the hindfoot (midtarsal joint). It is commonly thought that the midtarsal joint allows for articulation about two distinct axes [1]. The intertarsal joints describe the interfaces between the cuneiforms, navicular, and cuboid while the tarsometatarsal joints describe the interface between the metatarsals and the midfoot bones. Both the intertarsal and tarsometatarsal joints are less well studied than the other bones of the foot, however the general consensus is that they allow for only limited motion though in both planar translation and rotation modes. The metatarsophalangeal joints refer to the interface between the metatarsals and the proximal phalanges of the same ray.

1.1.4 Joint Angles and Positions

In recent years biomechanists have developed methods of describing joint angles and positions in 3D space. For example the International Society of Biomechanics approved the Joint Coordinate System method proposed by the Standardization and Terminology Committee [2]. Ideally, an extension of these methods should be applied to assessing joint angles in the foot for the purpose of orthotic intervention. However, it is not the intention of this dissertation to advance assessment methods, but rather to develop methods for carrying out prescriptions made during the assessment process. As such, the proposed methods will make use of the planar joint angle systems employed by traditional FO development theory as first described in the 1970's by Root et al. [3-5] and later and in greater detail by such works as, "The Functional Foot Orthosis" [6]. Though various aspects of the work of Root et al. have been questioned or criticized [7-10], it is still the predominant theory known and practiced today. How traditional FO theory is employed will be described in section 1.2. For now, the relevant joint angles and positions that will be necessary to carry out FO development are as follows:

- *Tibial stance angle* is measured in the frontal plane as the angle between a line bisecting the lower leg and vertical during standing (Figure 1.6 (a))
- *Subtalar joint angle* is measured in the frontal plane as the angle between the lower leg bisection line and a line bisecting the calcaneus (Figure 1.6 (b))
- *Midtarsal joint angle* is measured in the frontal plane as the angle between a line connecting the metatarsal joints along the plantar surface of the foot and the calcaneus bisection line (Figure 1.6 (c))

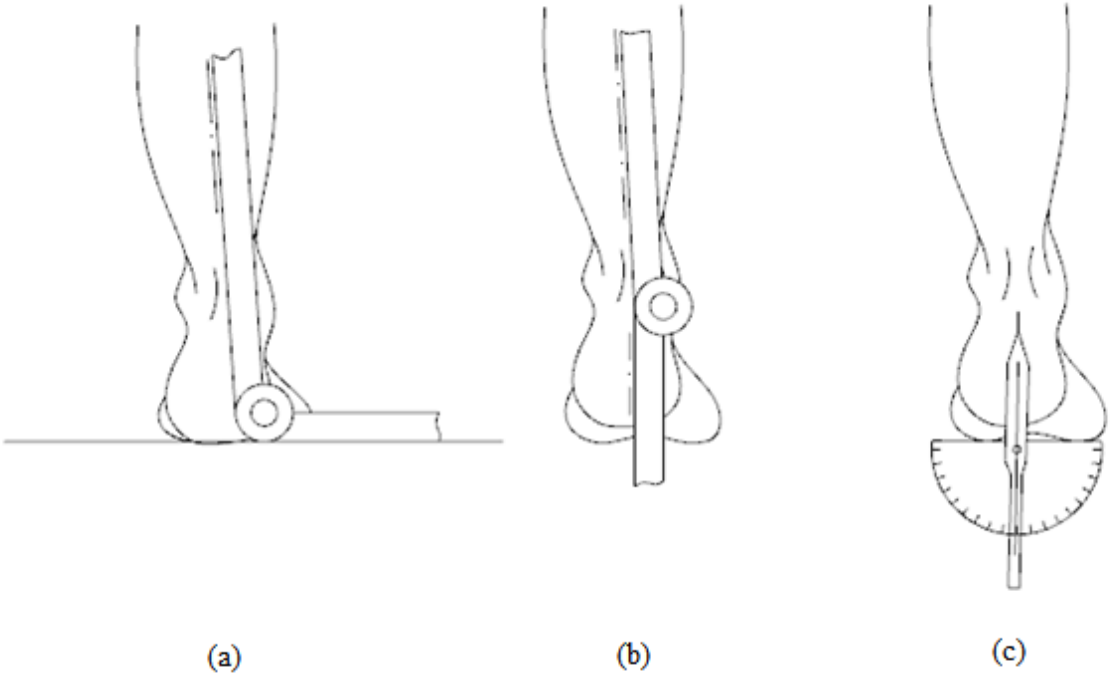

Figure 1.6: Joint angles: a) tibial stance angle, b) subtalar joint angle, c) midtarsal joint angle (adapted from [6])

These three angles are combined to arrive at the rearfoot and forefoot angles, which describe the orientation of the rearfoot and forefoot in the global system:

- The rearfoot angle is the addition of the tibial stance angle and the subtalar joint angle. Or, more simply, it is the angle between the calcaneal bisection and the sagital plane as viewed in the frontal plane (Figure 1.7).

- The forefoot angle is the addition of the rearfoot angle and the midtarsal joint angle. Or, more simply, it is the angle between a line connecting the metatarsal joints along the plantar surface of the foot and the transverse plane as viewed in the frontal plane (Figure 1.7).

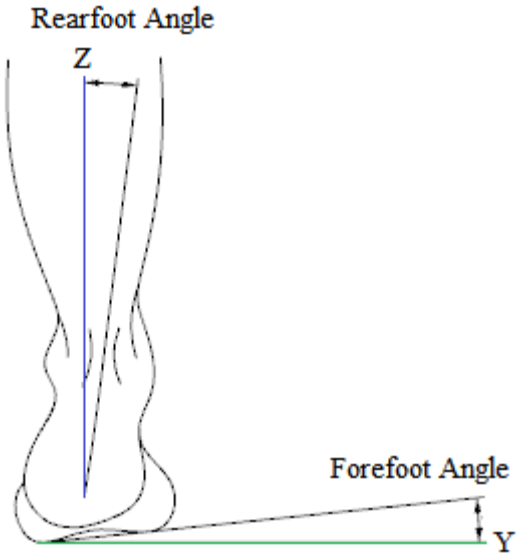

Figure 1.7: Rearfoot and forefoot angles with the midtarsal joint locked and the subtalar joint in neutral position (adapted from [6])

It should be noted that many practitioners currently employing traditional methods find measuring the tibial stance, subtalar joint angle, and midtarsal joint angle to be both time consuming and difficult to achieve with good repeatability. Instead, they prescribe the rearfoot and forefoot angles based on what has previously worked well.

To carry out the methods proposed by Root et al. [3-5], the above measurements must be taken while the foot is positioned in the subtalar neutral joint position with the midtarsal joint locked. Root et al. [3-5] described the subtalar neutral joint position first as the position of the subtalar joint as it is articulated two thirds of the way from full supination to full pronation, and second as the position where the medial and lateral aspects of the talus-calcaneus interface are palpated as congruous. The midtarsal joint locked position was described as occurring at the end range of articulation of the joint as the forefoot is dorsiflexed.

1.1.5 Primary Mechanisms of the Foot

The complexity of the foot's musculoskeletal system is closely matched by the complexity of mechanisms controlling its motion. The following sections detail the three most prominent mechanisms exhibited by the foot.

1.1.5.1 Arches

The arches of the foot provide shock absorption and store mechanical energy thereby reducing peak joint loads and increasing efficiency. Additionally, they prevent compression of the specific plantar regions of the foot that house muscles, nerves, and blood vessels.

There are three distinct arches in the foot; the lateral longitudinal, the transverse, and the medial longitudinal (Figure 1.8). The transverse arch includes the cuboid, cuneiforms, and metatarsals. The lateral longitudinal arch includes the calcaneus, cuboid, and fifth metatarsal. The medial longitudinal arch includes the calcaneus, talus, navicular, medial cuboid, and first metatarsal. Ligaments provide support to the arches. The plantar fascia joins with the medial and lateral longitudinal arches to create a truss structure capable of supporting large loads.

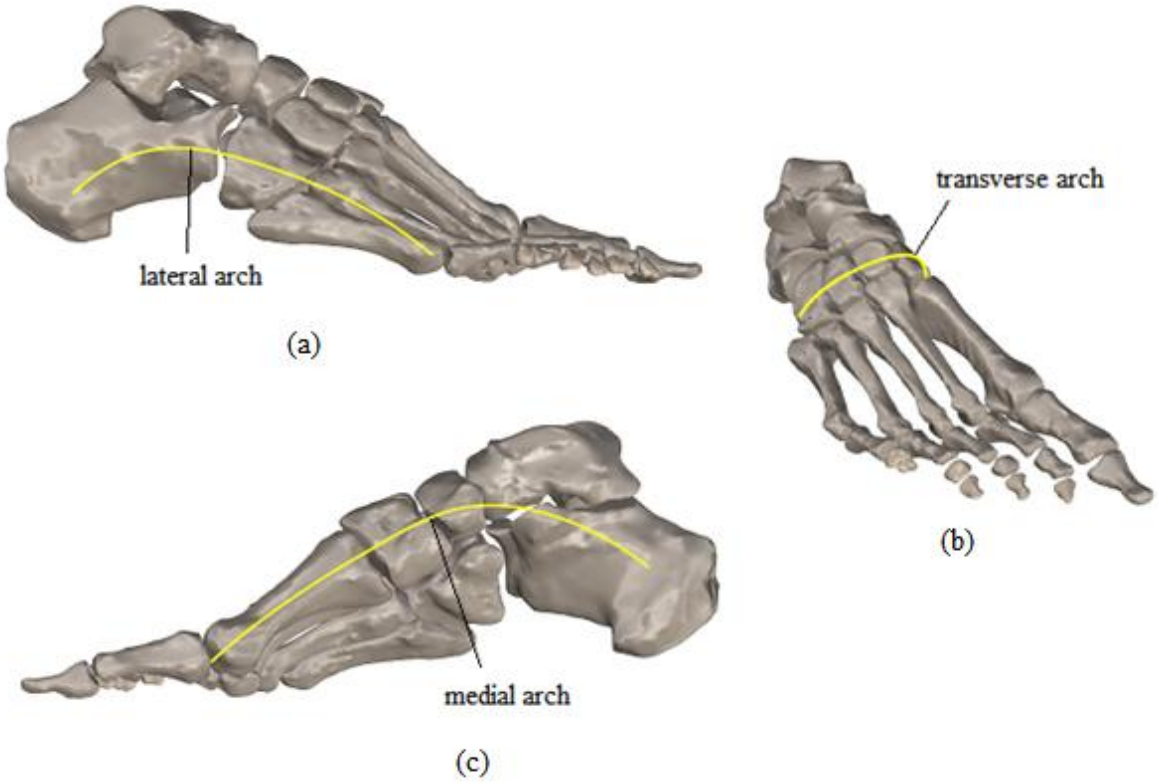

Figure 1.8: Arches of the foot: a) lateral arch, b) transverse arch, c) medial arch (adapted from [1])

1.1.5.2 Lever

Muscles in the posterior compartment of the lower leg act on the Achilles tendon (tendo calcaneus). The Achilles tendon pulls on the calcaneus and the entire foot (the lever) pivots about the articulating surfaces on the distal heads of the tibia and fibula (the fulcrum) and a moment about the ankle joint is created. During quiet standing, this moment counteracts the moment that results from the body's centre of gravity generally residing anterior to the ankle joint, thereby stabilizing the body. An increase in force on the Achilles tendon results in an anterior movement of the foot's centre of force on the ground. During gait, the force on the Achilles tendon can be significantly more than during quiet standing, particularly in the push off stage where the foot plantarflexes and helps propel the body forward (Figure 1.9).

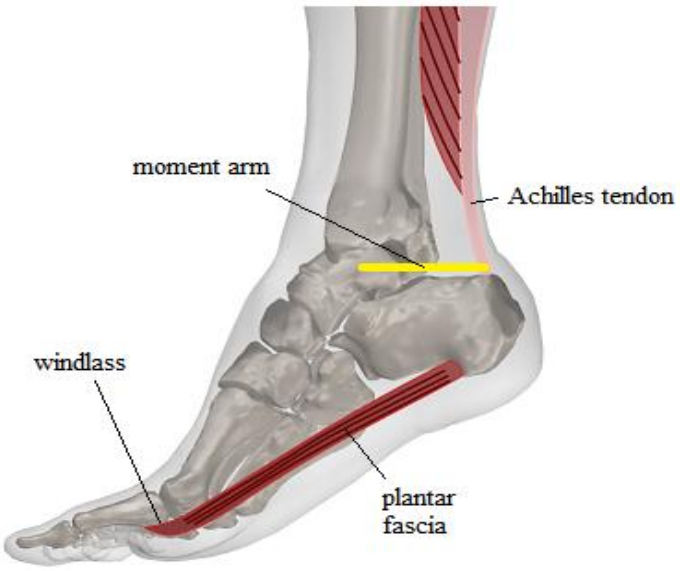

Figure 1.9: Lever and windlass mechanisms of the foot (adapted from [1])

The foot has been observed to change from being adaptable in the early phases of stance as it accommodates various uneven terrains and then converts to a rigid lever during push off. It has been shown that this is largely due to the axis of the midtarsal joint aligning with the subtalar joint axis and the direction of push [11]. This phenomenon is commonly referred to as 'midtarsal joint locking', leading to confusion as this term is also used to describe the midtarsal joint reaching its end range of articulation. For the purposes of this dissertation, the term will be assumed to refer to the midtarsal joint reaching its end range of articulation.

1.1.5.3 Windlass

The plantar aponeurosis is the deep thick portion of the plantar fascia (Figure 1.9). It is pulled taught as the toes are forced into dorsiflexion in the push-off stage of gait (windlass mechanism). As the plantar aponeurosis tightens it provides the extra rigidity the foot requires to support the force the body applies to the foot during push-off. Additionally, as the plantar aponeurosis is stretched, elastic energy is stored to be released as the push-off stage completes.

1.1.6 Foot Motion During Gait

Dorsiflexion and plantarflexion are the largest motions of the foot during gait (Figure 1.10) and occur predominantly about the ankle joint. On heel strike, the foot begins to plantarflex as the forefoot moves towards the ground. Through midstance, the foot dorsiflexes as the body's weight is shifted to

the forefoot in preparation for push off. During push off, the foot is forced into plantarflexion as the muscles acting on the Achilles tendon contract to provide the necessary propulsion.

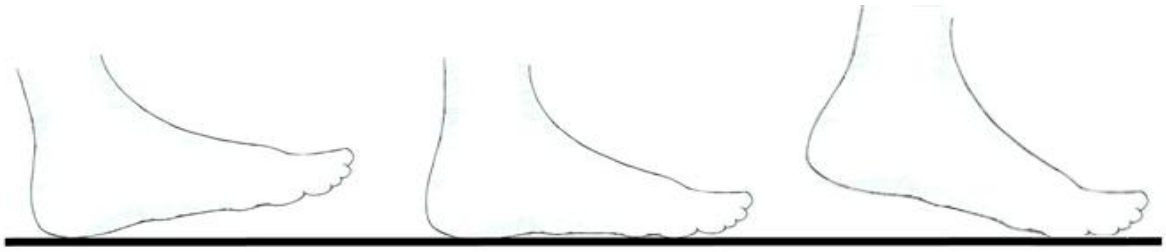

Figure 1.10: Heel strike, mid stance, and push off in the stance phase of gait

Adduction, abduction, inversion, and eversion occur to a lesser degree during gait than dorsiflexion and plantarflexion. Typically, the foot begins to pronate from heel strike to mid-stance and then suppinates until push-off. During changes in direction and as the foot adapts to uneven surfaces, articulation in all of the cardinal planes occurs. The foot also uses articulation to absorb and emit mechanical energy during the stance phase of gait.

1.2 The FO and its Development

The word orthosis stems from the Greek word, orthos, which translates to straight. An orthosis, or orthotic device is used to straighten or correct the posture of a part of the body. A FO is situated between the foot and the midsole of the shoe and replaces the insole. Foot orthoses (FOs) are intended to prevent or aid in the recovery of injury by acting to redistribute pressure experienced by the plantar surface of the foot and/or cause adjustments to relative joint positions during standing and gait. Two common terms used to categorize FOs are *functional FO* and *accommodative FO*. A *functional FO* is intended to achieve both pressure redistribution and postural correction while an *accommodative FO* is merely intended to achieve pressure redistribution.

1.2.1 Pressure Redistribution

FOs are designed to closely match the contours of the non-weight-bearing foot. This results in a more even distribution of pressure across the plantar surface of the foot than the foot experiences on a standard insole [6]. This duplicate surface serves as a base geometry and additional localized adjustments are made to achieve further control over the plantar pressure distribution.

In general, the geometry of all FOs differ from that of the foot in several ways: the region around the border of the heel and midfoot usually has a lower curvature than the foot to allow for tissue expansion, the medial arch area curves away from the foot to prevent the foot from landing on a sharp edge, and the toe region is flat to allow the toes to move freely during ambulation. In addition to these basic differences, there are several indications for further pressure adjustment. Diabetics are prone to ulceration due to reduced sensitivity and circulation in the extremities. As the lack of circulation in the foot causes the tissues to stiffen, they become prone to micro tears that lead to ulceration and infection. Additionally, the reduced sensitivity in the diabetic foot results in inadequate warning when tissue damage is occurring. FO treatment is used to redistribute the force so as to minimize peak pressure points and reduce pressure specifically in areas where ulceration is probable (heel and metatarsal heads). Plantar fasciitis is another condition that benefits from pressure redistribution. Excessive tension on the plantar fascia may result in inflammation at the proximal attachment of the plantar fascia on the calcaneus. Redistribution of pressure away from this inflamed and tender area is therapeutic.

1.2.2 Postural Correction

A second role of a FO is to correct foot posture thereby benefiting the foot as well as ensuring other parts of the body further up the kinematic chain are not compromised through compensation. To achieve corrections, the FO is designed such that it influences foot posture during standing and the gait cycle.

The feet are unique among parts of the body in that they alone contact the ground during standing and gait. Consequently, the foot's biomechanical function influences a greater number of body parts than the biomechanical function of any other part of the body. As a result, most dysfunctions in the foot can be shown to adversely impact other parts of the body. Some of the more common dysfunctions are caused by excessive varus or valgus deformities in the rearfoot or forefoot (resulting in excessive supination or pronation) and collapsed arches. Though a FO may not be able to eliminate these dysfunctions, it can in most cases actively correct them during standing and gait.

1.2.3 FO Development

There are a variety of methods for developing FOs. The methods can be categorized as either modern methods that employ technology made possible by the computer or traditional methods that rely on

physical manual techniques such as plaster casting. Despite their differences, the majority of both modern and traditional methods can be broken down into the following five steps.

(1) Patient assessing

(2) Foot geometry recording

(3) FO geometry developing

(4) FO fabricating

(5) FO fitting and adjusting

Step 1, *patient assessing*, is commonly carried out by podiatrists, choropadists, pedorthists, chiropracters, or orthotists at a clinic. From this point on, the individual prescribing the FO will be simply referred to as the practitioner. Step 2, *foot geometry recording*, is handled by an assistant. However, for simplicity, it will be assumed that the practitioner carries out this step. Steps 3 and 4, *FO geometry developing* and *FO geometry fabricating*, are most often performed at a lab by a technician. Finally, *FO fitting and adjusting* most often occurs back at the clinic and is carried out by the practitioner.

1.2.3.1 Traditional FO Development

Traditional methods for FO development vary between texts, schools, and practitioners. For the current work, the early theories proposed by Root et al. [3-5] and later described in greater detail by J.W. Philps in his 1990 text, "The Functional FO" [6], will be used.

Central to Root et al.'s [3-5] traditional FO theory is the concept that a FO should assist the foot in achieving an ideal midstance posture. Root et al. [3-5] claimed that this ideal posture is characterized by the adoption of the subtalar neutral and midtarsal joint locked positions (these positions were described in section1.1.4). The steps to develop such a FO can be broken down as follows:

(1) *Patient assessing*: The practitioner examines the patient while non-weight-bearing and during standing and gait. The tibial stance, neutral subtalar joint angle, and locked midtarsal joint angle are measured to arrive at the ideal midstance rearfoot and forefoot angles. Abnormalities such as a collapsed arch or a rigid Hallux are noted and appropriate corrections

to the positive cast prescribed. Various characteristics of the FO are decided at this point such as the FO's type, materials, and any local regions requiring decreased pressure.

(2) *Foot geometry recording*: The practitioner casts the foot while maintaining the subtalar joint neutral position and locked midtarsal joint as well as neutral ankle position where the ankle is neither plantar flexed nor dorsiflexed (Figure 1.11). The patient may be either supine or prone. Additional postural adjustments may be incorporated if the type of shoe the FO is intended for is known, for instance if it is a shoe with a high heel. A positive cast is created by pouring Plaster of Paris into the negative cast (Figure 1.11). A common variation on this step is to use a foam box to capture the negative mould of the foot (Figure 1.11) as the patient is sitting. The advantage of the foam box method is that the intended ground plane for the finished FO coincides with that of the casting procedure and thereby simplifies the process for the practitioner. A disadvantage is that the midtarsal joint can no longer be locked with the fingers and instead the reaction force of the foam must be relied upon.

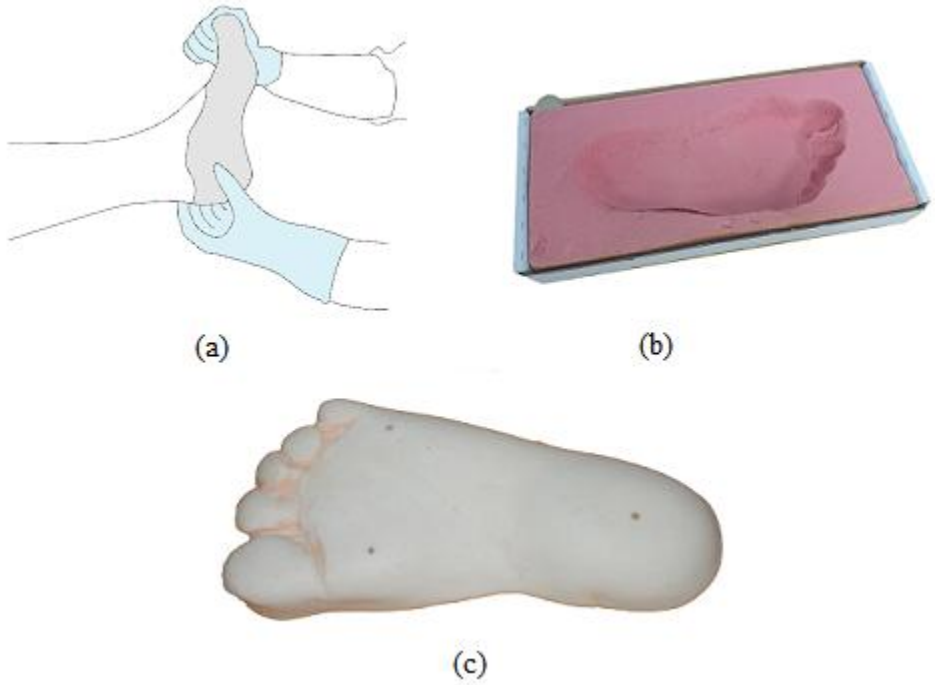

Figure 1.11: Capturing foot geometry: a) suppine plaster casting, b) foam impression, c) resulting positive cast

(3) *FO geometry developing*: A mould for developing the FO geometry about is formed by modifying the positive cast. Modifications are necessary to ensure the FO formed about the cast will achieve the functions prescribed by the practitioner and are achieved through the addition and subtraction of plaster. Firstly, plaster is added and removed from the cast to influence the pressure distribution the foot experience upon weight-bearing on the FO. Modifications for this purpose include the addition of plaster around the perimeter of the mould such that the resulting FO will provide space for the tissues to expand, and the addition and/or subtraction of plaster in various regions to decrease pressures in key locations. Secondly, modifications are made to achieve postural adjustments in addition to those that are achieved by controlling foot posture during casting. For example, material is washed away from the arch area to achieve a FO that lifts the arch to a greater extent and material is added

to cause additional adjustments to the forefoot and rearfoot positioning (commonly referred to as intrinsic posting). Common tools for adding and removing plaster include spatulas and wash clothes (Figure 1.12).

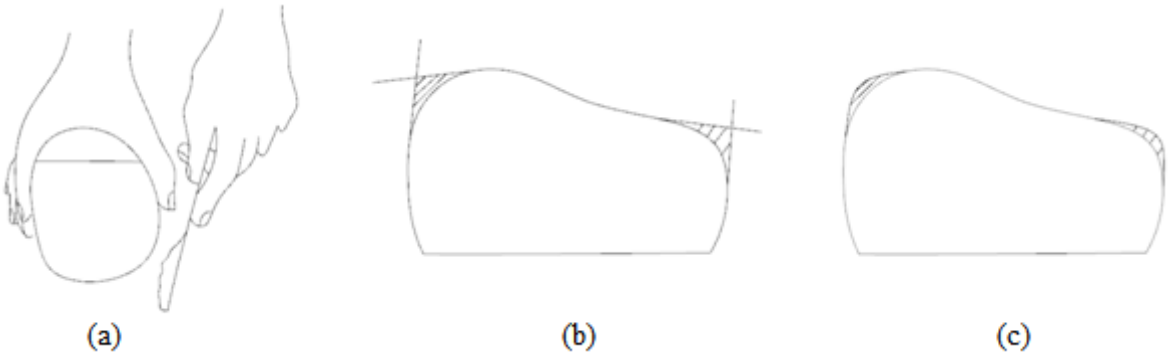

Figure 1.12: Modifying the positive plaster cast: a) adding plaster with a spatula, b) cast with added plaster, c) cast after smoothing out plaster addition (adapted from [6])

(4) *FO fabricating*: At this stage in the process, the manner in which the FO controls posture has already been determined through the preceding steps. The goal of this step is to fabricate a FO with a top surface that matches the altered positive cast from step 3 and attach support material to the bottom of the FO to ensure it remains oriented in the shoe as prescribed in step 1. The shell of the FO is created by vacuum forming material to the positive cast (Figure 1.13). The bottom supporting parts (also known as extrinsic posts) are created by vacuum forming materials to the bottom of the shell and grinding them to the angles necessary to support the FO as prescribed. Additional materials can be attached to the top surface of the FO such as metatarsal bars and pads, however, their purpose is more to cause pressure redistribution than postural correction.

Figure 1.13: Creating the FO shell by vacuum forming materials to the positive cast

(5) *FO fitting and adjusting*: Some adjustments may be necessary to fit the FO into the shoe. After the patient has had a chance to use the FO, adjustments to the way in which the FO controls posture and redistributes pressure may be deemed necessary. In some cases a problem can be solved through simply adding or removing material from extrinsic posts or adding components such as metatarsal pads. In other cases, the positive cast may need adjustment and a new FO fabricated. In the worst case, a new cast must be made.

The process requires extensive skilled manual labour and is thus expensive; a pair of FOs costs between three and five hundred dollars [12]. A second problem is the amount of subjective input required in the process. Controlling the foot's posture during geometry capture is done by hand, further postural adjustments and pressure adjustments are achieved through sculpting of the plaster cast, and fabrication is done manually including the addition of various features such as extrinsic postings and pressure adjusting components. All of these steps are subject to significant intra- and inter-operator error. For casting alone the repeatability has been shown to be poor [13, 14]. Modern digital methods are poised to reduce costs and eliminate some of the subjective component involved in traditional methods.

1.2.3.2 Modern FO Development

Modern FO development methods make use of technologies made possible by the computer such as digitizers, computer aided design (CAD), and automated manufacturing. During the mid 1980s researchers began to work on the use of computer enabled advancements for the application of orthosis and prosthesis development [15] and more specifically, FO development [16, 17]. Since then,

researchers have worked on the continuing advancements in digitizing [18-20], designing [21], optimizing [22-24], fabricating [25, 26] as well as advancements to overall procedures [27, 28] and computer enabled investigations of FO designs and design parameters [29-35] . Currently there are a multitude of companies employing solutions similar to those described in the literature and distributing them for the FO market: Delcam, Ideas, Varifit, Bodytech, JosAmericaLFT, Vorum, and Sharp Shape.

Steps 2 through 4 of the FO development process have been most influenced by technological advancement. Modern solutions replace traditional FO development with one or more of the following steps:

(2) *Foot geometry recording*: Modern approaches look to record the foot geometry as a digital rather than physical entity (Figure 1.14). Most commonly, one or more stationary or moving cameras capture images of the foot. The 3D foot geometry is developed by extracting depth from the images with such methods as triangulation of structured light or stereoscopy. Other varieties of digitizing include the active deformation of a foam block or bed of pins and then digitization of the foam box (the company Ideas uses this method) or recording the position of the pins (Varifit uses this method). There is considerable variation in how the foot is constrained during the scanning process. Scanners that allow for the foot's geometry to be captured with the foot fully non-weight-bearing while the practitioner locks the midtarsal joint yield results most similar to plaster casting (Sharp Shape uses this method).

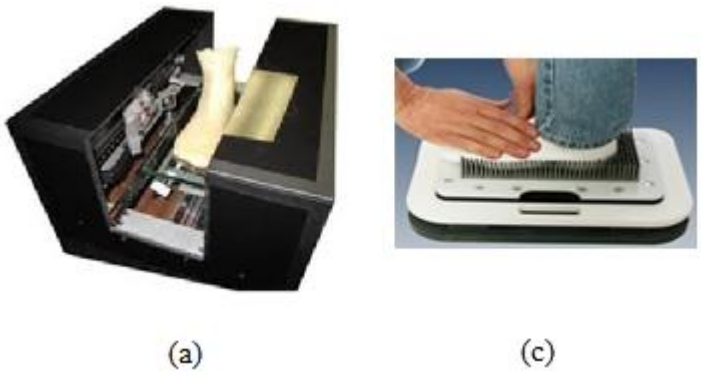

Figure 1.14: Capturing the foot's geometry: a) optically as the foot rests on a flat glass plate (Sharp Shape uses a variation on this scanner type to capture the non-weight-bearing geometry with the patient suppine), b) the Varifit device records the position of an array of pins (Ideas uses a variation on this where the impression of the foot made in a foam box is digitized)

(3) *FO geometry developing*: CAD is used to digitally develop the FO geometry from the foot geometry. Postural and pressure adjustments are made with various deformation functions. The model sent to the fabrication step is either a model of the actual FO or is a model of the mould that the FO is to be vacuum formed to (Figure 1.15).

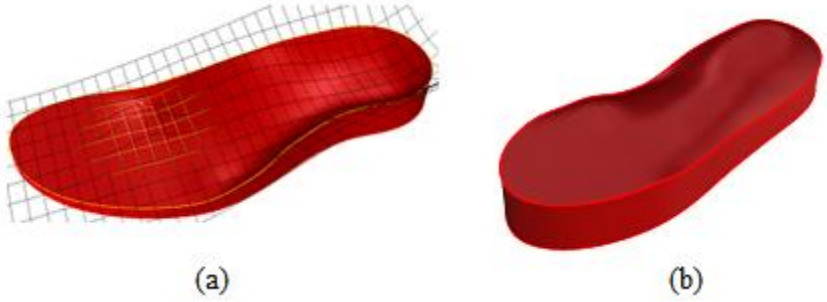

Figure 1.15: *FO geometry developing*: a) development of the actual FO, b) development of a mould about which the FO's materials are to be vacuum formed

(4) *FO fabricating*: A variety of automated manufacturing tools are used to fabricate the FO. Computer numerically controlled (CNC) machining is used to cut the FO or mould for vacuum forming a FO out of a block of material. A reconfigurable mould is used to

automatically develop a surface for vacuum forming a FO (Varifit), and additive manufacturing is used to build the FO layer by layer [25, 26] (Figure 1.16).

Figure 1.16: FO fabrication: a) vacuum forming the FO to a reconfigurable mould in the form of an array of pins (Varifit), b) CNC machining either the actual FO model or a mould for vacuum forming the FO

Though there is significant variation on FO quality and cost with the many different varieties of modern methods, the price of FOs yielded is generally less than that of traditional methods. Furthermore, the gap is growing as modern technologies improve and become more affordable while the cost of skilled manual labour increases.

Though modern methods continue to address the cost issue, there is still much progress to be made in reducing the subjective components required by practitioners and lab technicians to develop FOs; studies have found repeatability to be similar to that of traditional methods [14, 36]. Postural control during casting and manual techniques during fabrication still have a similar subjective component to traditional methods. Other subjective components have become digital rather than physical such as the way postural and pressure adjustments are made with various deformation functions instead of physical sculpting.

An additional problem in both traditional and modern FO development is that, unlike with off the shelf products, the patient is unable to try the FO prior to purchasing it. Both the problem of a large subjective component and the inability to test FOs prior to fabrication has a negative implication for the quality of FOs developed with traditional and modern development methods.

1.3 The Proposed Solution

The proposed solution introduces 2 new steps, both of which make use of an additional computer enabled technology that is not currently used in modern methods: the anatomically accurate simulation model. The first additional step is *postural adjustment simulating* where all postural adjustments occur via the simulation model. The second additional step is *FO design validating* where the simulation model will be used to test a FO prior to fabrication. If any problems are detected, the development processes is repeated starting with the postural adjustment step. The following are the new steps and how they differ from conventional steps.

(1) *Patient assessing*: This step is largely unchanged from conventional methods. The one proposed difference is the use of more advanced measuring tools. In the case of the current work, an Artec handheld scanner will be used to capture the various angles.

(2) *Foot geometry recording*: A digital scanner is used to passively capture the fully non-weight-bearing foot geometry. Given no interaction by the practitioner, the desirable outcome of an entirely undeformed plantar surface will result.

(3) *Postural adjustment simulating*: A simulation model is used to achieve all postural adjustments including rearfoot and forefoot alignment and adjustments to the arches and toes and heel height. The goal for this step is to place the foot in the ideal midstance posture such that a FO designed about the foot will hold it in this posture. This is distinctly different from conventional methods where postural adjustments are subjectively made in the FO geometry development step in the hope that they will cause the foot to assume the prescribed midstance posture. A further benefit of simulating the postural adjustments is that they can be done in such a way that the plantar soft tissues are left entirely undistorted.

(4) *FO geometry developing*: The FO is designed digitally about the posturaly adjusted digital foot model. A set of parameters exactly define the deviations between the FO geometry and the foot geometry. Unlike with conventional methods, these deviations are only intended to

achieve pressure adjustments; no postural adjustments are made in this step as they have already been fully achieved in step 3. The complete FO model is developed in this step, including any features of the FO such as extrinsic postings and plugs.

(5) *FO design validating*: In this step, the simulation tools are used to test a design prior to fabrication to detect potential problems. Depending on the type of problem, the process returns to either the postural adjustment step or the FO geometry development step.

(6) *FO fabricating*: Additive manufacturing will be used to automatically design the FO developed in step 4. The goal is to eliminate subjective operations that could influence the final outcome of the FO. Additive manufacturing is the ideal technology for this given the lack of restrictions on geometry it can produce.

(7) *FO fitting and adjusting*: This step remains unchanged from the conventional process. However, theoretically it should be less necessary given the proposed improvements to the process.

Given the deformable characteristics of the tissues of the foot, the finite element (FE) modeling method is appropriate. The FE foot model has become a common medical and engineering tool in recent years. Its application, however, has primarily been limited to research as few clinical applications warrant the development cost of a FE foot model. High cost stems from the MRI or CT scan and the skilled labour used to assemble the model for FE analysis. Consequently, the FE modeling approach has previously been out of reach for the application of FO development.

The proposed solution is to deform a detailed generic FE foot model to an inexpensive surface scan obtained from a modern digitizer to develop a patient-specific FE foot model.

1.4 Contributions of the Dissertation

The two primary short comings present in both traditional and modern FO development processes are first, the subjective input required throughout the process and second, the inability to validate designs prior to the fabrication step.

It is hypothesized that these short comings can be addressed through the incorporation of simulation techniques in the development process and improvements to the design and fabrication steps. The resulting novel FO development process is the overall contribution of this dissertation.

The parts required to create this novel process represent contributions in themselves. First, unlike other FE foot models described in the literature, the current model was developed with computational efficiency being a primary consideration. Second a novel procedure was developed for creating a patient-specific FE foot model by deforming a generic model derived from MRI data to structured light scan data. Third, novel methods were developed for designing and fabricating FOs. Finally, the simulation tools and FO design and fabrication methods were incorporated into a novel 7 step procedure for developing FOs.

1.5 Outline of the Dissertation

This dissertation is organized into 6 chapters. This first introductory chapter covered the basic anatomy and mechanics of the foot, described both traditional and modern methods of FO treatment and their short comings, and proposed an approach that incorporates simulation tools. The remaining chapters describe the development and implementation of the proposed approach.

In Chapter 2, a literature review of FE foot models is first provided, and the model developed for this dissertation is then described. The model differs from other models in the literature in that it is intended for use on a per patient basis rather than for research purposes. Given its application, computational efficiency is critical. The chapter describes all of the steps to develop the model, difficulties encountered, and the model's validation.

The goal of chapter 3 is to describe a method for rapidly and inexpensively developing patient-specific FE foot models. The method consists of a procedure for deforming a generic FE foot model, in this case the model described in chapter 2, to a specific surface model of a foot acquired from structured light scan data. Both the geometrical accuracy of the method and simulated pressure distribution accuracy are presented. Finally, the results and difficulties encountered are discussed.

In Chapter 4, the focus moves away from simulation techniques to developing design and fabrication tools necessary to produce a comprehensive solution for FO treatment. Each step of the design algorithm is described in detail as its unique aspects are pointed out. Similarly, the fabrication technique is explained and its uniqueness highlighted.

The purpose of chapter 5 is to demonstrate for a single subject the proposed FO treatment approach, and in particular the benefits of incorporating the simulation tools.

Finally in chapter 6, conclusions for the individual chapters, suggested improvements and advancements, and other potential applications that could benefit from the contributions of this dissertation are presented.

Chapter 2
Foot Modeling

Central to the proposed approach to FO development is a robust simulation model of the foot. Given the deformable characteristics of the tissues of the foot, the finite element (FE) modeling method is appropriate. The focus of this chapter is the development of a FE foot model.

Development of FE foot models is well documented in the literature. The model detailed in this chapter is unique in that computational efficiency was considered equally as important as plantar pressure prediction accuracy so that the model could be useful in clinical work rather than being of use solely for research applications.

The model developed in this chapter will serve as the generic model in following chapters where it will be morphed to foot surfaces and landmarks acquired from structured light scan data to inexpensively create patient-specific FE models.

2.1 Introduction

Finite element analysis (FEA) is a computational method used to approximately solve boundary value problems. A FE model is essentially a larger model broken down into many smaller elements of finite size. It is often used for analysis of fluid, structural, and field problems. FEA has been employed in analyzing human soft tissue behavior under pressure as far back as 1978 by Chow et al. [37], which developed a detailed FE model of a buttock and wheelchair seat that was used to investigate pressure distribution and the mechanics that lead to pressure sores.

The research of Chow et al. [37] was followed a few years later by Nakumara et al. in the first attempt at a FE model of a foot [38]. Their motivation was to investigate the shoe foot interface that influences the mechanics of diabetic feet. This model limited the analysis to a single plane and approximated the foot with four elastic bodies: the toes, the rest of the foot's bones, a region of lesser stiffness connecting them, and the soft tissues.

In 1993, Patil and Huson et al. followed up on Nakamura et al.'s work with a comparably simple 2D FE model limited to the medial arch [39]. The model included four bones and the forces exerted on the Achilles tendon by the triceps surae and the tibialis anterior. X-rays assisted in the design of

the model. Soft tissue was omitted as it was a study purely on joint stress. The work was motivated by a need for determining the altered joint stresses in leprotic and diabetic feet. In 1996 Patil and Huson et al. incrementally advanced their FE model to six bones, added cartilages and ligaments, and a greater number of muscles [40]. In the same year, the first 3D FE foot model was published on with Shanti Jacob added to the team and acting as the first author [41].

Since these early works, the number of publications, researchers, and uses of FE models of feet has been rapidly increasing. Figure 2.1 plots the number of papers being published versus time period[1]. Publications are turning up in journals with a wide variety of focuses such as biomechanics, ergonomics, prosthetics research, bionic engineering, industrial design, computer aided design, orthopedics, and medical engineering. Uses for FE foot models include advancing knowledge of FO design [23, 30, 32, 33, 42, 43], shoe design [39, 44, 45], ankle FOs [46], pathomechanics [47, 48], locomotion [49], plantar pressure [50-53], tissue mechanics [42, 54-56], plantar fasciitis [23, 48, 57], joint stress [58], and surgical interventions [43, 59, 60]. Many of these publications include details on the development and validation of their respective FE models. Others have published exclusively on development and validation [61-63]. Particularly relevant to the current work are the publications relating to FO design:

- Perhaps the most recent standard-setting and frequently cited FE foot model is Cheung et al.'s [30, 31, 42, 47]. Geometry was developed from MRI data, joint motion was achieved via surface-to-surface sliding interaction, the major ligaments and fascia were modeled as tension only trusses, and a hyperelastic material model was used to describe soft tissue mechanics. Cheung et al.'s models were used for a variety of purposes related to FOs including a study of the influence of FO geometry and material properties on plantar pressures.
- Goske et al. used FEA and experimental methods to compare peak plantar pressures felt by the heel of the foot while weight-bearing on a variety of materials, thicknesses, and conformity of the FO to the foot (full conformity, half conformity, and flat) [33]. It was concluded that conformity was the most influential parameter, followed by thickness, and finally, material. This study aimed to help those suffering with rheumatoid arthritis and plantar fasciitis.

[1] The search included database systems searched by Scholars Portal including Compendex, Inspec, and Medline and simple search terms relevant to FOs for demonstrative purposes: (finite element analysis and foot and orth*)).

- Bubhadhatti et al. created a FE model of just the first ray (first metatarsal and phalanges of the hallux) [43]. The model was used to analyze the effects of hallux limitus (limited dorsiflexion capability of the first ray), arthrodesis of the first ray (fussing the first ray at a specific flexion angle), and the influence on peak plantar pressures (along the first ray) of various materials that are used in footwear and FOs. Modeling was limited to the first ray to reduce computation times.
- Erdemir and Cavanagh et al. used FEA to study the effects of using plugs to reduce peak plantar pressures [32]. It was concluded that larger and softer plugs better reduced peak plantar pressures. Their numerical results were validated experimentally.
- Hsu et al. studied the influence of FO geometry on stress in the plantar fascia [23]. An optimization routine was used to develop a FO that minimized plantar fascia stress.

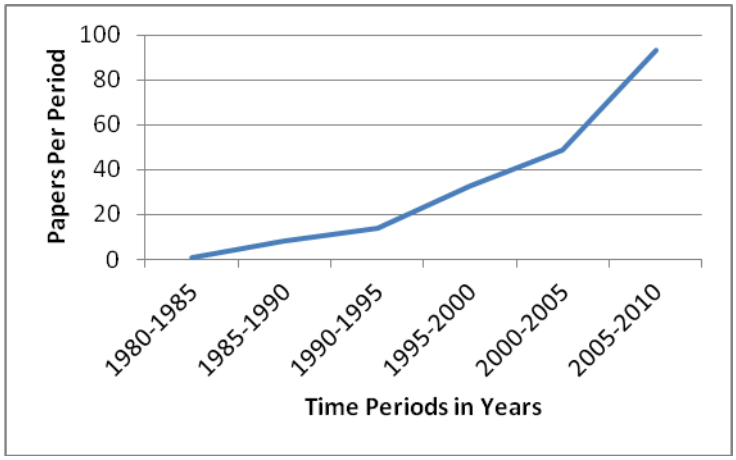

Figure 2.1: Publications found per time period

All of these studies have been geared towards advancing general knowledge of FO design. The intention of the current work is to instead apply the FE method to FO design in a clinical setting. This requires that the model be computationally efficient. The review of the literature on FE foot models turned up minimal attention to computational efficiency. The current work seeks to address this as various characteristics of FE foot models are evaluated and/or discussed in light of computational efficiency as a FE foot model is developed and validated for testing plantar pressure on flat ground and on FOs. Given any necessary design changes and validation, the model should also be suitable for other applications.

2.2 Methods

The methods used to develop the anatomically accurate foot geometry, joint articulation descriptions, interactions, loads, boundary conditions, steps, tissue properties, meshing, convergence, model simplifications, and experimental setup are described in this section.

2.2.1 Foot Geometry Development

An MRI (3.0 Tesla T2 weighted, 1mm spaced image slices with fat saturation) of a non-pathological human foot was taken while the subject was supine with their foot in a fixture that both contained a dedicated coil and restricted movement during the scan (Figure 2.2). The subject was positioned such that minimal force was applied to the plantar surface of the foot thereby minimizing compression of the plantar soft tissues. MIMICS was used to segment the scan images and reconstruct the bone and skin 3D geometry in mesh form (Figure 2.3, Figure 2.4, Figure 2.5). T-Splines were used to surface the mesh geometry while a Boolean subtract function in Rhinoceros 3D was used to generate the soft tissue volume (Figure 2.6). Rhinoceros 3D was used to draw the ligaments and fascia with guidance from Foot And Ankle Interactive (Figure 2.7). The model was initially oriented such that the posterior edge of the fibula was made parallel to the ZY plane and small rotations were later made to match up plantar pressure distributions with that of the pressure mat. Finally, the ground model was created in Rhinoceros 3D and the FO model was designed using the methods developed in chapter 4. All geometries were imported into Abaqus (Figure 2.8).

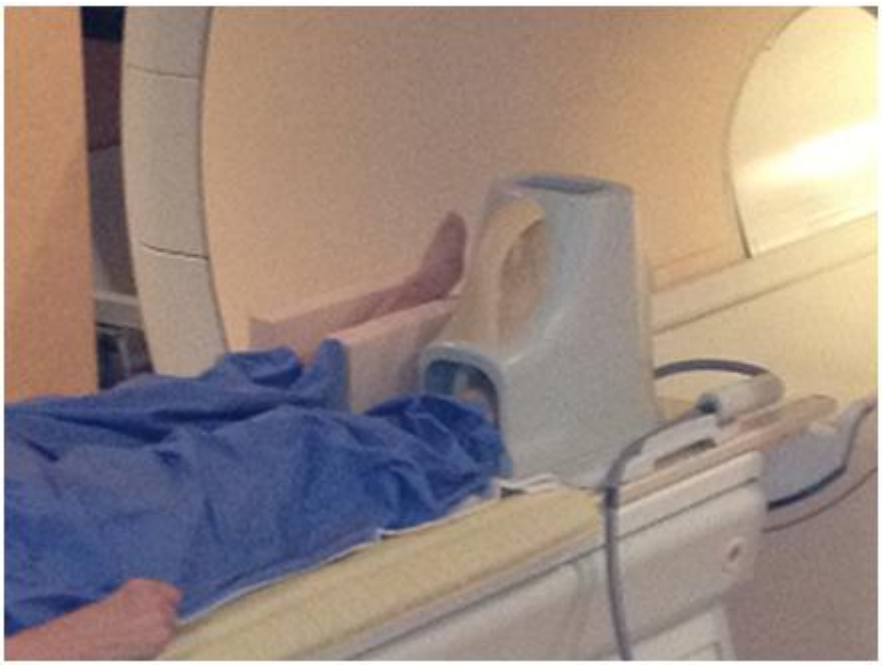

Figure 2.2: MRI scanning the foot with a fixture for both housing a dedicated coil and restraining the foot

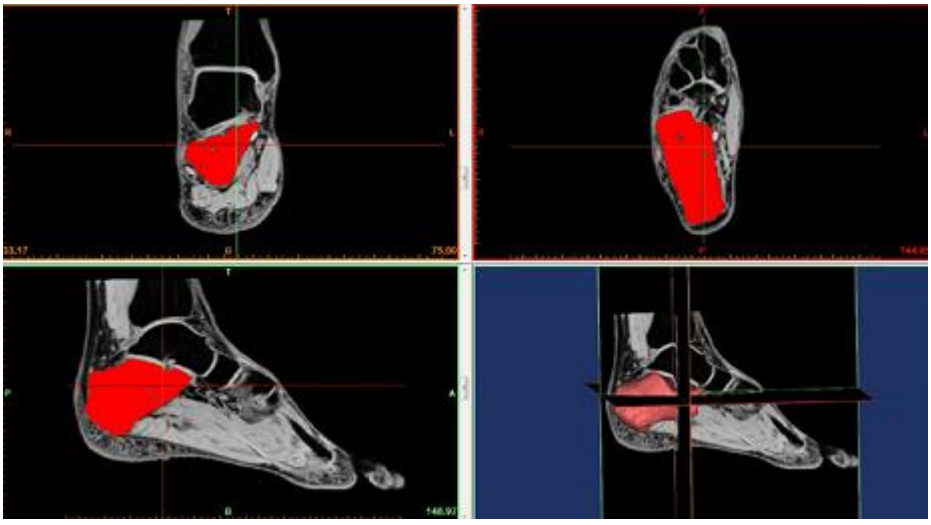

Figure 2.3: Cross sections of the foot and masking the bones with MIMICS

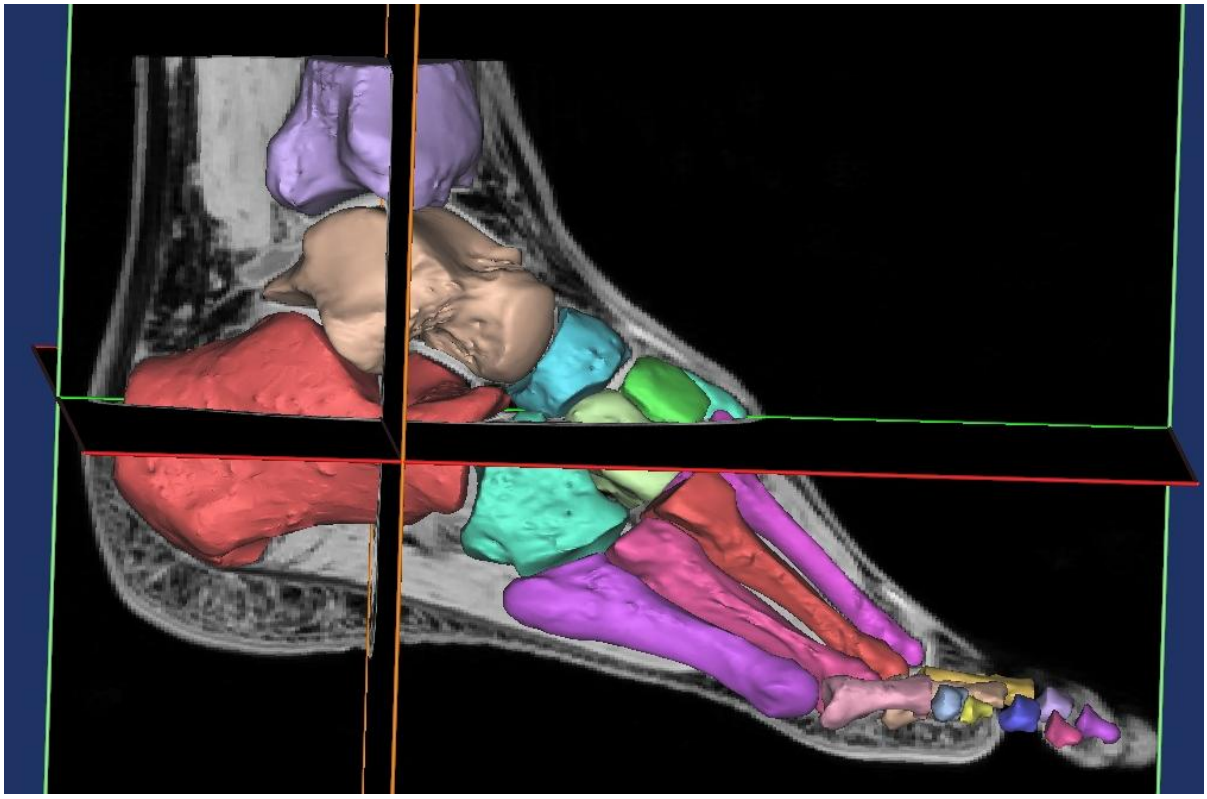

Figure 2.4: Reconstructed Bone volumes viewed in MIMICS

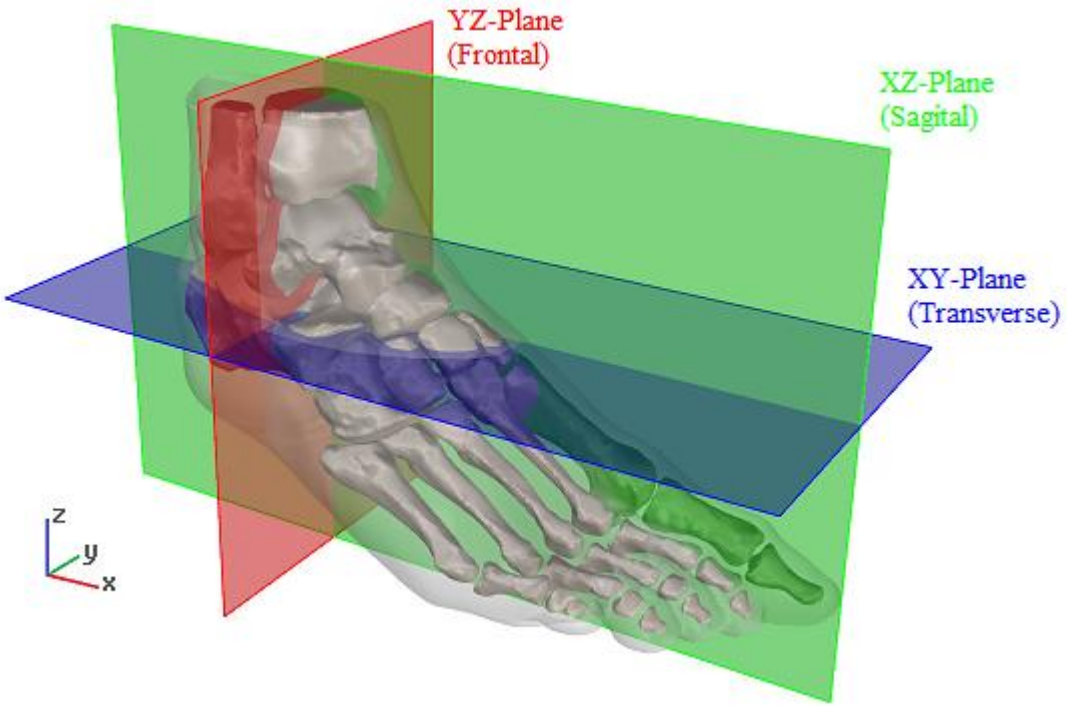

Figure 2.5: Skin and bone volumes after masking and reconstruction and the three cardinal planes

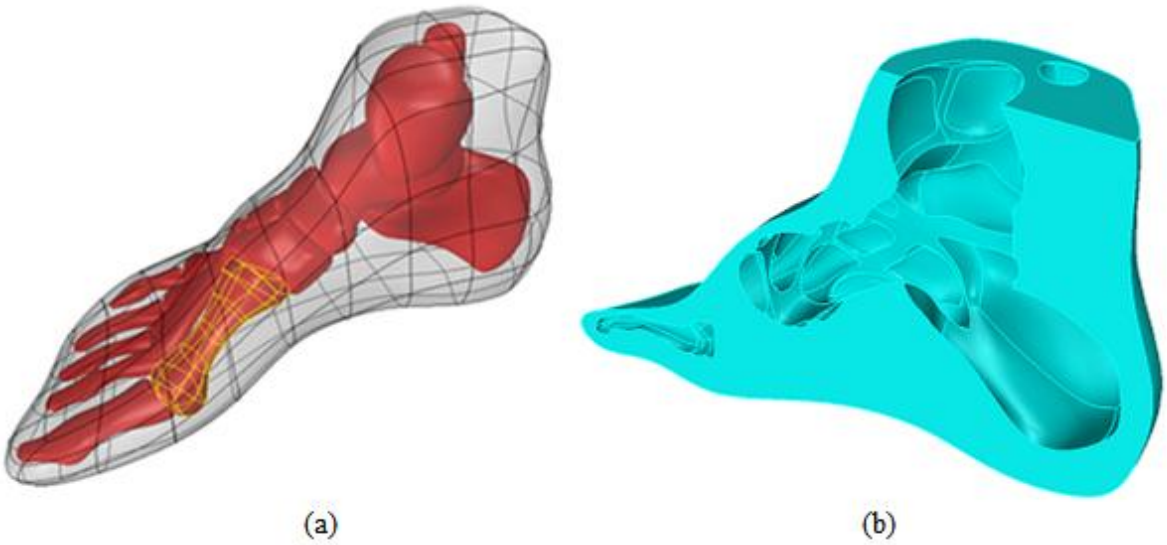

Figure 2.6: Anatomical surface model development: a) Skin and bones surfaced and converted to IGES, b) soft tissue volume created by a Boolean subtraction of the bones from the skin

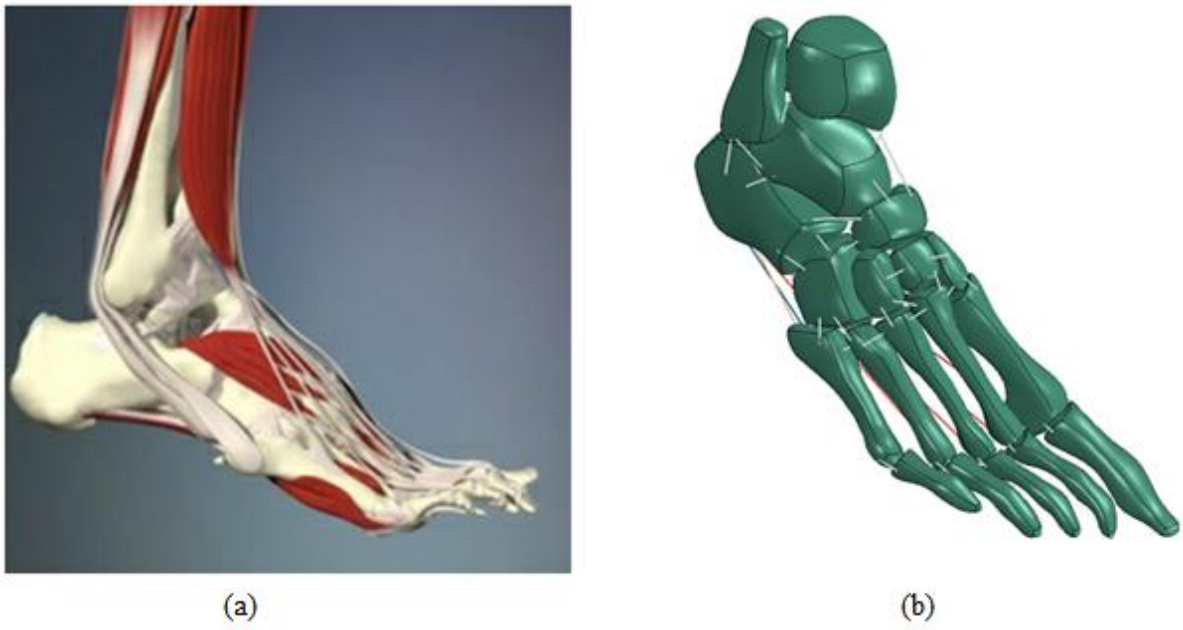

Figure 2.7: Locating ligaments and fascia: a) guided by the anatomy educational software Ankle Foot Interactive, b) located on the foot model

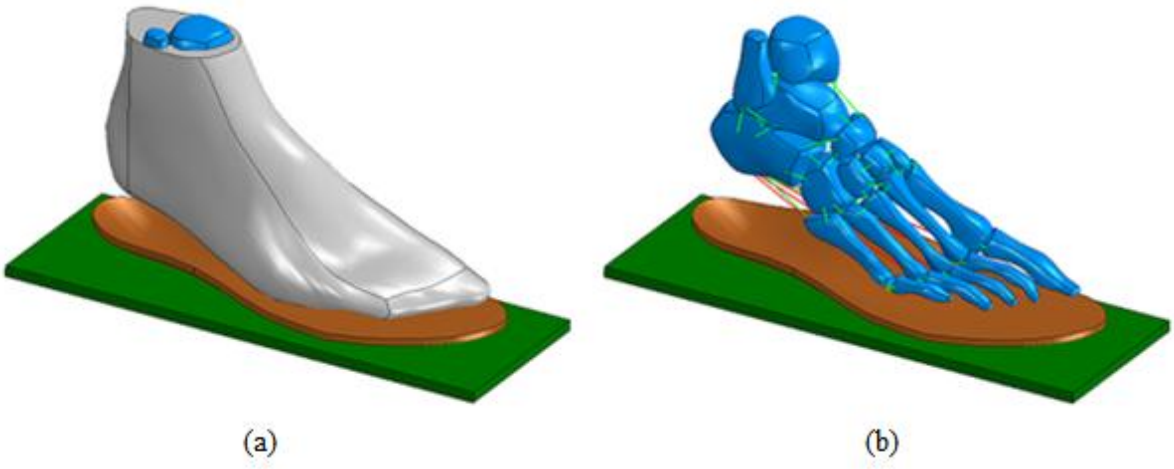

Figure 2.8: Assembly of the ground, FO, and foot model: a) view with soft tissue visible, b) view with tendons, fascia, and bones visible

2.2.2 Joint Articulation Modeling

Articulation of adjacent bones in the human foot is restricted by ligaments, manipulated by muscles via tendons, and allowed smooth movement by low friction cartilaginous layers covering the

contacting surfaces. In their FE foot model developed in 1981, Nakamura et al. achieved a simplistic model of a joint; a linearly elastic region of lesser stiffness than bone connected the toes to the rest of the foot [38]. This region allowed for articulation of the joint while resisting excessive joint excursion, thereby approximating the roles of both ligaments and cartilage. The primary disadvantage of this method is that the elastic region resists all degrees of freedom, including those of normal joint articulations that occur as the foot accepts weight, thereby introducing error when using the model to predict plantar pressures.

Cheung et al.'s recent work used a more realistic joint model; the ligaments that restrict joint motion were modeled as tension only trusses and cartilage on cartilage sliding was modeled as frictional surface-to-surface sliding interactions between contacting bone surfaces [30, 31, 42, 47]. A challenge in implementing this method is that the threshold technique for isolating bone in an MRI or CT is more difficult to apply to cartilage. The cartilage is more easily modeled manually on each contacting bone surface. Compared to the connecting elastic volume method, the joint contact modeling method is computationally more expensive due to the instability that results from the added degrees of freedom as well as the additional calculations required for contact modeling. It is perhaps for these reasons that many modern models still use Nakamura et al.'s method of attaching the bones with elastic volumes [61, 62, 64].

The proposed method describes relative joint motion kinematics with hinge and pin connections. In the context of predicting plantar pressures, this technique is biomechanically more realistic than gluing the bones together with elastic volumes and is computationally more efficient than contact modeling. A hinge joint allows for a single rotational degree of freedom while a pin joint allows for three rotational degrees of freedom. Neither joint allows for translational degrees of freedom.

The talocrural and the subtalar joints were modeled as hinges. The axes of the hinges were determined as described by Parr et al. [65]: For the talocrural axis, spheres were fit to the medial and lateral halves of the trochlear facet of the talus (Figure 2.9). The line connecting the centres of the spheres is the joint axis. Similarly, spheres were fit about the calcaneal and sustentaculum facets of the talus to determine the subtalar joint axis (Figure 2.10).

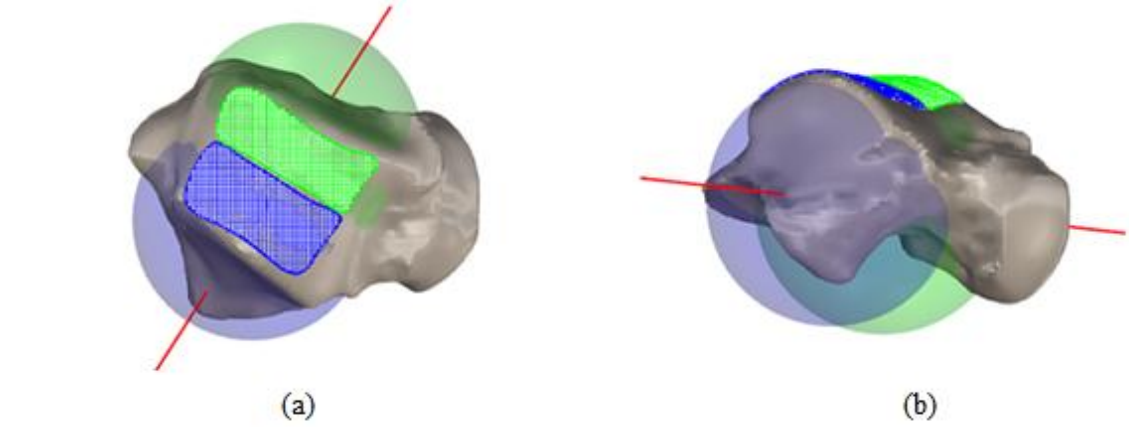

Figure 2.9: Talocrural joint hinge axis development on the talus: a) transverse view, b) sagital view

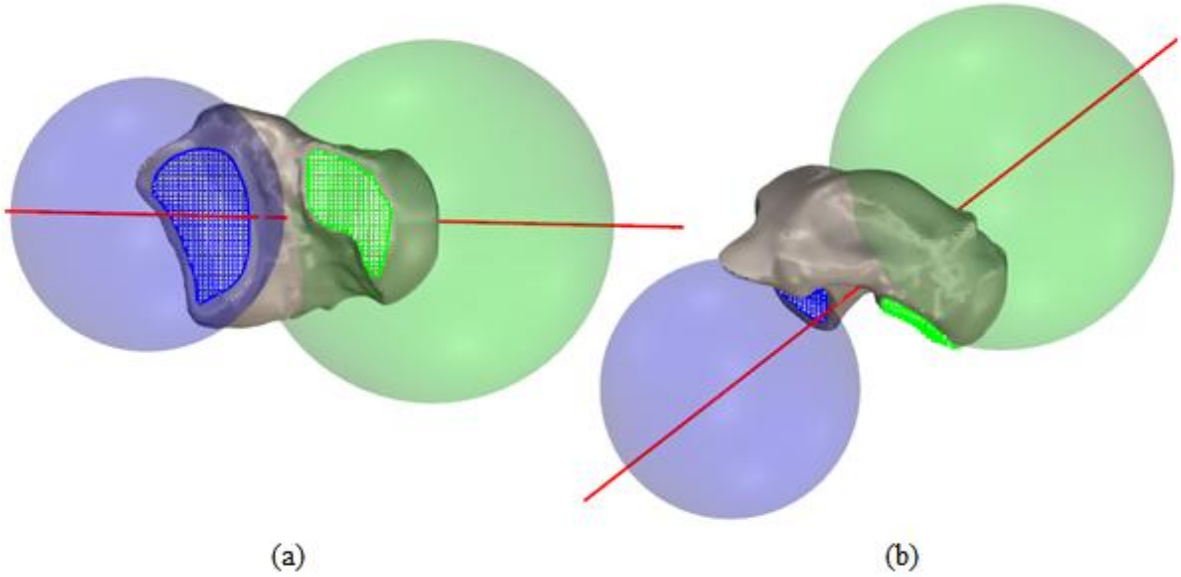

Figure 2.10: Subtalar joint hinge axis development on the talus: a) transverse view, b) sagital view

The midtarsal joint (also known as the transversetarsal joint) consists of the calcaneocuboid joint and the talonavicular joint. Similar to the subtalar and talocrural joint axes, the calcaneocuboid joint axis was determined by connecting the centres of two spheres fit to the superior and inferior parts of the posterior facet of the cuboid (Figure 2.11). The talonavicular joint was modeled as a ball joint centred about a sphere fit to the head of the talus (Figure 2.12). Interestingly, the axis of the

calcaneocuboid joint passes within 7mm of the centre of rotation of the talonavicular joint (less than 1mm when viewed in the sagital plane). This appears to support recent observations that the cuboid and navicular articulate as a single unit about a single midtarsal axis [66]. Furthermore, the orientation of the calcaneocuboid axis is within the range of the midtarsal axis described by Nester et al. [67].

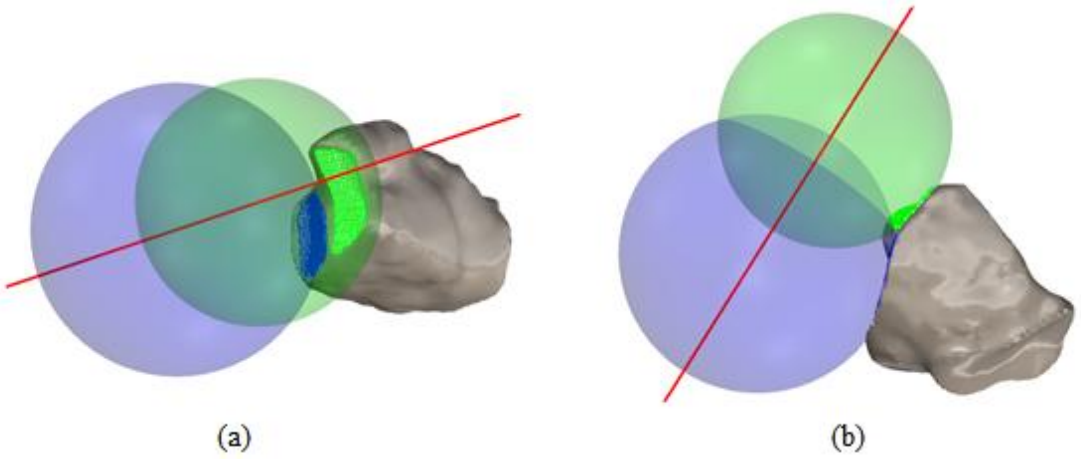

Figure 2.11: Calcaneocuboid joint hinge axis development on the cuboid: a) transverse view, b) sagital view

Figure 2.12: Navicular joint centre of rotation developed on the talus: a) transverse view, b) sagital view

Articulations of the intertarsal and tarsometatarsal joints are not as well studied as the other joints of the foot. Of all of these joints, the first metatarsocuneiform joint has seen the most attention where both rotational and translational motions have been reported [68, 69]. However, in all cases, observation of these joints has revealed limited mobility, perhaps due to the substantial network of

ligaments crossing the joints. For the current work, simple pin joints were used to approximate articulations of contacting bones in this region (Figure 2.13).

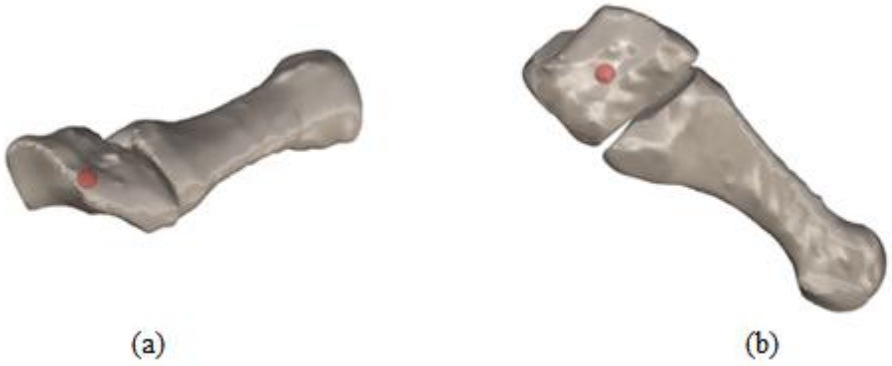

Figure 2.13: Metatarsocuneiform joint centre of rotation developed on the medial cuneiform and first metatarsal: a) transverse view, b) sagital view

Finally, the metatarsophalangeal joints were modeled as pin joints by fitting spheres to the articulating surfaces of the distal heads of the metatarsals (Figure 2.14). Figure 2.15 displays the various hinge and pin joints in the transverse and sagital planes.

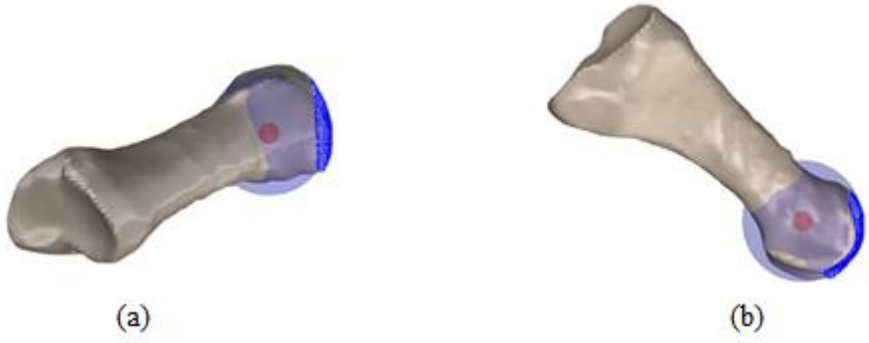

Figure 2.14: First metatarsophalangeal centre of rotation developed on the first metatarsal: a) transverse view, b) sagital view

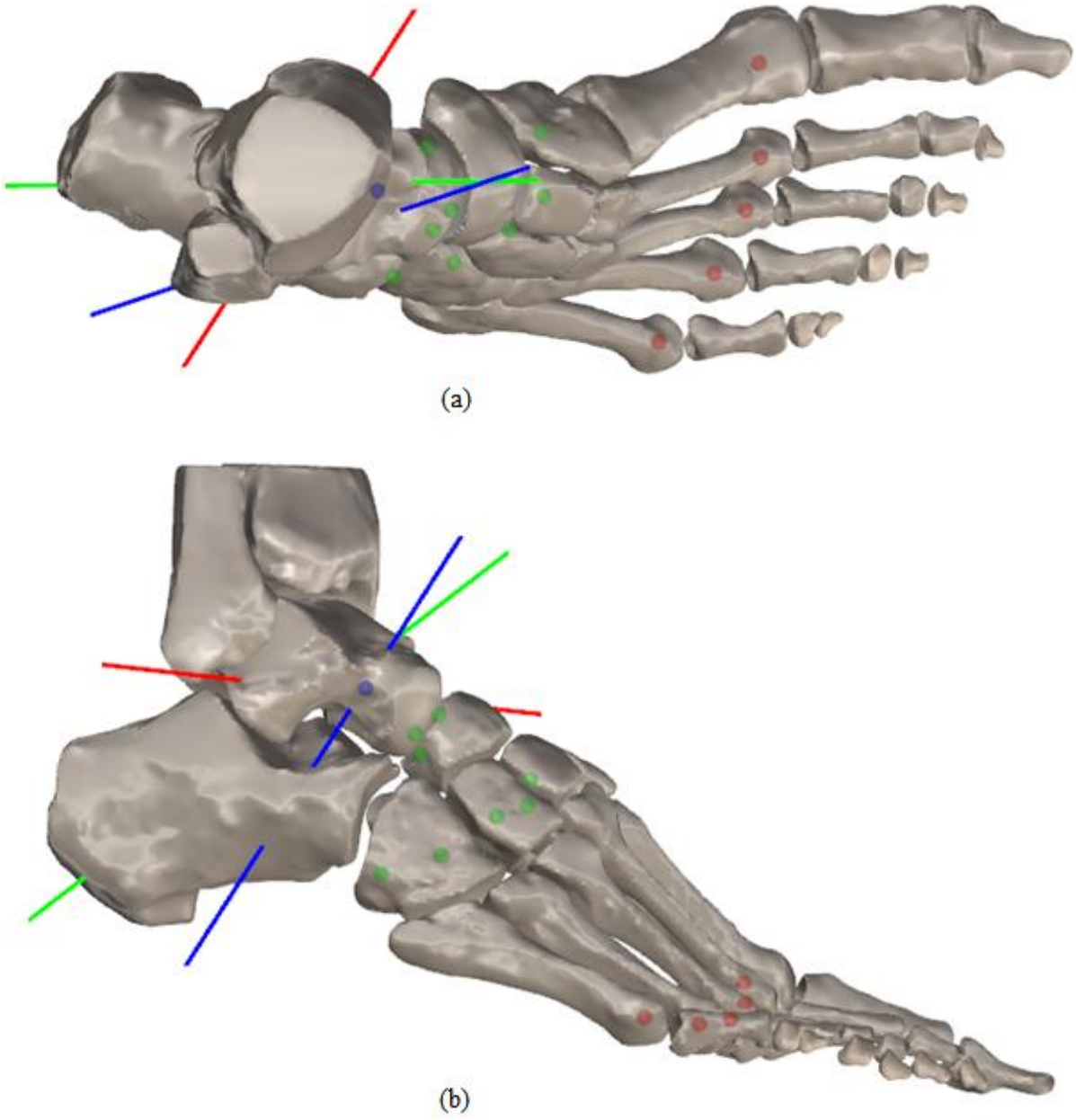

Figure 2.15: Talocrural hinge joint (red), subtalar hinge joint (green), calcaneocuboid hinge joint (blue), tarsonavicular pin joint (blue), intertarsal pin joints (green), and metatarsophalangeal pin joints (red): a) transverse view, b) sagital view

2.2.3 Interactions

Tie constraints were used to join the soft tissue volume and bone surfaces at their interface. Rigid body constraints were imposed on the bone shells with pin constraints used to connect the ligaments and fascia. A surface-to-surface interaction was setup to model friction between the plantar foot surface and the ground model with 0.3 coefficient of friction as suggested by Tadepalli et al. [70].

2.2.4 Loads, Boundary Conditions, and Steps

The forefoot is the lowest part in the model and thus contacts the ground first. Due to friction with the ground, the forefoot should act as an anchor point in the transverse plane while the ankle is free to move in the transverse plane. This was achieved by constraining translations about the X and Y axes for a point on the distal head of the first metatarsal and constraining translations along the X axis for a point on the distal head of the fifth metatarsal. The remaining degrees of freedom of the foot where constrained at the ankle; the tibia, fibula, and skin surface at a plane just above the ankle joint were constrained from translations along the Z axis and rotations about the X and Y axes (Figure 2.16).

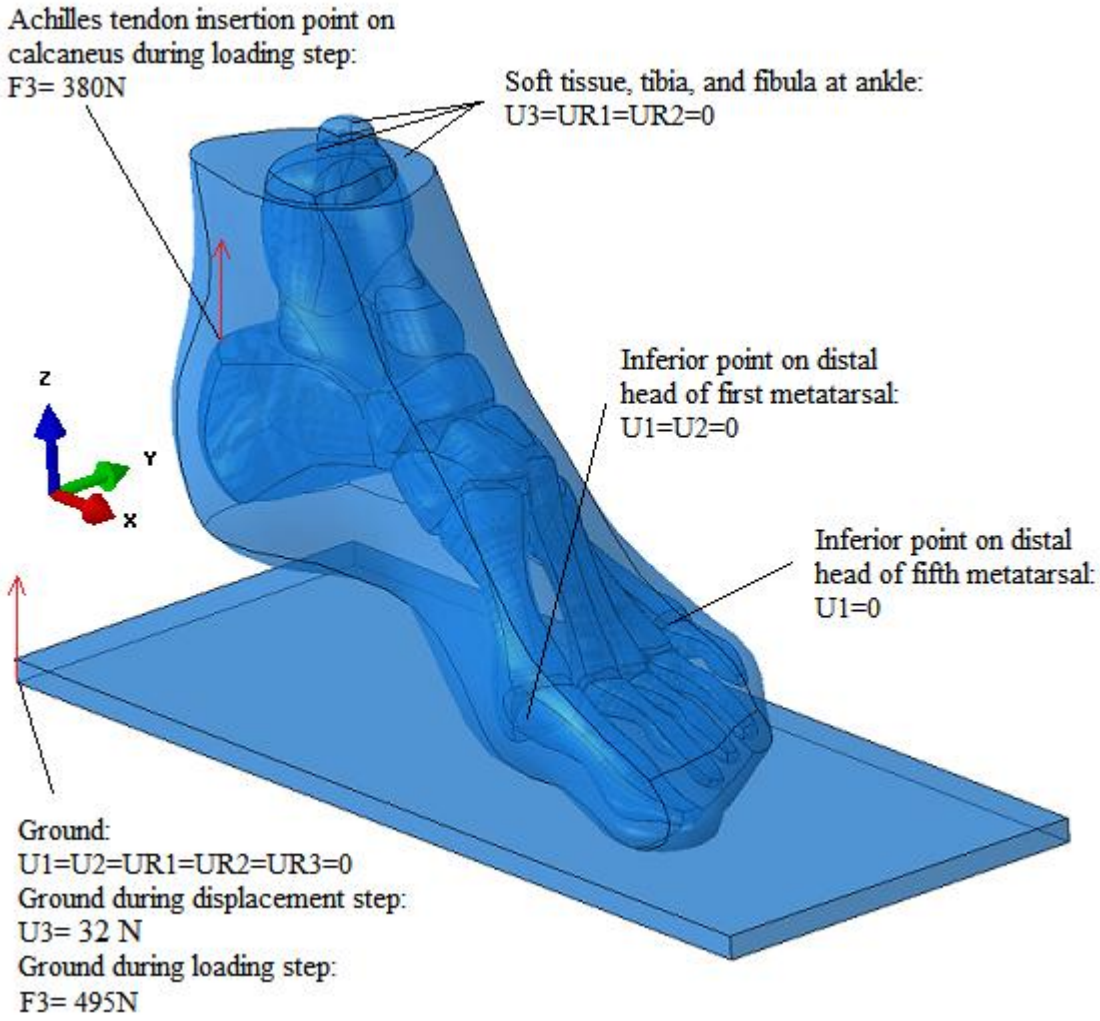

Figure 2.16: Boundary conditions and loads for the contacting and loading steps

The loading process (Figure 2.16) consisted of two general static steps: first the ground was displaced upwards to initiate contact and second a vertical force was applied to the ground (Figure 2.17). During quiet standing, the centre of mass of the body is anterior to the ankle joint. To oppose the resulting moment and achieve stability, muscles (primarily the gastrocnemius and soleus) pull upwards on the calcaneus via the Achilles tendon. As this force increases, the centre of pressure (COP) moves anteriorly. The magnitude of the force acting on the Achilles tendon during quiet standing has been measured to be 50% of the weight acting on the leg [71]. Cheung et al., however, found that 75% was required to match up COP for their model [47]. For the current work, values of 77% and 75% were found to match up COP for the flat ground and FO loading tests.

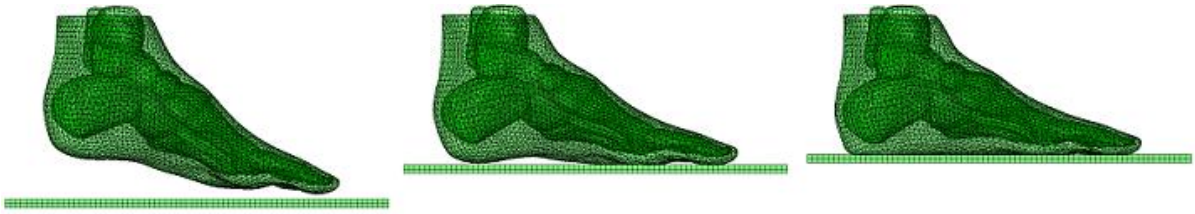

Figure 2.17: The foot model while in the initial, contacted, and loaded positions

Ligaments and fascia models were approximated as tension only trusses and attributed the elastic material models suggested in the literature (Young's moduli of 260MPa and 350MPa) [72, 73] and meshed with 2 node tension only trusses (T3D2). The bone models were approximated as rigid given their minimal deflection and thereby negligible effect on plantar pressure distribution during ordinary weight-bearing conditions. The bone models were meshed with linear quadrilateral shell elements (S4R). The ground model was attributed a high Young's modulus to approximate it as rigid and was meshed with hexahedral elements (C3D8) with a seed spacing of 5.05mm to mimic the cell spacing of the pressure mat used during experimental testing.

The material properties, meshing, and convergence for the soft tissue model required greater consideration than for the other tissue models as slight variations greatly influence plantar pressure distribution. As such the next section is devoted to determining the material properties, meshing, and convergence on just the heel portion of the foot while the section following describes the application of these to the entire foot model.

2.2.5 Patient Specific Soft Tissue Material Properties, Meshing, and Convergence

State of the art methods for acquiring force displacement data of soft tissue involve ultrasound transducers where tissue depth to the calcaneus is measured via ultrasound as the force is applied [56, 74]. Such a sensor was not available for the current work so instead, material testing was done on the plantar soft tissues of the subject using a force displacement sensor (Figure 2.18). The sensor apparatus includes a 1" diameter cylinder that is manually forced against the foot and a tube, essentially a thick wall bushing, that the displacement is measured relative to as it is held against the undeformed tissues of the foot. The experiment was repeated four times on the subject and the results are shown in Figure 2.19.

Figure 2.18: Force Displacement sensor applied to plantar heel soft tissue

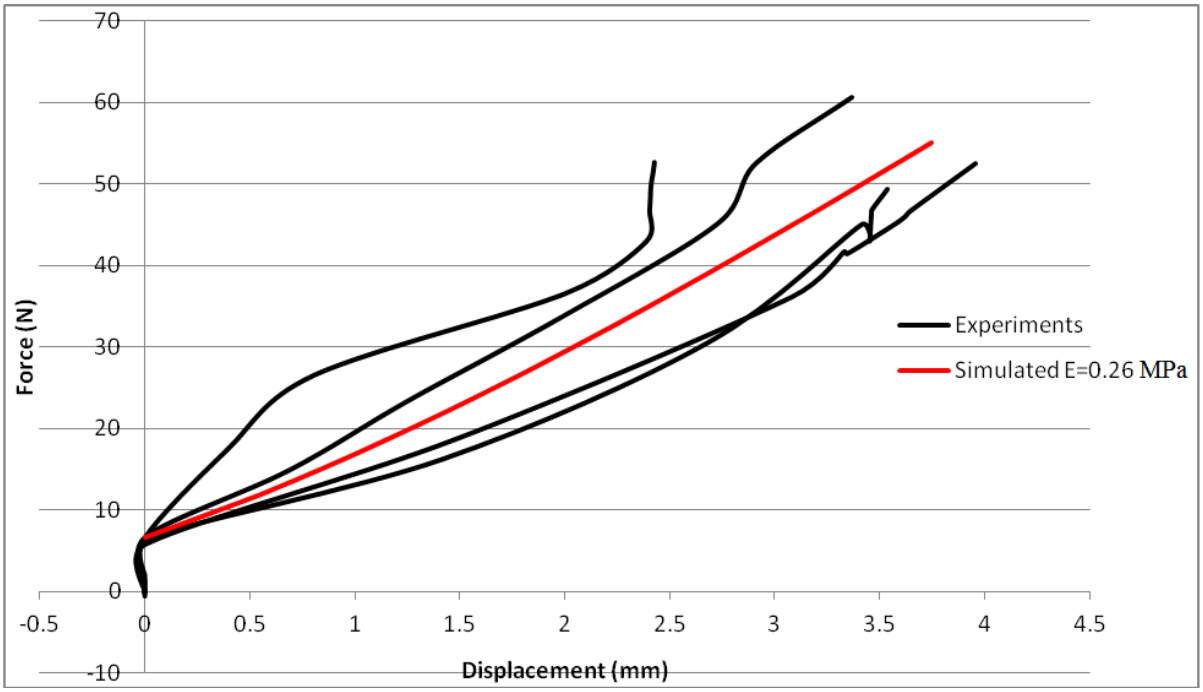

Figure 2.19: Force Displacement data from 4 experiments and the converged simulation

The experiment was replicated in the form of a FE model of the heel area of the foot using Abaqus (Figure 2.20). The 1" cylinder was approximated as an analytical rigid part. To limit the problem of excessive distortion of the soft tissue elements, a 0.5mm radius fillet was added to the cylinder edge.

Contact interaction between the soft tissue and probe was estimated to have a coefficient of friction similar to the foot pressure mat interface for the full foot model (0.3).The calcaneus was fully constrained (Encastre, all 6 degrees of freedom) via its rigid body reference point and the soft tissue was fully constrained at the top surface. The cylinder was restricted in all degrees of freedom except vertically (U3), such that the cylinder could only translate along its central axis to deform the foot's soft tissues. A first step displaced the cylinder 2mm vertically so that it came into full contact with the plantar soft tissues (approximately the same as with the experimental technique). A second step applied a vertical force of 55N (approximately the same as in the experiments) to the cylinder.

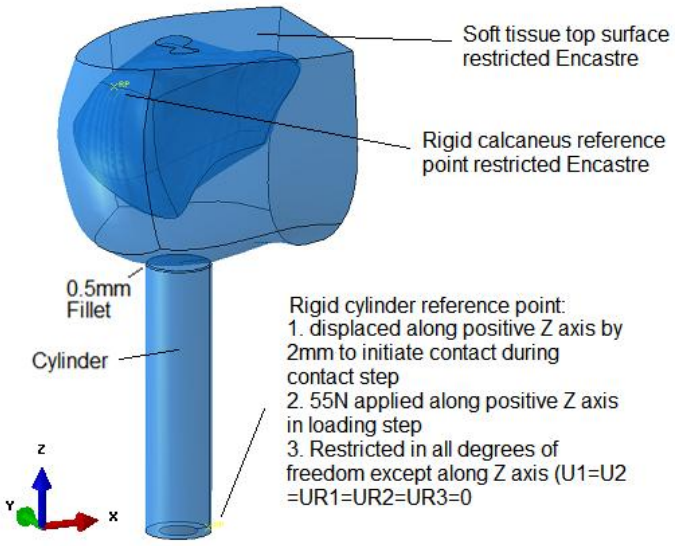

Figure 2.20: Plantar tissue testing simulation setup

The soft tissue was approximated as homogeneous and isotropic as has been deemed a reasonable approximation for the non-pathological foot [74]. Some researchers claim viscoelastic [75, 76] and hyperelastic [42, 55] models best describe the characteristics of plantar soft tissue. However, Tao et al. showed that linear elasticity is a good approximation for up to 35% tissue deformation [61]. For the current project, this claim appears valid as the maximum tissue deformation is 33%. Furthermore, the experimental and simulated force displacement curves have a similar shape throughout the loading step. The demonstrated accuracy and computational benefits make linear elasticity the best choice for the intended applications.

Tadepalli et al. recently published recommendations on element type for FE foot modeling [70]. Linear hexahedral (C3D8), linear tetrahedral (C3D4), and quadratic tetrahedral (C3D10) were

considered. They noted that while linear hexahedral elements afforded the fastest convergence rate and greatest accuracy, they have rightly been avoided for FE foot modeling due to their inability to be automatically meshed for organic geometry such as the soft tissues of the foot. It is for this reason that the majority of researchers have used linear tetrahedral elements for their FE foot models as opposed to linear hexahedral elements. However, Tadepalli et al. have claimed that linear tetrahedral elements yield inaccurate shear stress and pressure predictions due to their inherent problem of rigid shear locking. Quadratic tetrahedral elements were instead recommended.

The disadvantage of quadratic versus linear tetrahedral elements is their greater computational cost, which is of primary concern for the current application. Because of this, linear versus tetrahedral was reconsidered in regards to their pressure distribution predicting ability; the probe model was replaced with a model of the ground and the loading procedure was repeated while looking at plantar pressures. Tadepalli et al.'s findings that plantar pressures for the linear tetrahedral elements were high was confirmed when visualizing the pressure on the elements of the foot's soft tissues. When visualizing the pressures on the ground model, however, the linear and tetrahedral elements yielded similar pressure distributions and peak pressures (given both linear and tetrahedral models were meshed with sufficient density to converge). Furthermore, visualizing the pressure on the ground model is a better representation of the experimental testing of the full foot model as a pressure mat will be used to measure pressure distribution and the mesh seeding was set to match the sensor spacing on the mat (5.05mm). Hence, linear tetrahedral elements were selected for the current work as they predict similar plantar pressure at a lesser computational expense than quadratic tetrahedral elements.

Returning to the probe simulation test, the mesh was refined until a convergence with the linear tetrahedral elements reached a criterion of 2% probe displacement. Young's modulus for the soft tissue was adjusted until the simulation yielded a force displacement curve that was central to the corridor of experimental force displacement curves (Figure 2.19). The process of selecting mesh seed spacing (which controls mesh density) and Young's modulus was iterative as they influence one another. The process arrived at a mesh seed of 1mm and a Young's modulus of 0.26MPA (well within the range of Young's modulus of plantar soft tissues found in the literature by Tao et al. [61]). Such a high mesh density for convergence was due to the sharp edges of the probe causing large localized displacement. Loading the simplified heel model with a flat ground model rather than the probe is

more similar to the intended application and only required a 2mm mesh seeding to reach the 2% displacement convergence criterion. The 2mm seed spacing is better suited to the full foot model.

The above material properties, element types and mesh seeding were applied to the soft tissue of the full foot model. The simulation took 8 hours to solve, far too long for the intended application. While investigating the various model parameters' effects on simulation time, it was noted just how dependent simulation time was on soft tissue mesh seeding. The problem with reducing mesh seeding to take advantage of this relationship is that the mesh becomes excessively stiff. The solution is to correspondingly reduce material stiffness. By simultaneously varying Young's modulus and mesh seeding, an equally stiff model was obtained. The final Young's modulus selected was 0.22MPa and the mesh seeding was 5mm and simulated loading of the foot model onto flat ground took 29 minutes to solve. The final meshed assembly is depicted in Figure 2.21. The mesh consisted of 89,255 elements with an average shape factor of 0.654 (shape factor is obtained by dividing the element volume by that of an optimum element volume). Only 2 elements had a shape factor of less than 0.0001.

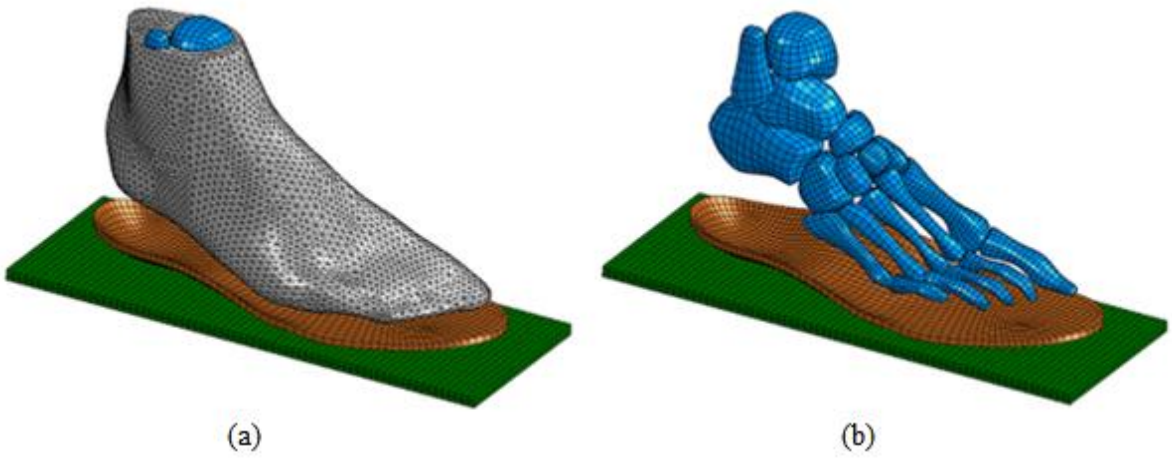

Figure 2.21: Assembly of the meshed parts: a) soft tissue visible, b) soft tissue not visible

2.2.6 Model Simplifications

The following are some adopted simplifications that researchers commonly use:

- Ligaments and fascia were approximated as linearly elastic tension only truss' [31]
- The sesamoids were included as part of the first metatarsal models [57]
- Relative movement of phalanges of each ray was not modeled [55]

- Bones were meshed with rigid quadrilateral shell elements rather than deformable solid elements [70]
- The bone and skin geometries were smoothed during the surfacing process [31]
- The fibula was fixed relative to the tibia [31]
- The soft tissues were approximated as a single homogenous volume [31]

2.2.7 Experimental Setup

To design a FO about the plantar foot surface, a single displacement step pushed the ground up to the foot until the heel just came into contact (this is a simplified method for adjusting foot posture; the method proposed in this dissertation is detailed in chapter 5) (Figure 2.17). The deformed soft tissue geometry was exported and used to design a FO model with the program that will be detailed in chapter 4. FOs are commonly made of, or have a top layer consisting of, a soft material that both absorbs shock and reduces plantar pressures. However, for the current work a stiff material was desired that could be approximated as rigid in the context of supporting the subject's weight so as to eliminate potential errors associated with developing a soft material model and CNC machining the material. Wood was selected. The FO model was meshed with linear hexahedral elements. The model, mesh, and CNC milled surface of the FO are seen in Figure 2.8, Figure 2.21, and Figure 2.22.

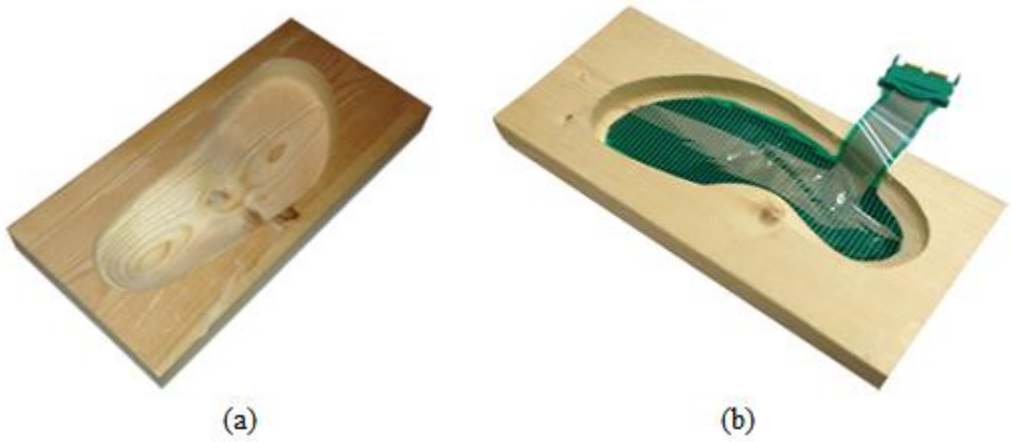

Figure 2.22: a) Machined FO surface, b) F-Scan sensor under trimmed and taped to the FO surface to minimize kinking

A TekScan HR Mat was used to experimentally measure plantar pressure while standing on flat ground and a TekScan F-Scan pressure sensor was used to measure plantar pressure while standing on

the FO. Because of the curvature of the FO's surface, the F-Scan sensor had to be under trimmed and adhered with double sided tape to the FO surface to avoid excessive kinking (Figure 2.22).

2.3 Results and Discussion

Figure 2.23 depicts the simulated and experimental plantar pressures for loading on flat ground and the FO. Average plantar pressure errors between simulated and experimental results were determined by overlapping the results (Figure 2.24). Average plantar pressure error between the experimental and simulated loadings for the flat ground test was 2.2% of peak plantar pressure and for the FO tests was 5.0% of peak plantar pressure. The greater error for the FO loading test was partly due to kinking of the flexible pressure sensor in the arch area as it conformed to the FO shape. Maximum strains occurred in the heel and first metatarsal areas and were 33% and 25%. The flat ground and FO simulations executed in 29 and 32 minutes on an Intel Core i7 CPU @2.67 GHz with 12.0 GB of RAM running Windows 7 64-bit. Peak pressure locations and magnitudes are similar between the simulated and experimental results. Both the simulated and experimental results demonstrate the FO's ability to redistribute load and reduce peak plantar pressures.

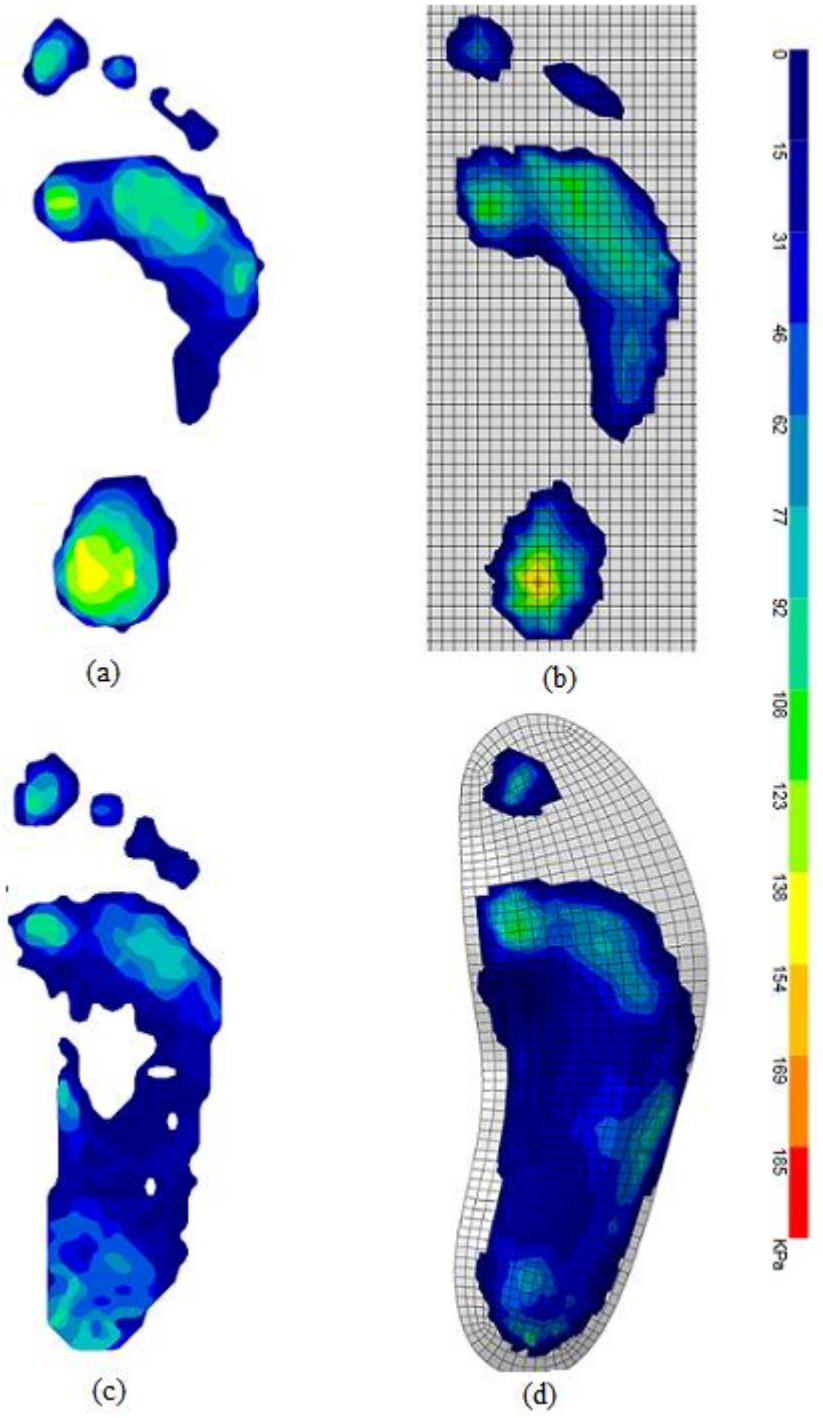

Figure 2.23: Plantar pressure: a) experimental on flat ground, b) simulated on flat ground, c) experimental on the FO, d) simulated on the FO

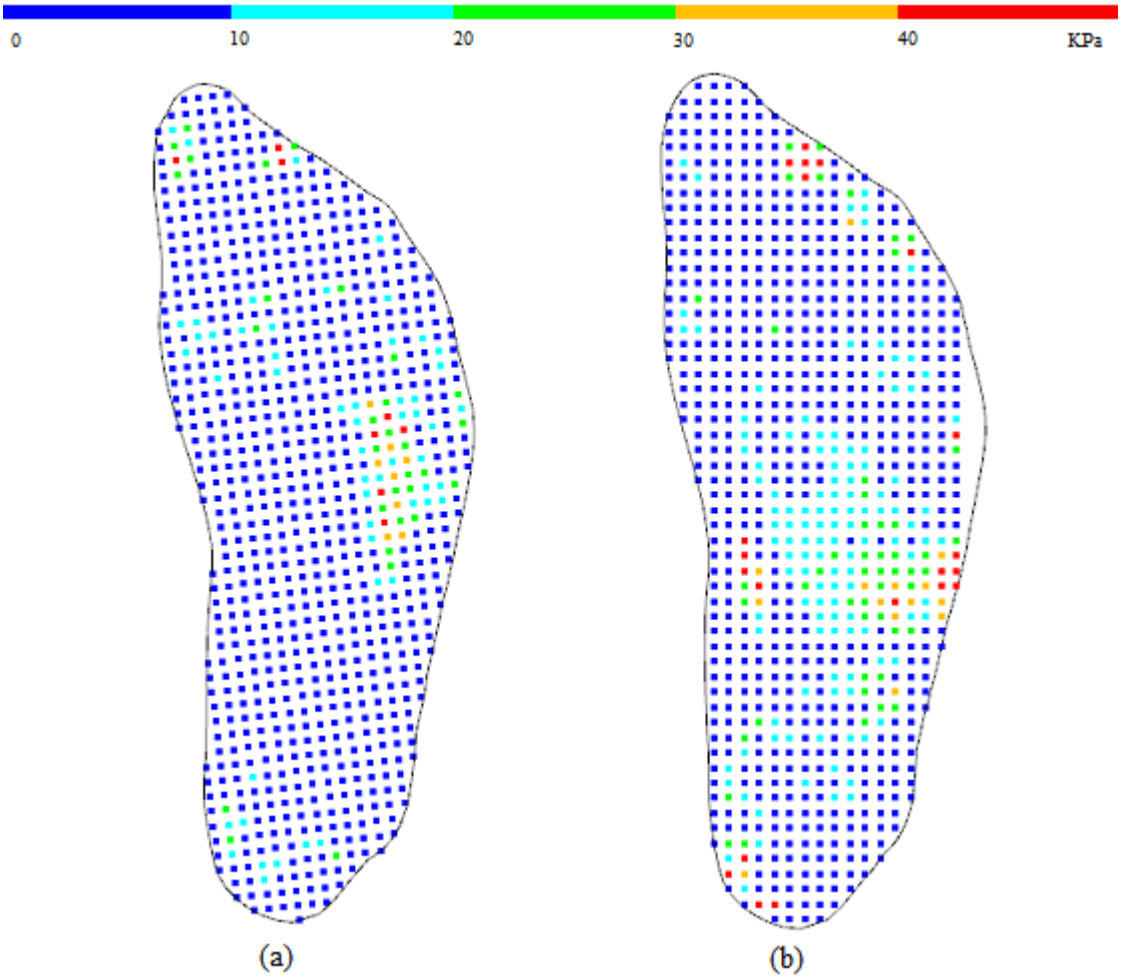

Figure 2.24: Plantar pressure error between experimental and simulated loading: a) on flat ground, b) on the FO

For the current FO, plantar pressures were significantly reduced in the rearfoot while less so in the forefoot. This is a consequence of the FO design method; the ground was pushed into the foot until the heel just came into contact. Thus the soft tissues of the rearfoot were unaltered while the forefoot tissues were compressed. The FO was designed about this geometry, and so reflected the flat forefoot region. Consequently, only minimal plantar pressure reduction in the forefoot resulted. The simulated results accurately predicted the experimental results in this regard.

In addition to using MRI data to develop the model and experimental testing to determine soft tissue stiffness, the following could further enhance patient specificity of the model:

- It was assumed that only the muscles pulling on the Achilles tendon were active as explained by Cheung et al. [31]. However, it is possible that other muscles could have been active during the test. To determine whether this is the case, EMG data should be collected during the pressure mat test for the various muscles likely to be active.
- The models were oriented such that the posterior edge of the fibula was made parallel to the ZY plane and small rotations were made to match up plantar pressure distribution with that of the experimental results. A more accurate method would be to determine the alignment of the lower leg during the experimental plantar pressure test and orient the simulation model similarly. Development of a FE foot model that included the lower leg would allow for this.
- The Achilles tendon was assumed to pull parallel to the Z axis. A better trajectory would perhaps be a line fit to the body of the Achilles tendon, although this was not tested.
- In addition to tuning of the soft tissue stiffness, plantar fascia stiffness could also be tuned. One possible method would be to adjust it until dropping of the arch upon loading matches up with weight-bearing scan data.
- Ligaments and fascia were located manually with guidance from Interactive Foot and Ankle and modeled as tension only trusses. In reality, they are non-homogeneous volumes and interact with the bones in a manner far more complex than a tension only truss can exhibit. Though picking up these geometries in MRI data would be challenging, it should be investigated.

Solution accuracy could be further improved by eliminating some of the simplifications listed in section 2.2.6, though at the cost of increasing solution time above 29 minutes. The biggest change would be to develop a model based on contacting elastic bones rather than the rigid body modeling approach. Models of this nature are described in the literature, although without mention of solution times. Early testing of this method, however, resulted in solution times in excess of 5 hours.

2.4 Summary

In this chapter a FE foot model was developed from MRI data and tuned. The emphasis placed on computational efficiency resulted in a unique design that combined rigid body models of the foot's bones with deformable solid modeling of the soft tissues. The model solved rapidly and accurately predicted plantar pressures on flat ground and a FO. Like other models in the literature, its

development required an order of skilled computer labour that can only be justified for research studies. Given the intention of this dissertation of applying FE foot models on a per patient basis to the FO development process, a more rapid method of developing FE foot models is required. This will be addressed in the next chapter.

Chapter 3
Development of a Patient-Specific Anatomical Foot Model and Finite Element Foot Model from Structured Light Scan Data

A single FE foot model was developed from MRI data in chapter 2. The objective of this dissertation is to incorporate such models into the FO development process. Though the development approach from chapter 2 resulted in an appropriate simulation model, it was expensive and time consuming. In the current chapter, an alternative approach is proposed that removes the need for an MRI and automates the assembly of the FE model.

The proposed approach morphs a generic FE foot model to a surface model and anatomical landmarks acquired from structured light scan data. To determine the geometrical accuracy of the morphing method, the technique was first tested for predicting bone and skin geometry. The process was next tested by morphing the completed FE foot model of chapter 2 to the foot surface geometry and anatomical landmarks acquired from structured light scan data. This chapter resulted in a publication in the journal, "Computer Methods in Biomechanics and Biomedical Engineering" [77].

3.1 Introduction

The development of FE models is expensive and laborious due to the need for MRI or CT scan data, the process of segmenting the data, reconstruction of the anatomical geometry, manual locating of tendons, ligaments, and fascia, and tuning of tissue properties. The reconstruction from MRI is particularly challenging due to the lack of contrast between soft tissues and bone. The CT scan fares better in this regard, though the subject's exposure to radiation leaves this method less desirable. Both methods for developing patient-specific anatomical geometry are time consuming, expensive, and impractical for use on a per-patient basis. Furthermore, assembly all of the components in an FEA program is also laborious.

Structured light foot scanners are a fraction of the cost of MRI and CT scanners to both purchase and operate and are gaining popularity in foot clinics; however, they are limited to digitizing the surface geometry and anatomical landmarks of the foot. This data alone is insufficient for developing the simulation models mentioned above. The proposed solution is to morph a generic anatomical foot

model (developed from MRI or CT) to the surface geometry and anatomical landmarks of a specific foot (obtained from a structured light foot scanner). Upon validating the accuracy of the morphed anatomical geometry, the same algorithm will be used to morph the entire FE foot model developed in chapter 2.

In the work of Sigal et al. [78] and Couteau et al. [79], generic FE meshes were morphed from generic to specific models of the human eye and the human femur. The current work differs in that the surface geometry and landmarks of the anatomy of interest (bones of the foot) are unknown; only the surface geometry and landmarks on the skin of the foot are known. In this regard, the problem tackled by Koikkalainen and Lotjonen [80] is more like the current problem: Detailed anatomical geometry of the human head obtained from MRI scans was morphed to surface geometry obtained from structured light scanning. The current work uses similar methods to Koikkalainen and Lotjonen for creating a 3D model of the human head [80], however the algorithms are derived specifically for developing surface models of foot geometry. As well, the results and discussion pertain specifically to morphing of the human foot. Once morphing of anatomical foot models has been validated, it will then be applied towards developing the entire FE foot model.

3.2 Anatomical Foot Model Morphing

Figure 3.1 depicts the overall anatomical foot model morphing process. The following sections detail the steps. The steps were programmed in the form of a Visual Basic plug-in for Rhinoceros 3D.

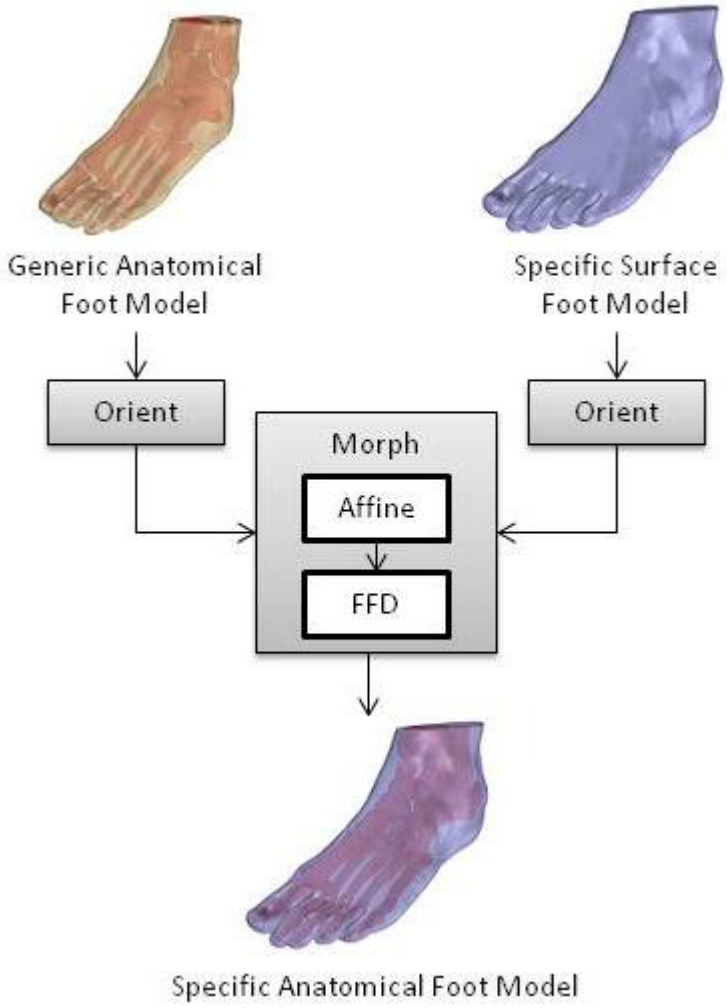

Figure 3.1: Diagram of morphing procedure

3.2.1 Generic and Specific Anatomical Foot Model Development

Three non-pathological feet (A, B, and C) from three subjects were scanned. A and B were scanned with MRI (3.0 Tesla T2 weighted images with fat saturation) and C with CT. Subjects were scanned while supine with their foot in a fixture to restrict movement during the scan. The subjects were positioned such that minimal force was applied to the plantar surface of the foot thereby minimizing compression of the plantar soft tissues. MIMICS was used to segment the scan images and reconstruct the bone and skin 3D geometry. Each model consisted of approximately 35,000 polygons. Figure 3.2 depicts the location of the anatomical landmarks selected (Table 3.1). Simulated palpation

was used to locate the anatomical landmarks on the three foot models; each landmark was located first on the bone and either pulled or projected to the skin surface geometry.

Landmark	Short Form
first ray distal phalange: anterior point	DP1A
second ray distal phalange: anterior point	DP2A
third ray distal phalange: anterior point	DP3A
fourth ray distal phalange: anterior point	DP4A
fifth ray distal phalange: anterior point	DP5A
first ray distal phalange: medial point	DP1M
first metatarsal phalangeal joint: medial point	MPJ1M
second metatarsal phalangeal joint: superior point	MPJ2S
third metatarsal phalangeal joint: superior point	MPJ3S
fourth metatarsal phalangeal joint: superior point	MPJ4S
first metatarsal phalangeal joint: medial point	MPJ5L
fifth metatarsal proximal head: lateral point	MPH5L
navicular: medial point	NM
medial cuneiform: superior point	MCS
medial malleolus: medial point	MMM
lateral malleoolus: lateral point	LML
calcaneal tubercle: superior point	CTS

Table 3.1: Anatomical landmarks and corresponding short forms

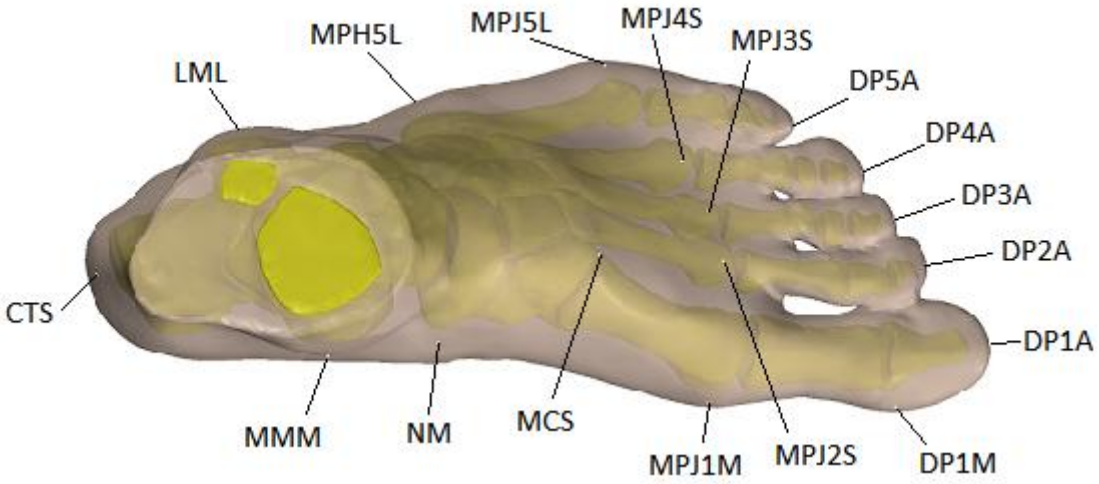

Figure 3.2: Anatomical landmarks

To maximize the number of experiments conducted with the three models, each model in turn served as the generic model as it was morphed to the remaining two models (specific models), thereby yielding six experiments labeled AB, AC, BA, BC, CA, and CB (Table 3.2). The intended application morphs a generic model to surface geometry and landmarks developed from a structured light scan, however, morphing to another anatomically detailed model allows for comparison between the actual bones and the morphed bones. The accuracy of the morph will be evaluated via the following errors:

(1) Skin Landmarks Error (SLE): the average distance between specific skin landmarks and morphed generic skin landmarks

(2) Skin Surface Error (SSE): the average distance between each specific skin mesh vertex and corresponding closest point on the morphed generic skin mesh

(3) Bone Landmarks Error (BLE): the average distance between specific bone landmarks and generic bone landmarks

(4) Bone Surfaces Error (BSE): for each bone, the average distance between each specific bone mesh vertex and corresponding closest point on the morphed generic bone mesh

3.2.2 Orienting and Positioning

All three models were oriented in a Cartesian coordinate system. The models were oriented such that the posterior edge of the fibula was made parallel to the ZY plane, the Achilles tendon was made parallel to the ZX plane, and the line passing from the calcaneal tuberosity at the Achilles tendon attachment through to the most superior palpable point of the second metatarsal phalangeal joint was made parallel to the ZX plane (Figure 3.3). All three models were positioned such that the point corresponding to the calcaneal tuberosity at the Achilles tendon attachment was situated at the origin.

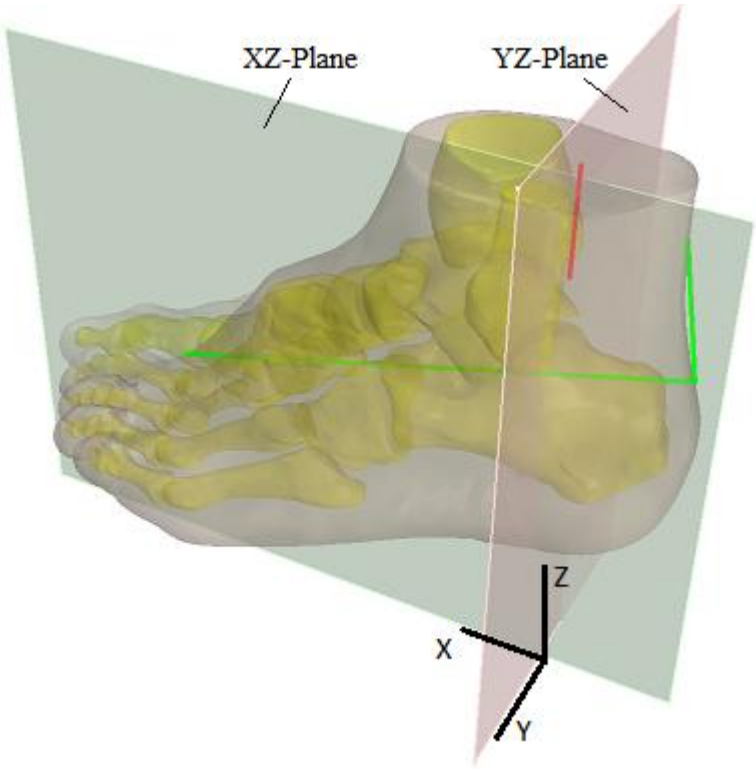

Figure 3.3: Sample model orientation

3.2.3 Morphing The Anatomical Model

To deform not just the surface geometry of the skin, but also the internal anatomy of the foot, it is essential that the deformation method deforms the entire volume within the surfaces. Furthermore, the deformation should be continuous and lack large gradients across the volumes. Free Form Deformation (FFD) is a robust deformation technique that meets these criteria. It will be implemented similarly to the work of Kokkalainen and Lotjonen [80]: morphing consists of applying affine transformations followed by iteratively applying Free Form Deformation (FFD) to adjust the geometry of the generic model to match the geometry of the specific model.

3.2.4 Affine Transformations

Three affine transformations scale the length, width, and height of the generic foot to match that of the specific foot. Width and length are calculated from a bounding box of the entire foot model. Height is calculated as the distance along the Z axis from the lowest point on the heel pad to the average of the medial and lateral malleolus points.

3.2.5 Free Form Deformation

FFD, proposed by Sederberg and Parry in 1986 [81], deforms points or mesh vertices within a deformation region as follows: A point of interest (or mesh vertex) is assigned a unitized coordinate (s,t,u) within the volume of the deformation region (1). A lattice of control points, $P_{i,j,k}$, dictate the deformation (2) (Figure 3.4). After repositioning the lattice control points, the point of interest is transformed with a trivariate tensor product Bernstein polynomial deformation function (3).

$$s = \frac{x - X_{min}}{X_{max} - X_{min}}, t = \frac{y - Y_{min}}{Y_{max} - Y_{min}}, u = \frac{z - Z_{min}}{Z_{max} - Z_{min}} \quad (1)$$

$$P_{i,j,k} = \left(X_{min} + \frac{i}{l}(X_{max} - X_{min}),\ Y_{min} + \frac{j}{m}(Y_{max} - Y_{min}),\ Z_{min} + \frac{k}{n}(Z_{max} - Z_{min})\right) \quad (2)$$

$$X_{ffd} = \sum_{i=0}^{l}\binom{l}{i}(1-s)^{l-i}s^{i}\left[\sum_{j=0}^{m}\binom{m}{j}(1-t)^{m-j}t^{j}\left[\sum_{k=0}^{n}\binom{n}{k}(1-u)^{n-k}u^{k}\right]\right]P_{i,j,k} \quad (3)$$

(X_{min}, Y_{min}, Z_{min}) and (X_{max}, Y_{max}, Z_{max}): corners of the deformation region

s, t, and u: unitized position of a point of interest inside the deformation region

i,j,k: indices of control points in the lattice

$P_{i,j,k}$: position of control point i, j, k

l, m, n: degrees of the FFD function (lattice will have (l+1, m+1, n+1) control points)

X_{ffd}: the deformed point of interest

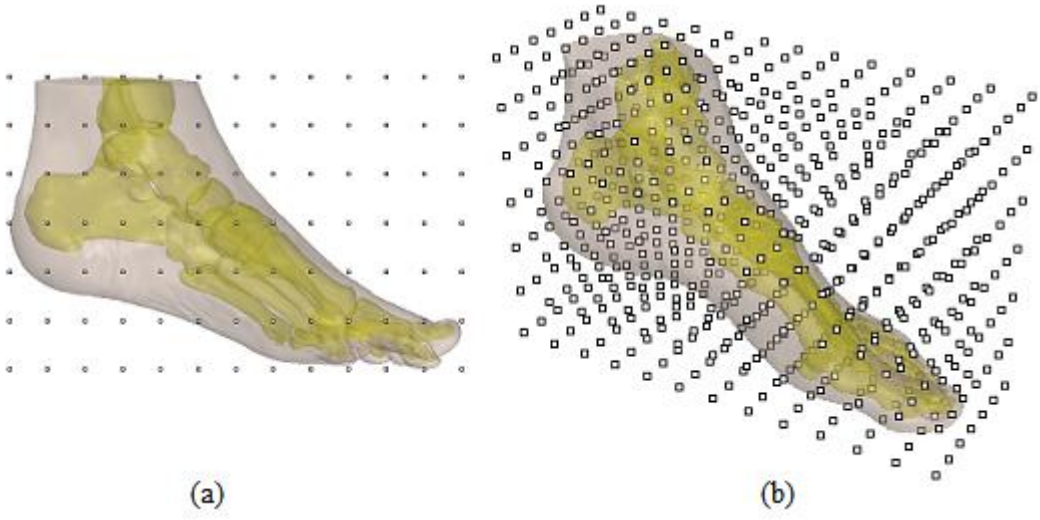

Figure 3.4: An example of a 13,7,7 lattice: a) side view, b) perspective view

3.2.6 Algorithm

The algorithm consists of a sequence of modules. In each module, FFD iteratively adjusts the position of landmarks and mesh vertices of the generic foot. Each module differs by whether it uses landmarks or skin mesh vertices to guide the adjustments, by the density of the FFD lattice used, and the number of iterations to be made. A single iteration consists of the following: for each lattice point a vector between each generic landmark (or each generic skin mesh vertex) and the corresponding specific landmark (or closest vertex on the specific skin mesh) is calculated. The respective lattice control point is translated by the weighted (cubically by distance to the lattice control point) average of the vectors.

Various lattice grid densities were tested. To match the aspect ratio of the foot, more lattice points were used in the X direction than the Y or Z. Ten iterations of FFD guided by landmark locations with a low density FFD lattice (6,4,4) yielded a SLE of 4.01mm and a BLE of 4.52mm. Ten iterations of FFD guided by landmark locations with a high density FFD lattice (13,7,7) yielded a SLE of 2.62mm and a BLE of 4.86mm. Thus, higher density lattices are better at matching up surface landmarks. However, the high density lattice resulted in more localized deformations thereby causing a higher BLE. Instead a low density lattice was used for approximate deformation followed by use of a high density lattice to achieve further refinement. Five iterations of FFD with a low density lattice followed by five iterations of FFD with a high density lattice resulted in smaller error than using strictly high or low density lattices: SLE of 2.53mm and BLE of 3.51mm.

Similarly, FFDs guided by skin landmarks were used first in the algorithm as they achieved more global deformations than FFDs guided by skin mesh vertices. Furthermore, matching up mesh surfaces prior to aligning critical locations such as the metatarsal phalangeal joints would be disadvantageous; FFDs guided by mesh vertices pay no heed to landmark locations and thereby may actually increase SLE. Given it is of critical importance to most simulation techniques to have accurate joint locations, FFDs guided by mesh vertices should be followed by FFDs guided by landmark locations. Finally, fewer iterations should be made with FFDs using higher density lattices due to their higher computational cost.

The proposed algorithm alternates between FFDs guided by landmark location and FFDs guided by mesh vertices as lattice density is gradually increased and iteration count is gradually decreased. After testing various combinations the following sequence of modules was arrived at:

(1) Guidance: Landmarks; FFD Lattice (x,y,z): 6,4,4; Iterations: 15

(2) Guidance: Mesh Vertices; FFD Lattice (x,y,z): 6,4,4; Iterations: 10

(3) Guidance: Landmarks; FFD Lattice (x,y,z): 9,5,5; Iterations: 10

(4) Guidance: Mesh Vertices; FFD Lattice (x,y,z): 9,5,5; Iterations: 3

(5) Guidance: Landmarks; FFD Lattice (x,y,z): 13,7,7; Iterations: 6

(6) Guidance: Mesh Vertices; FFD Lattice (x,y,z): 13,7,7; Iterations: 3

(7) Guidance: Landmarks; FFD Lattice (x,y,z): 13,7,7; Iterations: 3

3.3 Anatomical Morphing Results and Discussion

Refer to Table 3.2 for the errors of the six experiments. Complete models of the morphed generic feet and the specific feet were overlaid (Figure 3.5). Topology deviation maps were prepared (Figure 3.6 - Figure 3.9) and certain bones were isolated for detection of orientation problems (Figure 3.10). The six experiments yielded average SLE, BLE, SSE, and BSE of 1.55mm, 3.14mm, 1.77mm, and 2.53mm. The experiments took on average 2 minutes and 17 seconds to execute on an Intel Core i7 CPU @2.67 GHz with 12.0 GB of RAM running Windows 7 64-bit.

Experiment							
	AB	AC	BA	BC	CA	CB	average
SLE (mm)	1.39	2.06	1.37	1.44	1.54	1.48	1.55
BLE (mm)	2.90	2.89	2.64	3.35	3.16	3.90	3.14
SSE (mm)	1.80	1.58	1.97	1.78	1.61	1.85	1.77
BSE (mm)	2.62	1.78	2.72	3.05	1.84	3.17	2.53

Table 3.2: Skin Landmark Error (SLE), Bone Landmark Error (BLE), Skin Surface Error (SSE), Bone Surface Error (BSE), and average errors for the six experiments

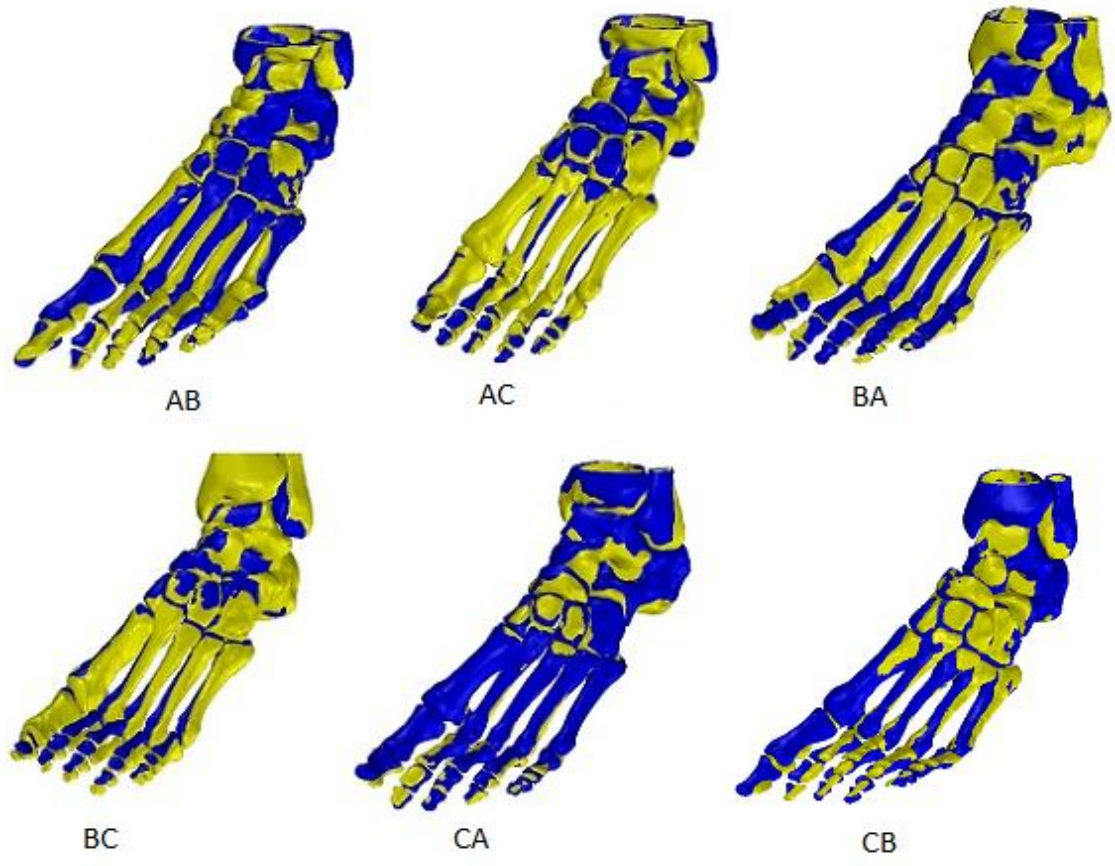

Figure 3.5: Original bones (blue) overlaid with morphed bones (yellow) for six experiments

The skin and bone topology divergence maps for experiment AC were typical of all experiments in that they show the morphing was most accurate in the mid-foot region and less accurate in the fore-foot and rear-foot regions (Figure 3.6). The lowest BSE was achieved for the fifth metatarsal for

experiment AC (just under 1mm, Figure 3.7). This is a consequence of the fifth metatarsal having two landmarks to guide the morphing algorithm and not being overly crowded by other landmarks to influence the morphing. Though the remaining four metatarsals, three cuneiforms, navicular, and cuboid had only one or no landmarks at all, they also performed well due to neither overly crowded nor overly sparse landmark spacing. Higher BSE was found in the rear-foot due to sparse landmark spacing and in the fore-foot due to overly crowded landmark spacing.

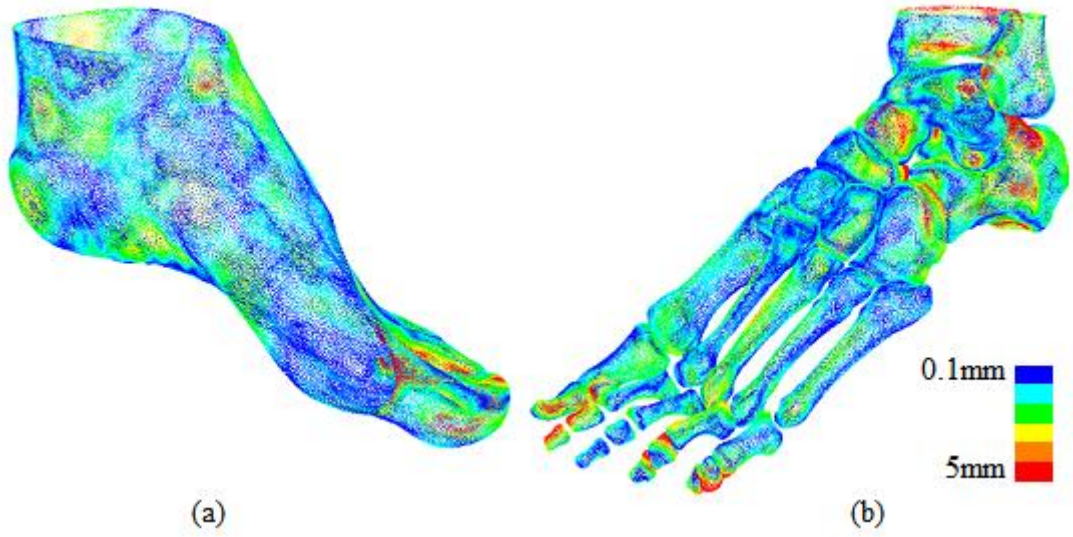

Figure 3.6: Topology deviation maps between generic and specific models for experiment AC (colour scale in mm): a) skin models, b) bone models

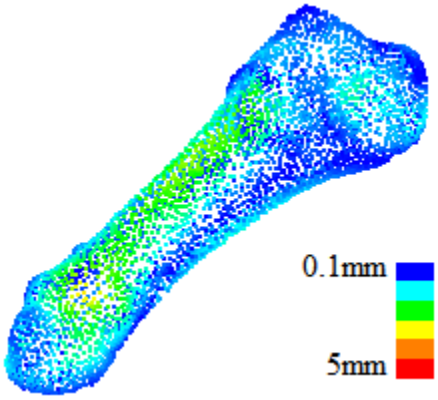

Figure 3.7: Topology deviation map between generic and specific fifth metatarsal models for experiment AC

BSE in the rear-foot could be decreased by increasing landmark count. However, besides the malleoluses and calcaneal tubercle, there are no other bony prominences that could be palpated with accurate repeatability. Consequently, BSE on the inferior surface of the calcaneus was relatively high, particularly for experiment AB (Figure 3.8). The talus and fibula results suffered similarly (Figure 3.8 and Figure 3.9).

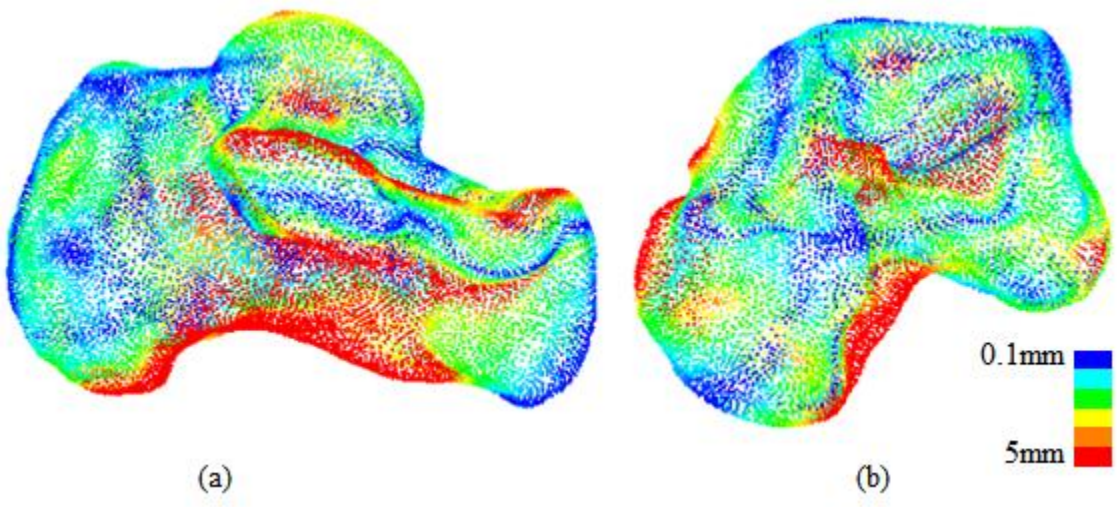

Figure 3.8: Topology deviation maps between generic and specific models for experiment AB: a) calcaneus models, b) talus models

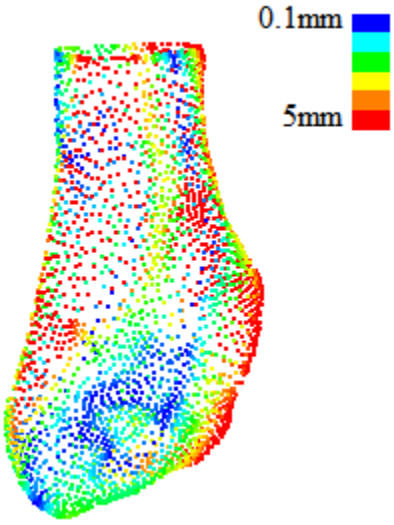

Figure 3.9: Topology deviation map between generic and specific fibula models for experiment AB

More bones are found in the fore-foot than the rear-foot and mid-foot combined and all are smaller. Furthermore, geometry and orientation of bones in the fore-foot are more variable than their mid- and rear-foot counterparts. Using landmarks on the metatarsals and ends of the toes is sufficient to accurately guide the morphing procedure for most cases. However, the accuracy of the intermediate phalanges can be compromised by a lack of local morphing guidance (Figure 3.10). Applications requiring consistently high accuracy of the intermediate phalanges should use additional landmarks and additional steps with finer lattice spacing.

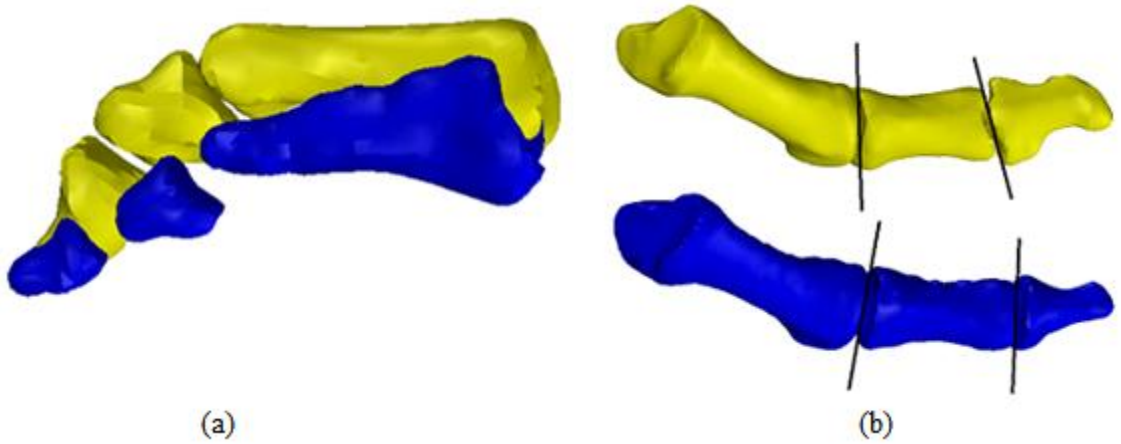

Figure 3.10: a) an example of poor intermediate phalange accuracy due to the lack of a local landmark, b) morphing the exceptionally long first toe of subject B resulted in shearing of the toe joints axes

A study on digit ratios reported the average ratio of first toe length to second toe length to be 1.28 with a standard error of the mean of 0.03 [82]. Subjects A and C were close to this ratio (1.37 and 1.24) while subject B had an abnormally high ratio (1.60). Consequently, morphing subjects A and C to subject B resulted in a large deformation gradient between the first and second toe. As a result, the articulating axes of the morphed first toe appeared sheared when compared to the actual first toe articulating axes (Figure 3.10). It is predicted that similar problems would arise when morphing to feet with irregularities such as bunions and hammertoes. Such problems could be avoided by morphing generic foot models that exhibit similar irregularities as the specific foot. Extending this, morphing the anatomy of a healthy foot to a foot with a collapsed arch may detract from the realism of simulations. Instead, the anatomy of a foot with a collapsed arch should be morphed to the patient's foot. The same is recommended for patients exhibiting pathologies such as hallux rigidus, excessive pronation or supination, and plantar fasciitis. A comprehensive library of foot models with known irregularities and pathologies should be developed and the most appropriate model should be deployed when generating a patient-specific foot model with the proposed morphing procedure.

Ligaments, tendons, and fascia were neglected in the current work as sufficient landmarks were already in use to evaluate the morphing procedure. For future work, their inclusion in the morphing procedure is done by adding the attachment sites to the array of points to be morphed.

The 3D coordinates of the landmarks were determined by manually selecting what appeared to be the center of the landmarks in the scanned model. Doing this twice successively yielded an average variability of 0.92mm. Users of the methods employing manual palpation should be able to achieve comparable variability; Telfer et al. [83] were able to achieve an average variability of 1.5mm using manual palpation and 1.1mm with a palpation tool they developed. In the current work, virtual landmark palpation variability was highest for the medial and lateral malleolus landmarks due to the high radius of curvature of the palpable bony prominences. Consequently, the BLEs for the tibia and fibula were high. In general, a future study of all landmark possibilities, their exact definitions, and variability should be undergone. The study should be based on physical rather than virtual palpation as was used in the current work

In search of ways to increase accuracy, experiment AB was repeated with eight additional steps reaching a final FFD lattice density of 64,29,29. Computation time increased to 3 hours and 27 minutes (from 2 minutes and 17 seconds) while accuracy only improved slightly to SLE:1.17mm, BLE:2.65mm, SSE:1.57mm, BSE:2.23mm (from SLE:1.39mm, BLE:2.90mm, SSE:1.80mm, BSE:2.62mm). Depending on the application, this increase in accuracy may be justified despite the disproportionate increase in execution time.

3.4 FE Foot Model Morphing

The methods presented above yield the patient-specific surface geometry of the bones and skin of the foot. Development of other patient-specific anatomy such as the ligaments and plantar fascia is only a matter of including the geometry in the morphing procedure. This can be done by including all of the nodes in the input file of the generic FE foot model developed in chapter 2 in the morphing procedure.

3.4.1 FE Model Morphing Methods

The proposed procedure was tested for three non-pathological feet. For each subject, landmarks were palpated and marked on their right foot. In addition to the landmarks listed in Table 3.1, two more landmarks were used. The first additional landmark was the lateral most point on the proximal head of the fibula. This landmark was included to assist in orienting the foot in the design session. The second additional landmark was a point on the anterior lateral aspect of the trochlear facet of the talus which is most readily palpated while the foot is plantar flexed . This landmark was included to increase the landmark density in a previously sparse region thereby improving morphing accuracy.

The foot was scanned with an Artec handheld scanner as the patient was prone and the foot was fully non-weight-bearing (Figure 3.11).

Figure 3.11: Prone, non-weight-bearing position during scanning foot with landmarks

Next, the foot was oriented in the design session by aligning a vector passing through the lateral maleolus landmark and the proximal fibula head landmark parallel to the Z axis. The FE model nodes were then morphed to the surface and anatomical landmarks and a script swapped the original nodes in the FE model input file with the morphed nodes.

The input file was opened with Abaqus. The subject's plantar pressure distribution was measured with the HR mat. The load applied by the ground to the foot was set to match the load applied to the HR mat by the foot. The load acting on the calcaneus via the Achilles tendon was adjusted until the centre of pressure predicted by the FE model simulation matched up with that of the pressure mat reading. The loads for the three subjects are listed in (Table 3.3). Small rotations about the X axis were made to better match up the pressure distributions.

	Ground Load (N)	Achilles Tendon Load (N)	Ratio
Subject 1	382	220	0.58
Subject 2	438	295	0.67
Subject 3	440	200	0.45

Table 3.3: Loads and ratio of loads for the three subjects

During early testing, excessive element distortion caused the simulations to fail. The problem was likely caused by the morphing algorithm excessively distorting the elements before the simulation even began. The problem was partly solved by turning off the "adjust slave surface initial position" setting in the soft tissue to bone tie constraint. Removing this was beneficial as the node adjustments required to match up the soft tissue and bone surfaces caused initial mesh distortion thereby exacerbating the problem. However, the downside was that the resulting displacement discontinuity at

the bone skin interface slowed the simulations down by as much as a factor of four. Despite this setting adjustment, the morphed models would only solve with higher soft tissue Young's modulus. Attempts with other techniques such as adaptive meshing (actual incremental remeshing was unavailable for the orphan meshes resulting from the morphing method) and artificial stiffening were tried without success. The simulations were compared to experimental pressure mat data and the results are below.

3.4.2 FE Model Morphing Results and Discussion

Subject 1 required a soft tissue Young's modulus of 0.3 to solve (Figure 3.12). This results in much higher peak plantar pressures than that measured by the HR pressure mat. However, the relative pressure distribution is similar; average plantar pressure error between a scaled and simulated pressure distributions was 2.2% of peak plantar pressure (Figure 3.12). The simulation results for subjects 2 and 3 were also scaled, resulting in average plantar pressure errors of 4.7% (Figure 3.13) and 2.8% (Figure 3.14). The plantar pressure errors between the experimental and simulated tests are shown in Figure 3.15. These results are exceptional given the average of the three (3.2%) is only slightly higher than the master FE foot model achieved (2.2%) despite its advantage of being developed about anatomical geometry acquired directly from an MRI scan. The same recommendations for increasing patient specificity and improving accuracy of the generic model are applicable to the morphed model.

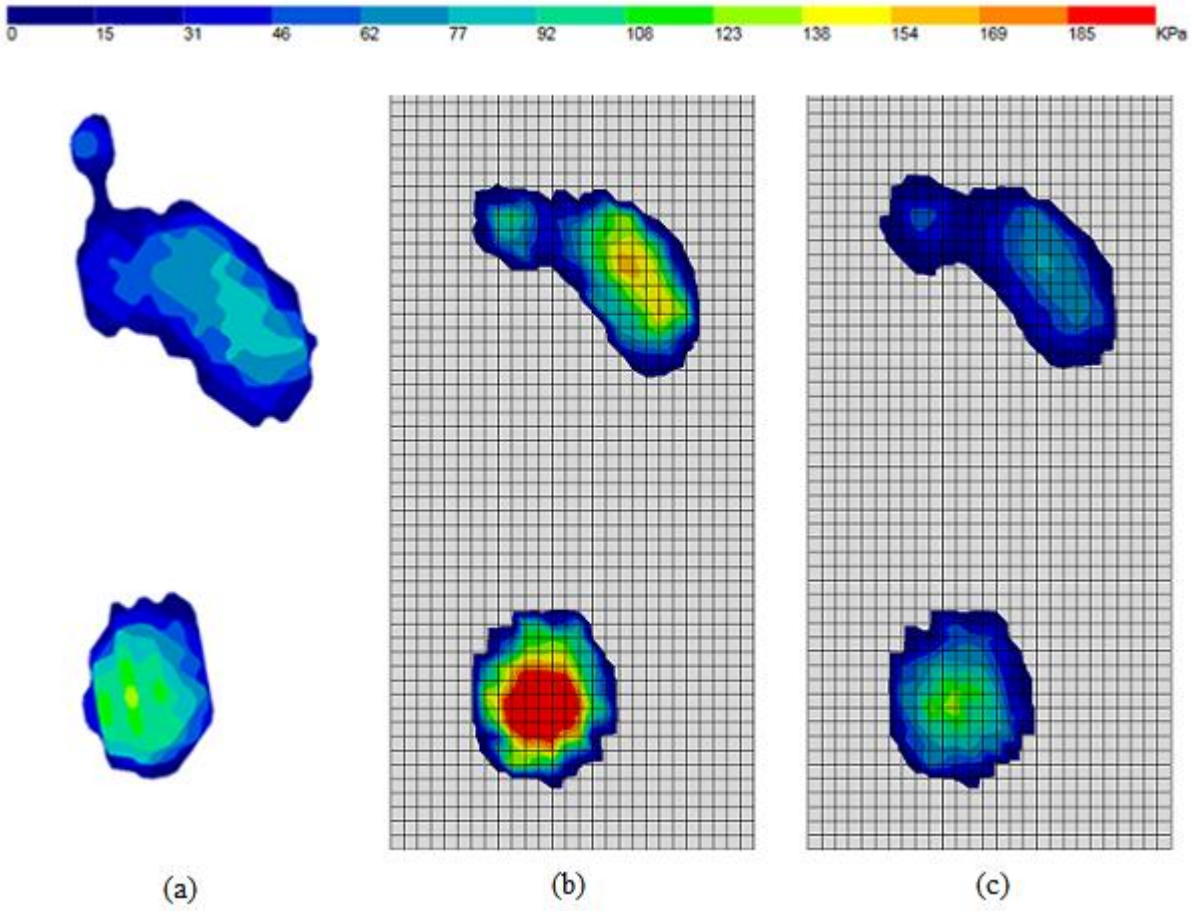

Figure 3.12: Plantar pressure for subject 1: a) experimental, b) simulated, c) simulated (after scaling)

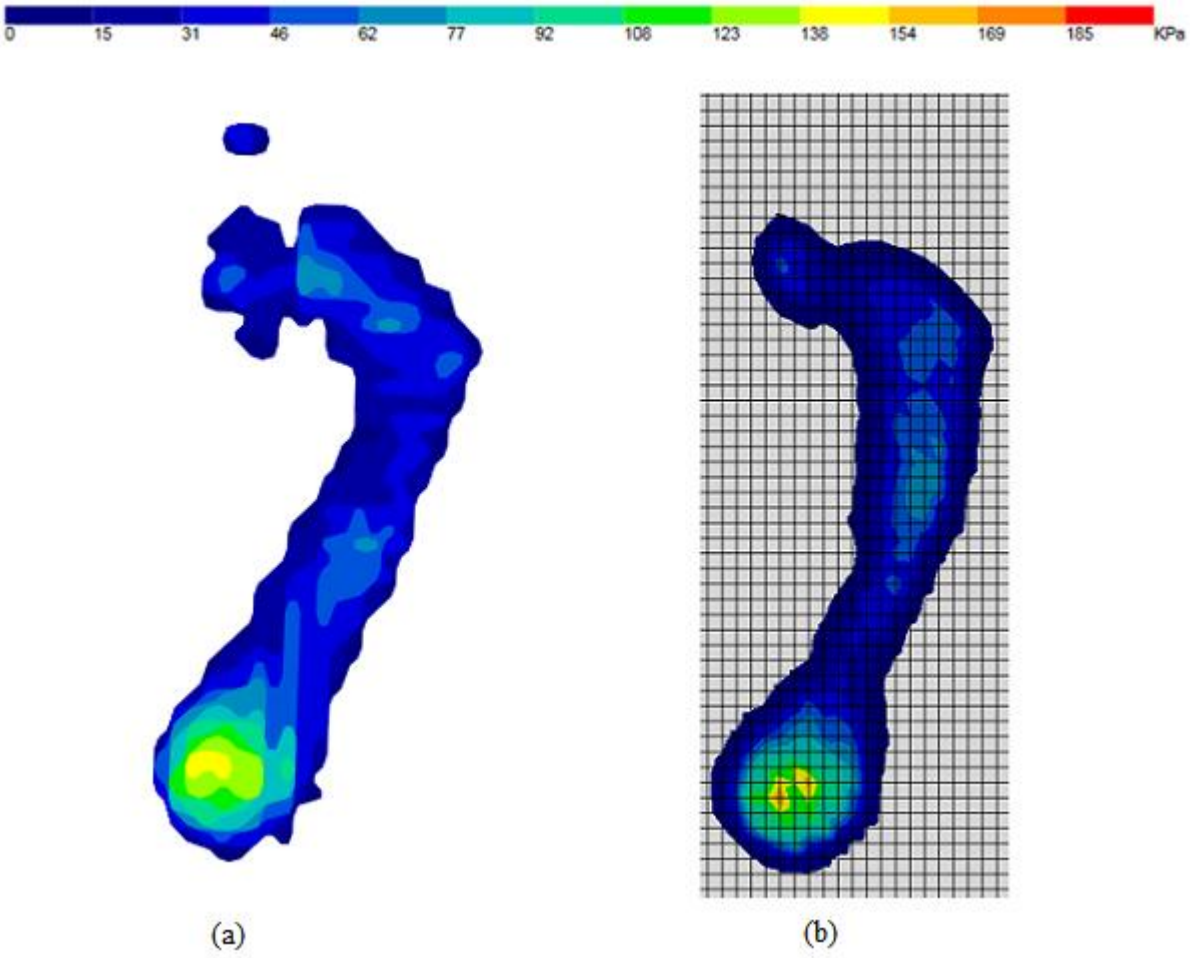

Figure 3.13: Plantar pressure for subject 2: a) experimental, b) simulated (after scaling)

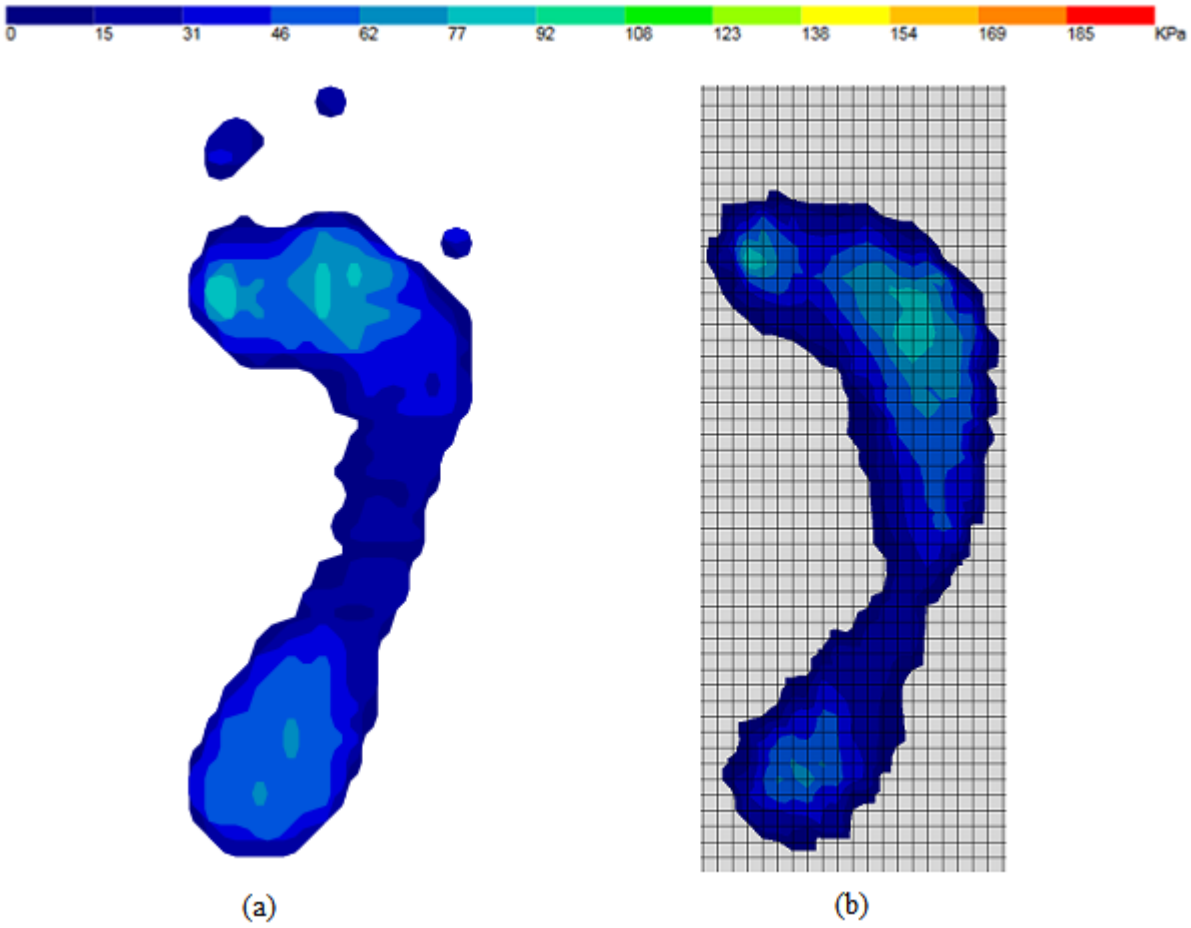

Figure 3.14: Plantar pressure for subject 3: a) experimental, b) simulated (after scaling)

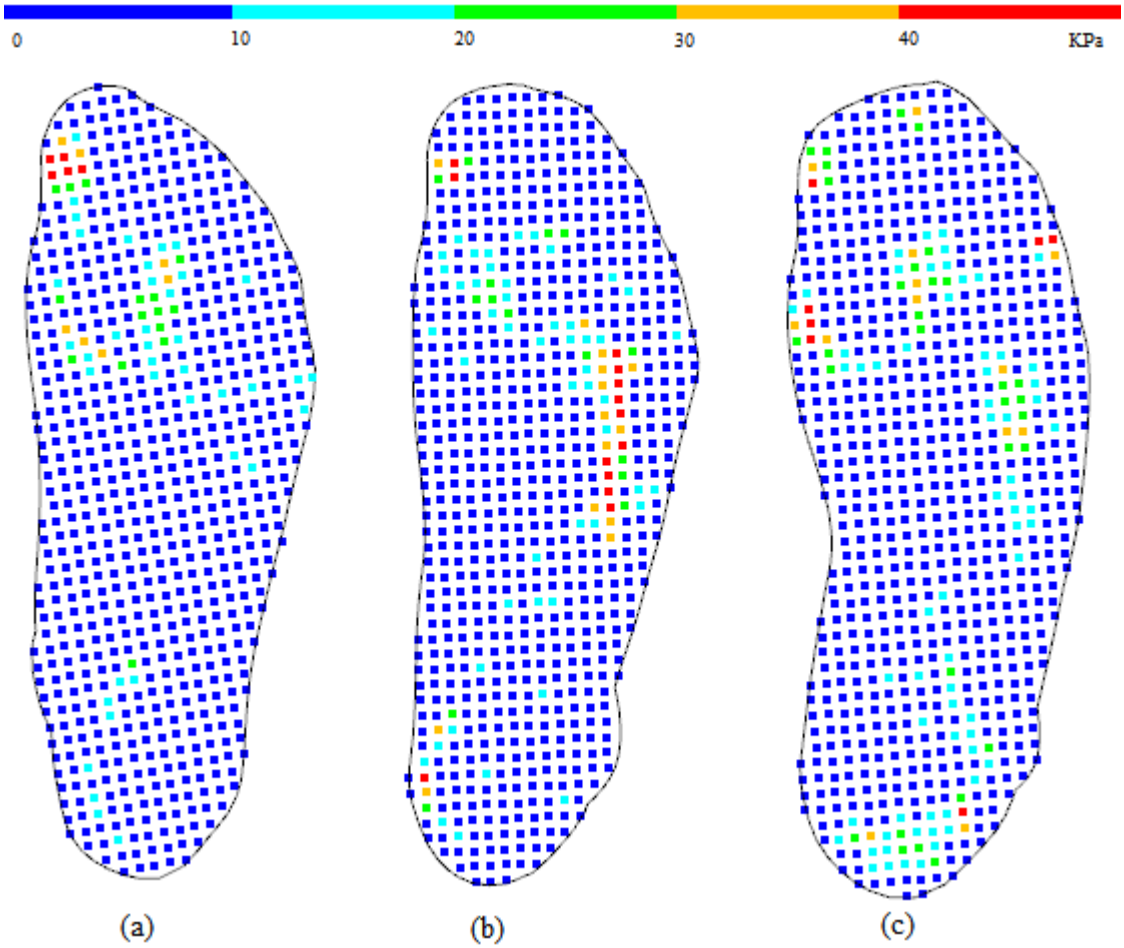

Figure 3.15: Plantar pressure error between experimental and simulated for: a) subject 1, b) subject 2, c) subject 3

In addition to accuracy, speed is the other criteria for determining the usefulness of the method. Unfortunately, the simulation times averaged approximately 80 minutes (nearly three times as long as the master FE model). The relatively longer simulation times were primarily due to the settings adjustments required for the model to solve a mesh already partially distorted by the FE procedure.

This problem could be avoided by meshing the models after morphing takes place or by remeshing at each increment. The drawback of this is the extra computing required for meshing. Furthermore, Abaqus is unable to mesh polygon models (it requires analytical geometry); an additional program or script would need to be introduced to perform this meshing.

Another promising approach that could at least partially address the excessive distortion problem is to combine the soft tissue and bones as a single part and seamless mesh (Figure 3.16). This results in a more regular mesh that can undergo greater deformation before excessive distortion becomes a problem. The method was first attempted with a partial foot model and proved to be more computationally efficient. However, difficulties were encountered in implementing the method for an entire foot model with ligament, fascia, and joint connections. With further development time, this would be the first step in solving the excessive distortion problem of morphed models. In addition to this, the locations and manner in which the morphing algorithms distort the meshes should be studied and possible adjustments to the morphing algorithm considered. Possible alterations to the morphing approach include substituting the bezier functions with b-splines or hierarchical b-splines to achieve more localized deformation.

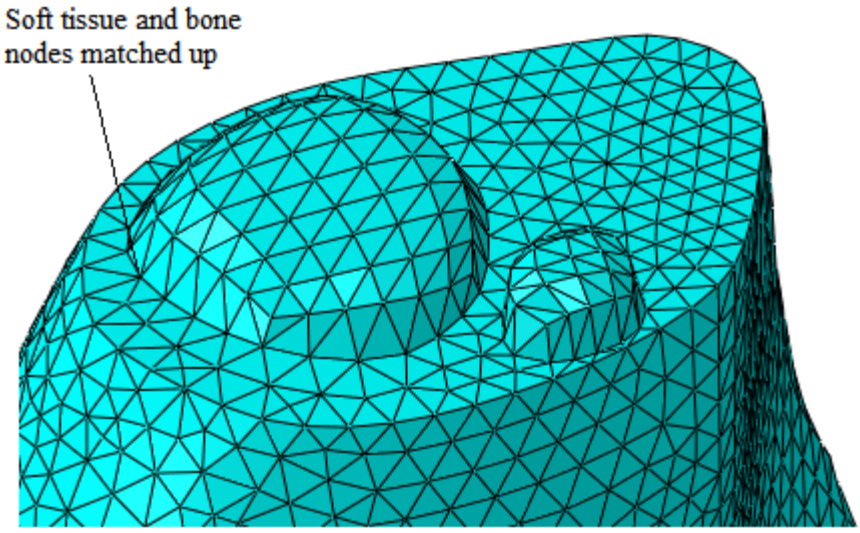

Figure 3.16: Mesh of a single part foot model

3.5 Summary

The proposed morphing approach for rapidly and inexpensively developing FE foot models to be incorporated in the FO development process has been described in this chapter. The approach was first validated for its ability to predict anatomical geometry. Second, the approach was tested for developing complete FE foot models. Future work was recommended for addressing difficulties encountered with element distortion.

Chapter 5 will demonstrate the incorporation of simulation models into the FO development process. Prior to that, however, additional tools are required to provide a comprehensive FO development procedure. In particular, methods for designing and fabricating FOs are required. These will be described in the next chapter.

Chapter 4
FO Design and Fabrication

Thus far, methods for rapidly developing simulation models have been covered. Prior to an explanation on how to incorporate these models into the overall FO development process, a modern digital method for designing and fabricating a FO must be obtained. A variety of tools exist commercially, however the literature on the topic is lacking. Furthermore, some improvements are apparent that would make these tools a better match for the overall goal of reducing subjective input in the FO development process. In this chapter, tools and methods for designing and fabricating a FO are developed. The FO design portion of this chapter resulted in a publication in the journal, "Computer Aided Design and Applications" [84].

4.1 Introduction

To review, the proposed method of developing a FO can be broken down into the seven steps below (see chapter 1 for a full description of the steps). The current chapter pertains to steps 4 and 6.

(1) Patient assessing

(2) Foot geometry recording

(3) Postural adjustment simulating

(4) FO geometry developing

(5) FO design validating

(6) FO fabricating

(7) *FO fitting and adjusting*

The geometry of a FO closely resembles that of the plantar surface of the foot. Any deviation between the FO and foot geometry is intentionally developed to influence the FO's ability to control posture and pressure distribution. However, for the current purposes, all postural adjustments will have already been achieved in the *postural adjustment simulating* step. Traditional methods control the deviation for pressure adjustment through the addition and subtraction of plaster. The problem

with these techniques is that they are more subjective than scientific. Consequently, accuracy and precision are difficult to achieve. Though modern methods are also capable of producing this deviation, the methods are not clear nor documented in the literature. Trinidad stated, "The replication of [custom foot orthosis] geometry using CAD tools is time consuming and almost impossible to accurately represent" [22], and proposed that any digital FO model be acquired through scanning of a manually fabricated FO . Furthermore, it is often implied that there is no deviation, that the FO geometry is simply a duplicate of the foot's plantar surface geometry [26, 85].

The proposed method is to design the FO digitally and use parameters to determine where and by how much the FO geometry differs from that of the foot. In this chapter, the development of this method of FO design will be explained. To complement this technique, a fabrication method will be described that similarly reduces the subjective input required by the operator.

4.2 Proposed System

The detailed description of the proposed FO design method will start with the assumption that a digital representation of a foot's surface has been acquired and the foot's posture has already been adjusted with the simulation model (the full process including adjusting the foot's posture will be described in the next chapter). The digital representation of the foot's surface is simply a mesh made up of vertices and normals (Figure 4.1). With this scope, the first step in the process is to obtain the anatomical landmarks of the foot. A Visual Basic plug-in for Rhinoceros 3D for designing a FO was developed based on the following sections.

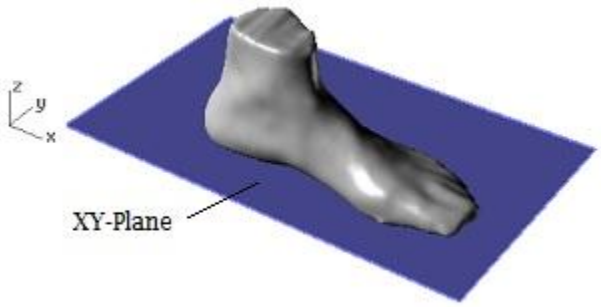

Figure 4.1: A 3D model of a foot composed of approximately 8000 vertices and 16000 triangles. The XY plane represents the ground plane

4.2.1 Manual Anatomical Landmark Selection

In chapter three, 19 landmarks were used for the morphing procedure (Figure 3.2). The landmarks were located by palpation and application of markers prior to scanning. Each landmark was visible on the resulting foot model. Though this method of landmarking is more accurate, the simpler method of locating the landmarks on the digital model has the advantage of reducing the time expenditure of the individual operating the scanner. Though either method is possible with the proposed system, the latter method is described here.

Physiologically, one human foot form is similar to the next. This would suggest that landmarks could be automatically detected on the foot mesh with relative ease. However, the geometry of various tissues may vary dramatically from one foot to the next making automatic landmark detection challenging (Figure 4.2 (a)). Thus the current system uses manual landmark selection as it only takes a few seconds and does not significantly detract from overall automation. The four key landmarks that are required for the FO design process are as follows:

- MPJ1Medial - the most medially prominent point of the first metatarsophalangeal joint
- MPJ5Lateral - the most laterally prominent point of the fifth metatarsophalangeal joint
- HalluxAnterior - the most distal point on the first ray
- MPJ2Inferior - the most inferior point of the second metatarsophalangeal joint

To get these points, the user is provided with a bottom view of the foot and is asked to click on the various landmarks. The first three selections are constrained to the outside edge of the foot projected onto the XY plane (Figure 4.1) while MPJ2Inferior is provided no constraints (Figure 4.2 (b)). Afterwards, the 3D version of the points can be obtained by projecting a ray vertically and finding the intersection with the foot mesh.

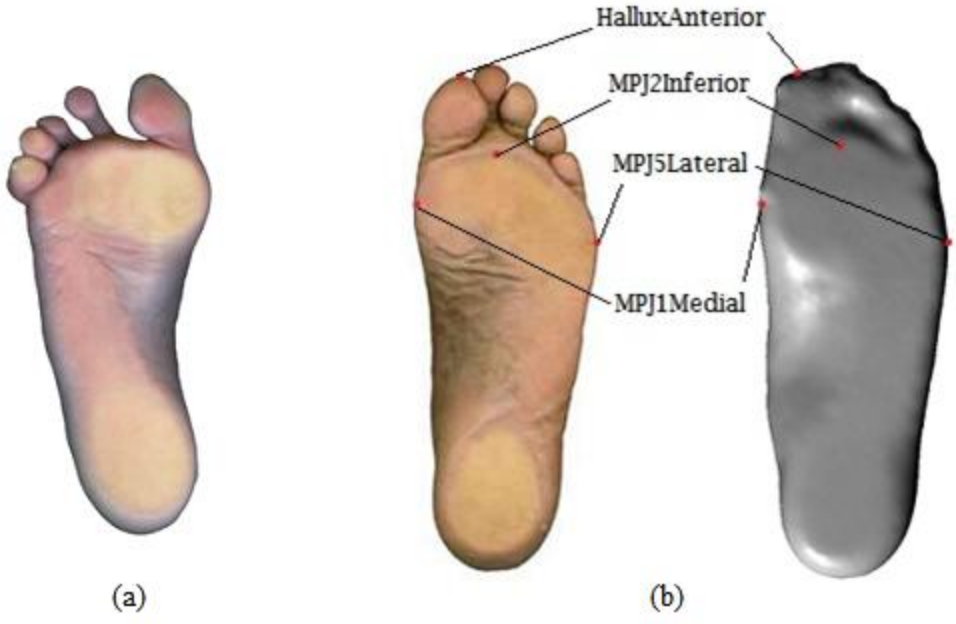

Figure 4.2: a) Common deformities make automatic landmark detection from a 3D model challenging, b) Landmarks to be manually selected by user shown first on a digital image of the plantar surface of the foot and then on the corresponding 3D model

4.2.2 Foot Alignment

Prior to designing the FO, the central axis of the foot is aligned with the X axis in the design session. There are two common methods for determining the central axis. Witana et al. describe the methods as follows [86]:

- Brannock - The central axis starts at the pternion. The pternion is an anatomical landmark defined as the most posterior point on the foot (gauged from initial approximate alignment of the foot). The central axis is then constrained to pass 1.5" from MPJ1Medial (Figure 4.3).

- Second Toe - The posterior point is calculated as the furthest point on the projected outline from the tip of the second toe. The central axis starts at the posterior point with a direction towards the tip of the second toe (Figure 4.3).

The Brannock method uses the 1.5" constraint for feet of all sizes. Consequently, the Brannock method will result in central axes positioned too far laterally for narrow feet and too far medially for wide feet (Figure 4.3). The second toe method is sufficiently defined and operates independent of foot size; however, it often fails due to common irregularities of the second toe (Figure 4.2 (a), Figure 4.3) and the posterior calcaneus surface (Figure 4.3). In light of these difficulties, the following extension of the second toe central axis technique will be used:

- Rather than using the tip of the second toe as the anterior point, MPJ2InferiorXY is used as it is far less subject to deformities. Additionally, the posterior point is replaced by the posterior contact point, where it is the furthest point on the foot from MPJ2InferiorXY that lies on the XY plane. These two changes will result in central axes that are less subject to minor foot deformities. The foot in Figure 4.3 exhibits deformities for which the Brannock and Second Toe methods perform poorly but the proposed method performs adequately.

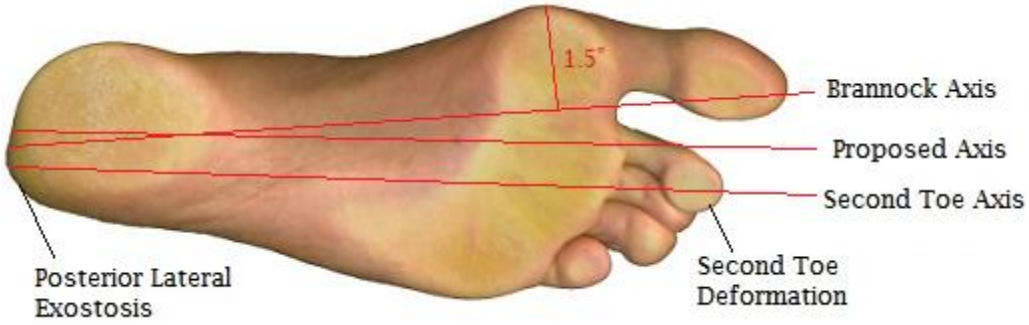

Figure 4.3: An example of the Brannock and second toe method performing poorly. The large size of the foot results in an overly medial Brannock central axis while the deformed second toe and posterior lateral exostosis undesirably influence the central axis

4.2.3 Boundary Geometry

In addition to landmarks on th foot, the outer boundary of the FO must be known prior to designing the FO surface. This information can be determined from the shoe geometry. A shoe's geometry is dictated by its corresponding shoe last's geometry (a shoe last is a mould about which materials are assembled to manufacture a shoe). However, it is a rare case when making FOs that the digital

geometry of the respective shoe last is known. Thus the current system asks the operator to select an appropriate last from a database and grades it to the size of the intended shoe with independent 1-dimensional linear scaling along the X, Y, and Z axes. Its central axis is then lined up with the model foot central axis followed by any further manual orientation adjustments that may be necessary. The primary piece of geometry required from the shoe last is the outside silhouette when viewed from the top. This will serve as the FO boundary. To capture this, an outline of the last is created in the XY plane. This will be referred to as BoundaryXY (Figure 4.4).

Figure 4.4: BoundaryXY determined from a standard shoe last

4.2.4 Surface Design

The next step in the process is to build a FO surface about the foot geometry and bounded by boundaryXY. The FO surface differs from the posturaly adjusted foot surface as follows: The FO surface must allow space for the tissues of the foot to expand and avoid sharp edges for the foot to land on. As described by Philps in "The Functional FO", the tissues of the foot expand during weight-bearing [6]. This phenomenon will be accommodated by allowing the FO surface to deviate from the foot surface near the perimeter of the FO. Additionally, the geometry of the foot in the toe region is highly irregular and thus is not suitable as a FO surface. To address this, the forefoot will be provided a smooth surface that does not closely match the geometry of the toes.

The first consideration is primarily relevant to the rearfoot and midfoot whereas the second issue is applicable primarily to the forefoot. To accommodate this, the rearfoot and midfoot sections will be designed first in a single surface called the posterior FO surface and then the forefoot will be addressed with the anterior FO surface. A direct transition between surfaces of differing methodologies will inevitably result in discontinuities. To avoid this adverse result, the transition FO surface will provide a smooth blend (Figure 4.5).

Figure 4.5: First the posterior FO surface is designed, then the anterior FO surface, and finally the model is completed by adding the transition FO surface

It should be noted that what is being created is considered a full length FO. A common alternative is the 3/4-length FO which ends just posterior to the ball joints. Full length FOs are beneficial as the pressure distributing characteristics are included in the ball joint region (this is critical for patients requiring decreased pressure in this region). Furthermore, use of a full length FOs eliminates the potential discontinuity that results during significant forefoot posting [6]. The challenge in developing a full length function FO is that the hind three quarters are commonly rigid to achieve functional correction while the transition zone must be flexible to allow for bending during toe off. This non-homogeneous material requirement will be addressed in the section on FO fabrication.

4.2.4.1 Posterior FO Surface Design

The rear and mid parts of the foot contain all geometry posterior to the ball curve and the surface of the foot in this region will be referred to as the posterior foot surface. For the most part, the posterior FO surface resembles the posterior foot surface. Where they differ is near the perimeter where adequate space must be allotted for tissue expansion. Traditional manual techniques achieve this through the addition of plaster to the plaster cast of the foot (Figure 4.6). Philps describes the use of a spatula for smoothing down added plaster and describes the process as follows: "... the convex shape is maintained but some allowance is made for the spreading of the soft tissues on weight-bearing" [6]. Philps also points out that the amount of added plaster varies with the location on the foot. The result is a casting that no longer represents the foot, but rather the geometry of the eventual FO.

The proposed solution takes a fundamentally different approach. The foot remains in its unaltered natural shape at all times. Rather than modifying the foot, the deviations between the foot and FO are achieved via parametric equations. Below is an explanation of the proposed algorithms.

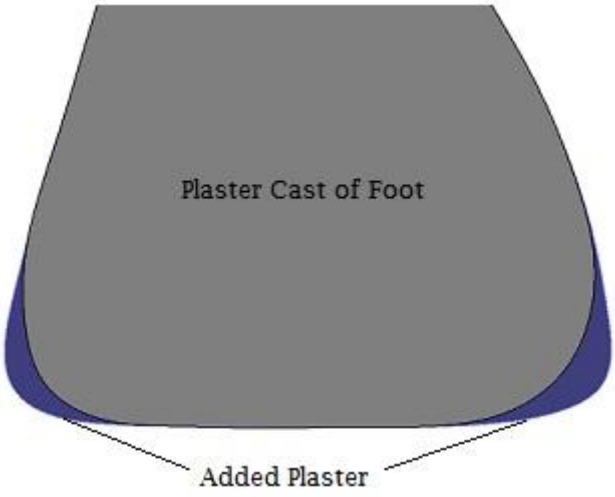

Figure 4.6: Traditional manual techniques add plaster to the plaster cast of the foot. A FO built about the modified cast will allow for tissue expansion during weight-bearing

A series of points are found on the domain of BoundaryXY that are posterior to the ball curve. At each of these points, an arc is created (Figure 4.7). The arcs deviate from the foot surface and represent the region of the FO that allows for tissue expansion on weight-bearing. Referring to Figure 4.8, the arc at each point is fully defined by four parameters:

(1) Start Angle: The angle between the XY plane and a vector tangent to the foot's surface. This angle dictates the final contact point of the FO with the foot's surface (while non-weight-bearing). The user has control over this parameter.

(2) End Angle: The angle between the XY plane and a vector tangent to the arc at the arc's end point. This angle dictates the geometry of the FO around the boundary. The user has control over this parameter.

(3) Start Point: The point at the start of the arc is found by incrementally seeking a point on the foot's surface that satisfies the start angle. This point is dependent on the start angle, the geometry of the foot, and the geometry of BoundaryXY.

(4) End Point: The point at the end of the arc has the same X and Y coordinates as the corresponding point on BoundaryXY. Its Z coordinate is driven by the above three parameters.

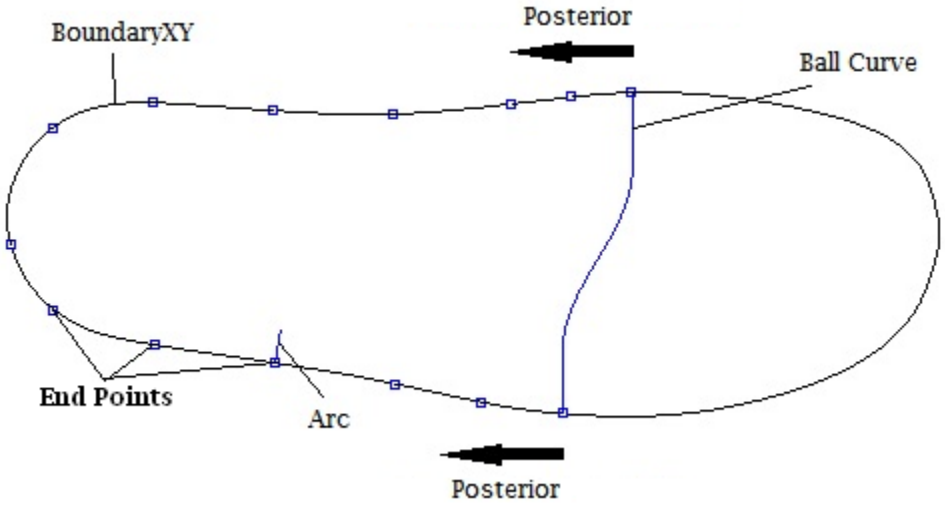

Figure 4.7: A series of points are found along BoundaryXY posterior to the ball curve and an arc is created for each point

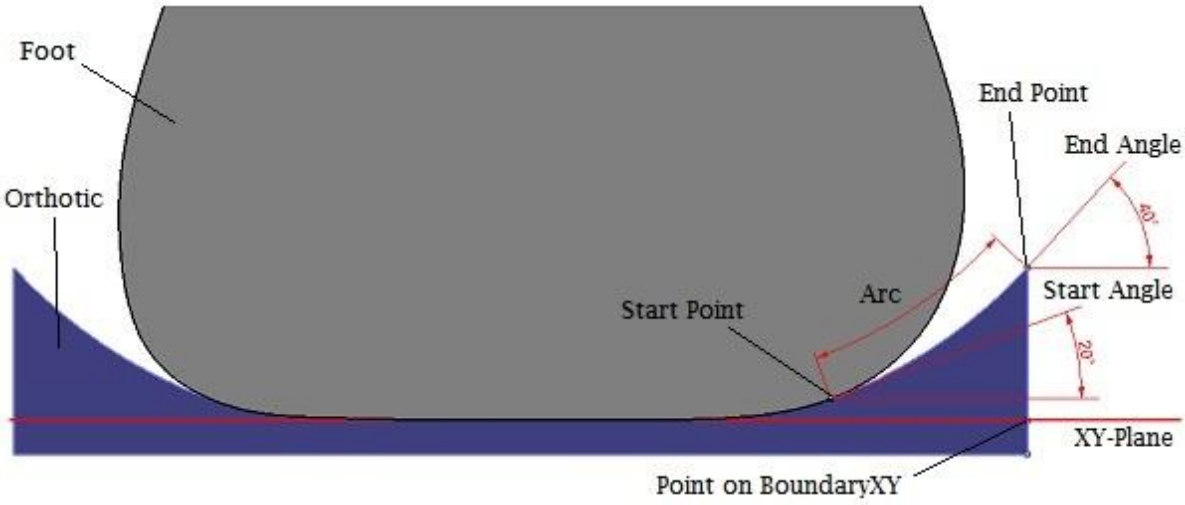

Figure 4.8: Designing the arc. Note that the extension of the FO beyond the edge of the foot is exaggerated for clarity

The amount of tissue expansion around the rearfoot varies depending on the region of the foot. For example, the heel tissue tends to expand more than the arch tissue. Thus the system is designed to allow independent inputs for the start and end angles for the arcs corresponding to various regions of the foot. A lower start angle leads to more space for expansion.

Preliminary experimentation found 40 degrees to be an acceptable end angle for most regions. This is not so steep that the material becomes fragile, but nicely cups the foot. The arch region is unique in this respect. To reduce the overall height of the FO, a lower end angle may be used, perhaps even 0 degrees (Figure 4.9). This can save considerably on material usage (see manufacturing steps below). Furthermore, Phelps recommends this technique to avoid the problem of blistering in the arch area [6]. The start and end angles for the arc are important inputs for the system and further analysis may show that they should be properly considered and adjusted on a per patient basis.

Figure 4.9: An end angle of 0 is advisable for the arch region of the foot

Next, a surface will be fit through the arcs in combination with other geometry to create the posterior FO surface. The remaining geometry required is created as follows:

The ball curve is projected vertically to the foot. A curve is interpolated through the start points of the arcs and joined with the projected ball curve. This curve is pulled to the foot to ensure full contact (now referred to as the Inner Perimeter). An array of points is projected to the surface of the foot that is contained by the Inner Perimeter (now referred to as Contact Points). The Outer Perimeter is created by interpolating the ends of the arcs and then pulling the interpolated curve to a surface created by extruding BoundaryXY vertically. The Outer Perimeter curve is closed by joining it with the projected ball curve. The Posterior FO Surface is created by fitting a surface through Contact Points, Outer Perimeter, Inner Perimeter and the arcs followed by trimming it to the Outer Perimeter (Figure 4.10).

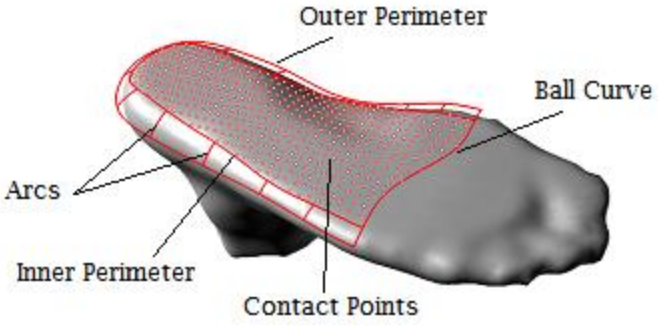

Figure 4.10: Curves and points used to construct the posterior FO surface

4.2.4.2 Anterior FO Surface Design

The anterior FO surface differs considerably from the anterior foot surface; the anterior FO surface is relatively flat and does not mimic the complex geometry exhibited by the toes. Rather, it provides a smooth forgiving surface that can easily accommodate shifts in position of the toes. The geometry is created as follows:

Referring to Figure 4.11, a primary arc is created that starts at the first ball joint inferior point. This arc is tangent to horizontal at the start. The radius of the arc is determined by incrementally decreasing it from a large initial value until it intersects the Hallux. This arc is a building block for a smooth surface that just contacts the Hallux. Normally, this technique will result in a near flat curve and could easily be replaced by a straight line. However, the use of an arc provides a more robust solution that can adapt to a greater variety of possible postural adjustments or foot irregularities.

Next, the arc is copied to the fifth ball joint at either end of the ball curve, extending the start of the arc as necessary. A surface is then fit through the ball curve and the arcs. Finally this surface is trimmed by a line slightly anterior to the ball curve (a predetermined ratio of foot length) and the projection of BoundaryXY onto the surface. The resulting trimmed surface is the anterior FO surface (Figure 4.11).

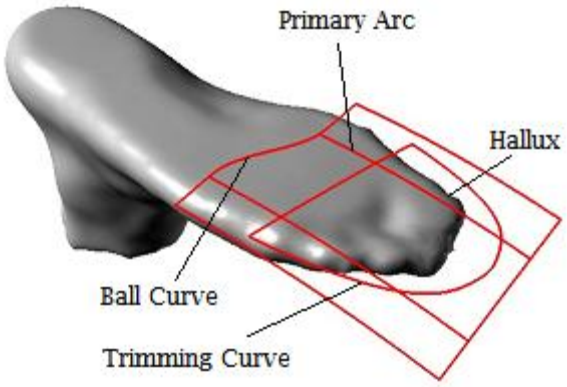

Figure 4.11: Curves used to construct the anterior FO surface

4.2.4.3 Transition FO Surface Design

Aside from the divergence near the edge, the posterior FO surface closely resembles the foot geometry whereas the anterior FO surface is considerably different from the foot geometry. A direct transition between the posterior FO surface and the anterior FO surface would result in discontinuities. The transition FO surface provides a smooth blend between the posterior and anterior FO surfaces:

A surface is fitted through a series of curves passing from the posterior FO surface to the anterior FO surface. Each curve is a degree 3 Bezier curve (four control points) where the start of the curve is tangent to the posterior FO surface and end of the curve is tangent to the anterior FO surface. Fitting a surface to these curves results in the transition FO surface (Figure 4.12).

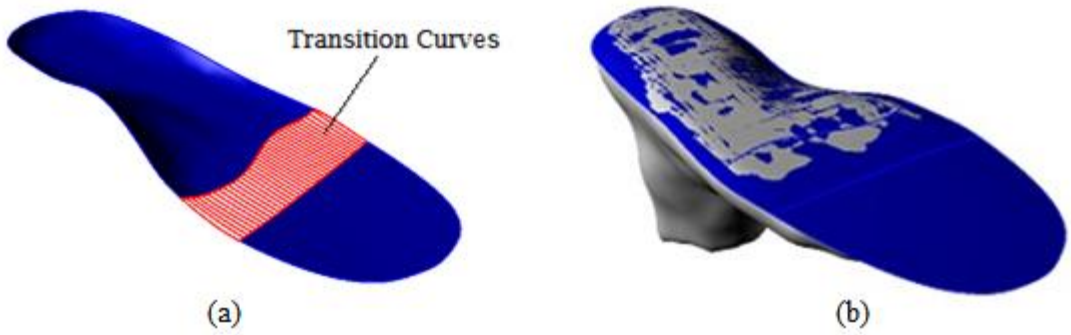

Figure 4.12: a) Curves used to construct the transition FO surface, b) finished FO surface. The splotchy pattern corresponds with a close match between the FO and foot surfaces

4.2.4.4 Additional Pressure Adjustments

Further reduction of plantar pressures in specific regions may be required to address pathologies such as diabetic ulceration or plantar fasciitis. Such pressure adjustments can be achieved through the repositioning of the control points that define the FO surface (Figure 4.13). The control points can be adjusted individually, or with a blending function guided by a point or a line. Holes for plugs can be cut from the part.

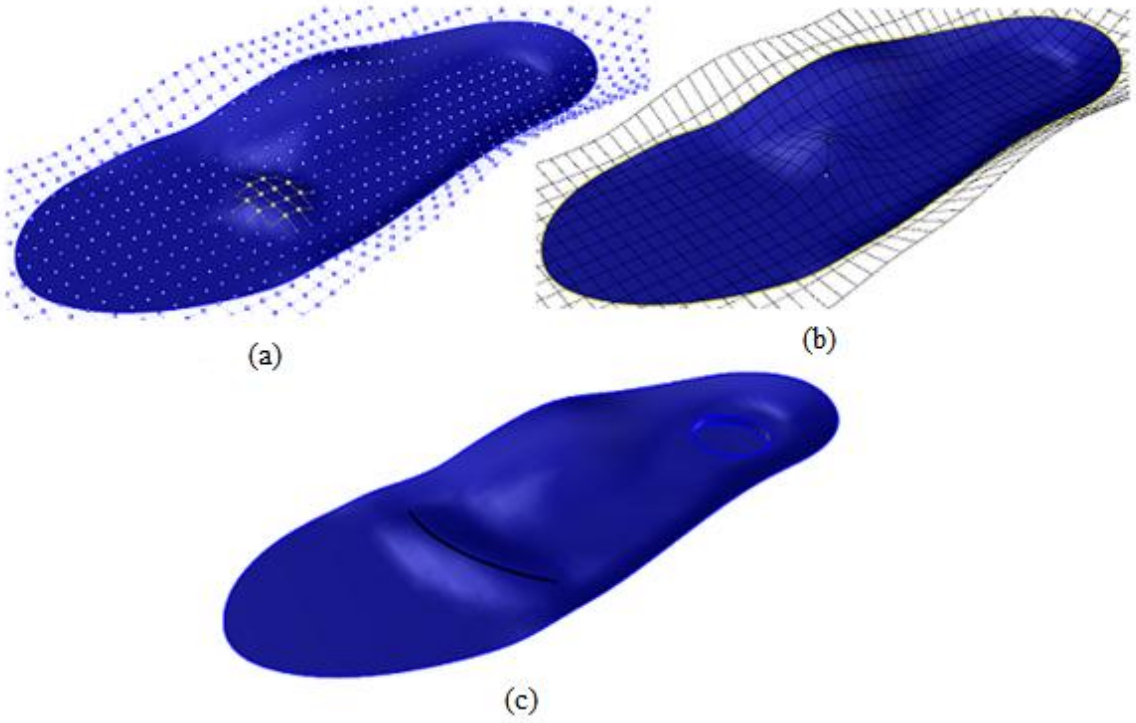

Figure 4.13: Additional pressure adjustments: a) manual control point repositioning, b) blended control point adjustment from a point, c) blended control point adjustment from a line and a cavity created for a heel plug

4.2.5 Fabrication

The traditional method of fabricating a FO is to vacuum form various materials to the positive plaster cast. Modern variations on this technique include using a CNC machined cast or a reconfigurable mould to take the place of the plaster cast. Though vacuum forming is fast and inexpensive, it has the disadvantage of only controlling the top surface geometry of the FO. If the FO body is to have

anything other than uniform thickness, it must be achieved in a subsequent step. For example, extrinsic posting in the forefoot or rearfoot must be attached and ground to the desired shape.

CNC machining is becoming a popular method of FO fabrication. Though it is slower than vacuum forming, requires expensive machinery, and results in more wasted material, it has the advantage over vacuum forming of being able to produce parts of non-uniform thickness through two sided machining. Though this works fine for rigid materials, softer materials require freezing if they are to be machined on both sides [28]. Given a full length FO requires softer materials in the ball joint area to allow for bending during the push off phase of gait, this is a problem for the technology.

Similar to CNC machining, additive manufacturing (AM) has the advantage of allowing for a part of complex geometry, even more so in fact than CNC machining. Various types of AM methods have previously been tested for FO fabrication including selective laser sintering (SLS), steriolithography (SLA), and fused deposition modeling (FDM) [25, 26]. The methods have previously only been used for fabricating the rigid portion of the full length FO. Additive manufacturing machines generally print one material type (multiple material printing is available, though at a considerably greater cost) while the FO is commonly made up of multiple materials of varying stiffness. AM can satisfy this requirement by using the relatively stiff print material to form the shell and postings of the FO and then using printed cavities for injecting softer materials to form the other regions of the FO (the heel plug, top covering, metatarsal pad, and flexible transition zone). Consequently, it is the only technology that can manufacture the entire FO without any of the geometrical outcome being subjectively influenced by manual operations. Its disadvantage is that it is perhaps the slowest and most costly of the manufacturing methods. However, AM is rapidly evolving as its number of applications and popularity continue to grow and increases in speed and affordability follow suit.

FDM will be used for the current work. FDM uses an extrusion nozzle to melt and deposit beads of thermoplastic material to create a part one layer at a time. A second material that can later be dissolved is printed to support the part material. The support material will also be used to print thin walls to form cavities for injecting material to form the flexible or softer regions of the FO (Figure 4.14). Columns of support material will be used to provide support inside the cavities. Another potential benefit of using AM is that the shell part of the FO can have ribbing such that a higher stiffness to weight ratio can be achieved in the arch area than with uniform thickness shells. Though there is no limit to the number of materials that could be used in this manner to form the FO, for the current purposes the printing, supporting, and injecting materials are: ABS-M30, SR-30, and a silicon

rubber compound called Dragon Skin (shore A hardness of 20). An example FO CAD model and finished part are depicted in Figure 4.15 and Figure 4.16. In this first example, the cavity was created with print material rather than support material. Some additional details need to be worked out in order to print the cavity with support material.

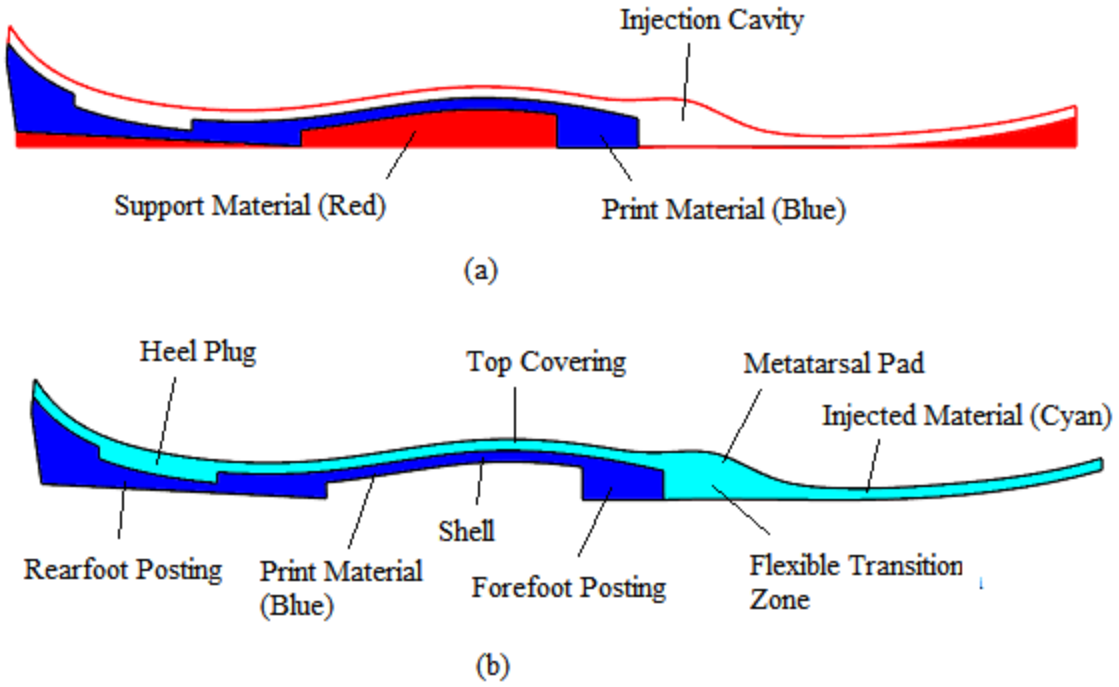

Figure 4.14: Conceptual model of additive manufactured part: a) including support material, b) after material is injected into the cavities and the support material has been dissolved

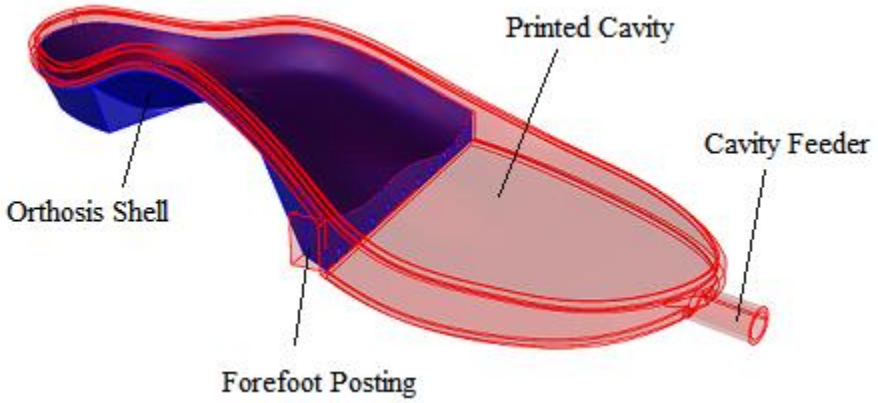

Figure 4.15: 3D model of the FO to be sent to the FDM software

Figure 4.16: Printed FO

4.3 Summary

In this chapter, novel methods for designing and fabricating FOs have been described. A primary consideration in the development of the methods was to reduce the required subjective input of the system operator. For the FO design method, this was achieved by describing the variation between the FO and the foot geometry with a series of input parameters as opposed to the traditional method of adding and removing plaster from the positive cast. Though the user can select these values, recommended defaults are provided to present the opportunity for full automation. For the FO fabrication method, reduction of the subjective component required by the system operator was achieved through the use of a novel AM technique that combined building the FO with the print material and a flexible material formed by injecting it into a printed cavity.

Algorithms were developed for automatically designing the FO top surface geometry. Building the full body of the FO was done manually. Similarly, preparation for the printing process was done manually. Although this method offers qualitative advantages over other methods, further work must be done to fully automate it to arrive at a competitive cost.

Up to this point in the dissertation, all of the components required for the proposed FO development process have been developed. In the next chapter, these components will be linked and the overall procedure will be demonstrated for a single subject.

Chapter 5
The Proposed Foot Orthosis Development Process

Thus far, a procedure for rapidly and inexpensively developing computationally efficient simulation models along with tools for designing and fabricating FOs have been described. The aim of the current chapter is to incorporate all of these tools into the proposed process for developing FOs. A review of conventional FO development methods and how the proposed methods differ (chapter 1) would be beneficial to the reader at this point as the current chapter delves directly into an example of the proposed method.

5.1 Demonstration of the Proposed Method

Figure 5.1 depicts the conventional and proposed methods.

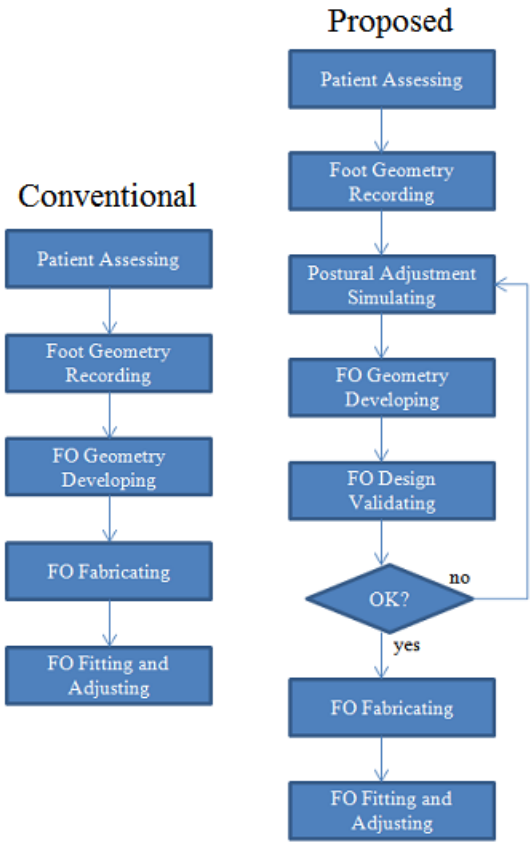

Figure 5.1: Conventional methods and the proposed method

Subject 1 from chapter 3 was selected to demonstrate the proposed method as follows:

(1) *Patient assessing*: The tibial stance angle was measured during weight-bearing and the subtalar and midtarsal joint angles were measured with the patient prone and the foot in the subtalar neutral position with the midtarsal joint locked as described in section 1.1.4. The resulting angles were 5.7° valgus, 2.1° varus, and 6.6° varus yielding a rearfoot angle of 3.6° valgus and a forefoot angle of 3.0° varus. Other postural adjustments decided upon at this point were positioning the foot for a 10mm heel height and for a toe spring with a 100mm arc radius.

(2) *Foot geometry recording*: The landmarks described in chapter 3 were palpated and marked on the subject's foot. The Artec scanner was used to capture the foot's non-weight-bearing geometry while the subject was prone and foot relaxed as described in chapter 3.

(3) *Postural adjustment simulating*: The generic FE foot model (developed in chapter 2) was morphed to the subject's foot with the method developed in chapter 3. Boundary conditions were applied to the bones to achieve the posture prescribed in step 1 as follows (Figure 5.2, Figure 5.3, Figure 5.4):

    a) The foot was fully constrained in all DOF at the ankle (tibia and fibula).

    b) Points on the inferior surface of the distal heads of the first and fifth metatarsals were displaced along the Z axis to achieve a heel height of 10mm and a forefoot angle of 3.0° varus.

    c) A point on the posterior/inferior surface of the calcaneus was displaced along the Y axis to achieve a rearfoot angle of 3.6° valgus.

    d) A point on the anterior surface of the first toe was displaced along the Z axis to achieve a toe spring with a 100mm radius.

e) A point on the inferior surface of the intermediate cuneiform can be displaced vertically to increase arch height of the resulting FO. This adjustment was not used as the current subject had a high arch and did not need any further support from a FO in the arch area.

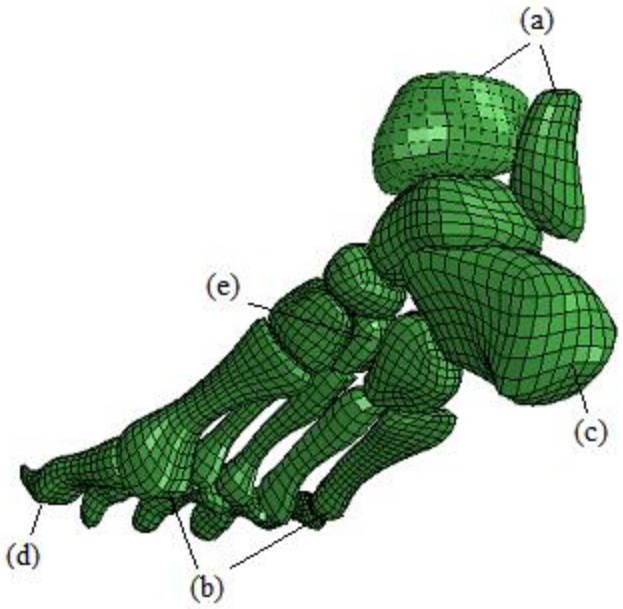

Figure 5.2 Points where boundary conditions are applied to achieve postural adjustments

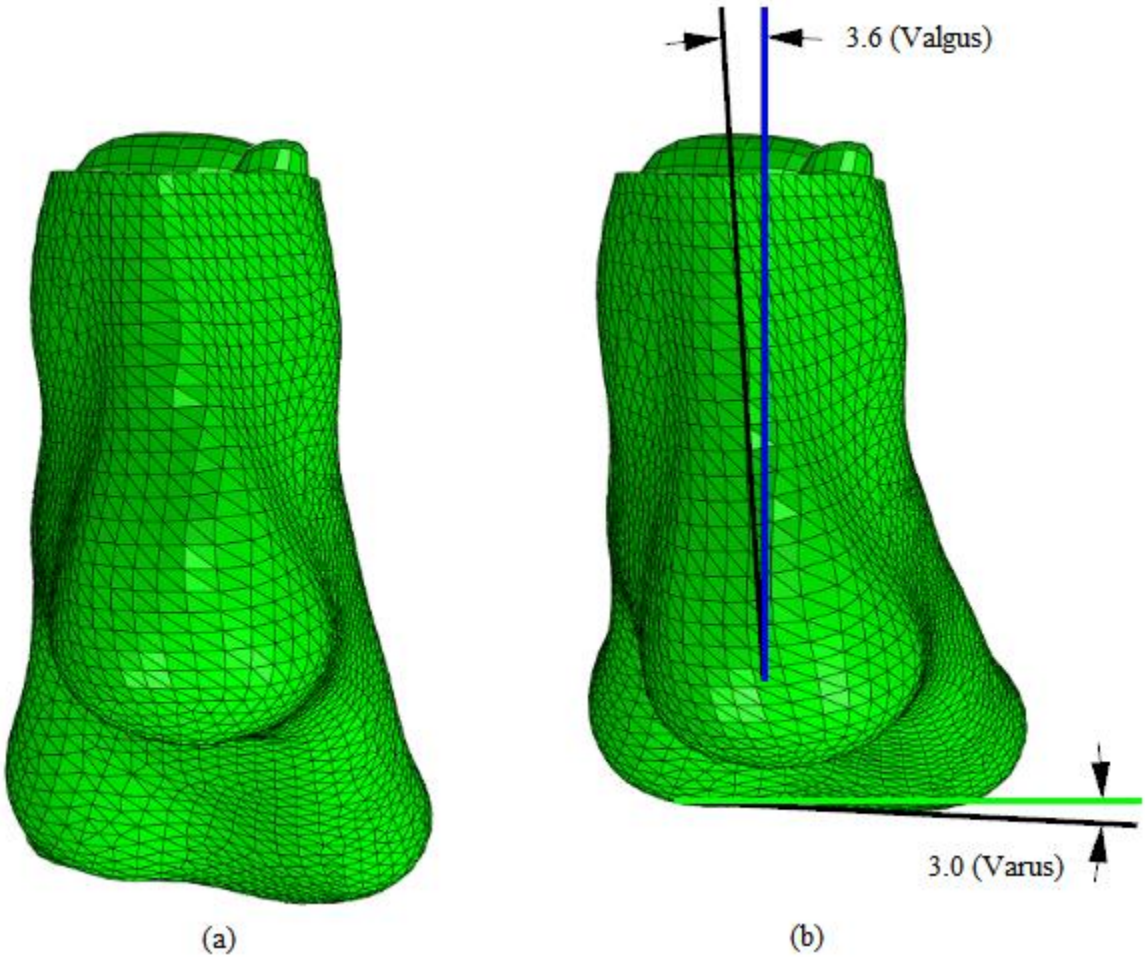

Figure 5.3 Posterior view of the foot with Y (green) and Z (blue) axes: a) before postural adjustment, b) after postural adjustment

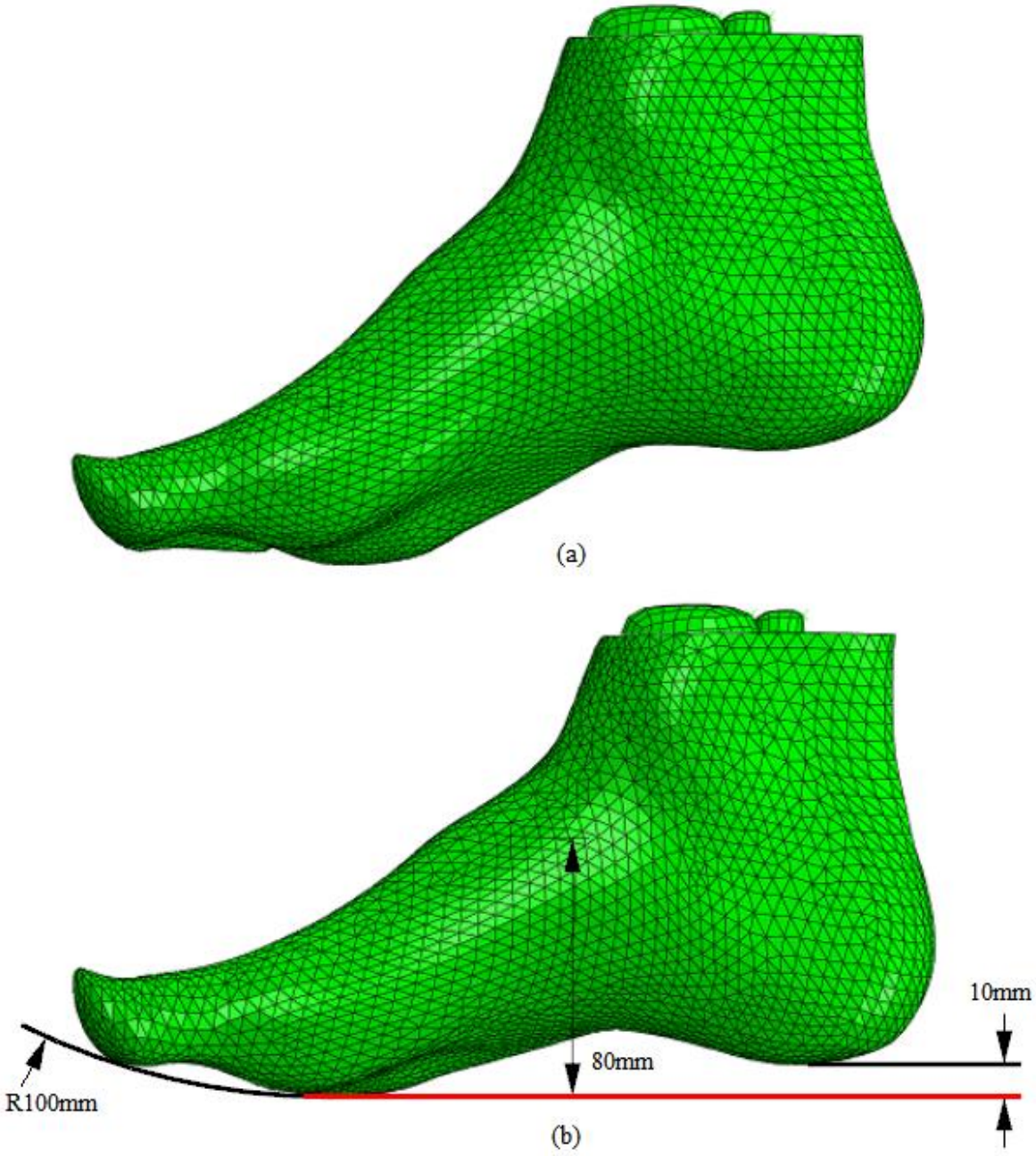

Figure 5.4 Medial view of the foot with X axes (red): a) before postural adjustment, b) after postural adjustment

(4) *FO geometry developing*: The FO was designed about the posturaly adjusted foot from step 3 using the FO design program from chapter 4 (Figure 5.5). The default design parameters were used. Ordinarily, in this step the complete foot model including extrinsic posts and other features is developed and prepared for additive manufacturing. For the current purposes, only a uniform thickness part was designed for analysis in the next step.

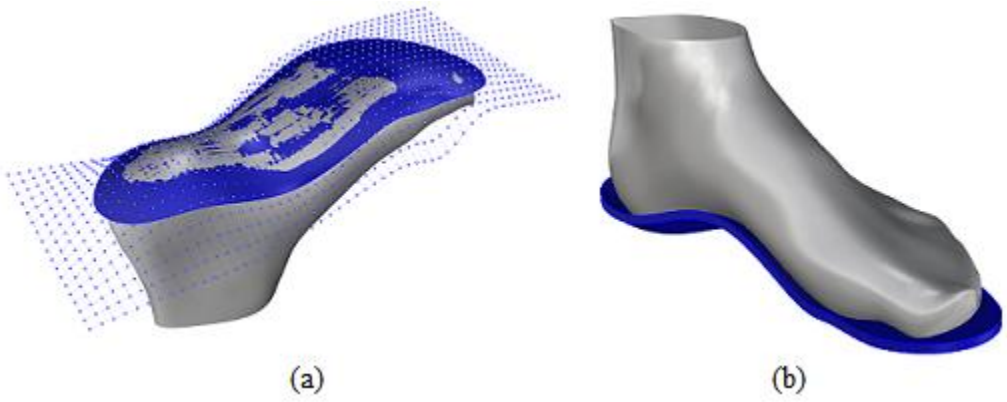

Figure 5.5 FO: a) initial surface design, b) body design with uniform thickness for FEA use

(5) *FO design validating*: The simulation of weight-bearing on the FO was carried out as described in chapter 2. Figure 5.6 (a) depicts the resulting simulated plantar pressure distribution. The highest pressure occurred along the lateral arch and the head of the fifth metatarsal. To reduce the pressure in this region, the FO design was modified by reducing the height of the surface in this area by 2mm (Figure 5.6 (b)) and then by 4mm (Figure 5.6 (c)). The 2mm adjustment was preferred as, unlike the 4mm adjustment, it reduced the pressure in the region of interest without significant adverse effect to other regions.

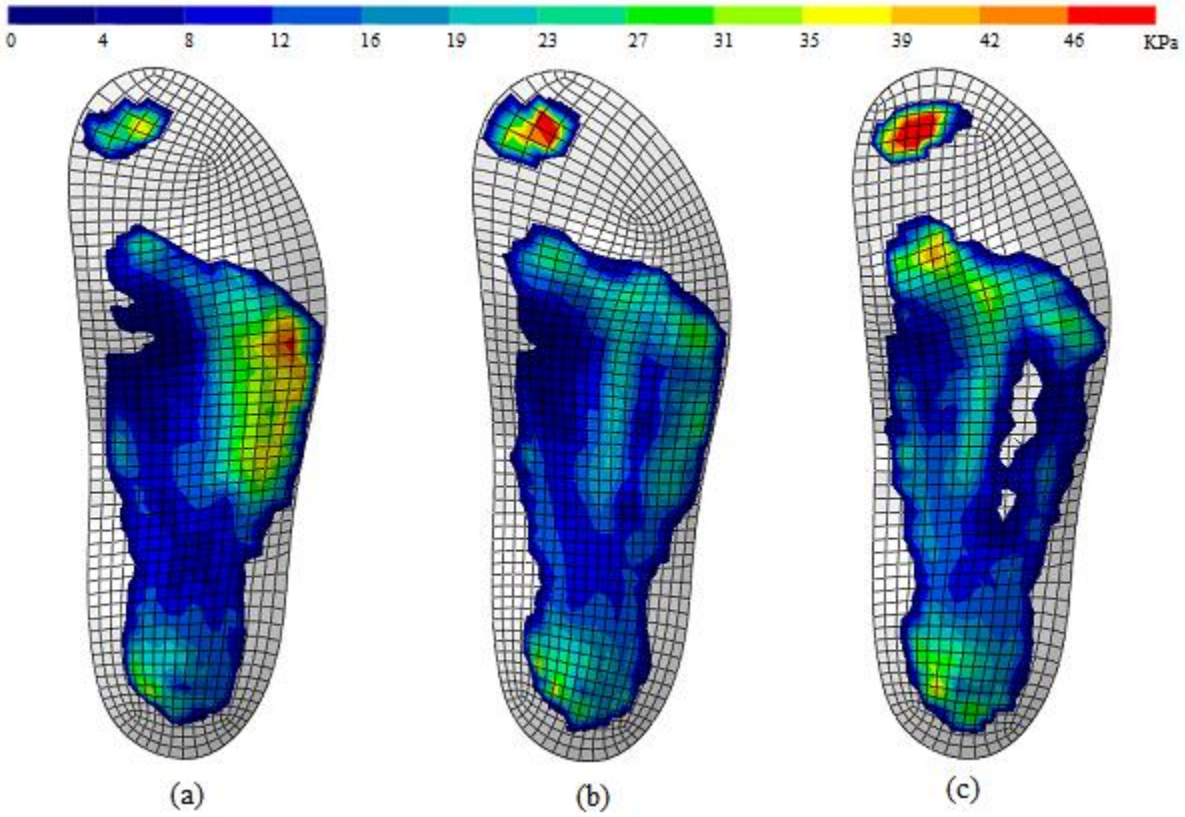

Figure 5.6: Plantar pressure distributions: a) initial FO, b) FO with 2mm drop along lateral arch and fifth metatarsal head, c) FO with 4mm drop along lateral arch and fifth metatarsal head

(6) *FO fabricating*: The next step in the process is to fabricate the FO with additive manufacturing as described in chapter 4.

(7) *FO fitting and adjusting*: This step remains unchanged from the conventional process. However, theoretically fewer adjustments should be required given the addition of the design validation step.

5.2 Comparison with a Common Modern Scanning Method

The introduction of computer enabled technologies has spawned a great variety of modern methods for capturing foot geometry. Perhaps the most popular method consists of the patient sitting in a chair and gently resting their foot on a flat glass plate as the plantar foot geometry is scanned from below.

This section will compare a FO designed about foot geometry resulting from this method to a FO designed about foot geometry resulting from the proposed method.

To rapidly carry out the test, physical resting of the foot on a flat glass plate was substituted with a simulation; the foot model of subject 1 was loaded onto flat ground until the heel just touched the ground surface (about 1mm of heel tissue deformation). The FO was then designed about the resulting foot geometry using the FO design program from chapter 4. To test the design, the foot was then loaded on the FO model and the resulting pressure distribution (Figure 5.7 (b)) compared to the pressure distribution resulting from the proposed method (Figure 5.7 (a)).

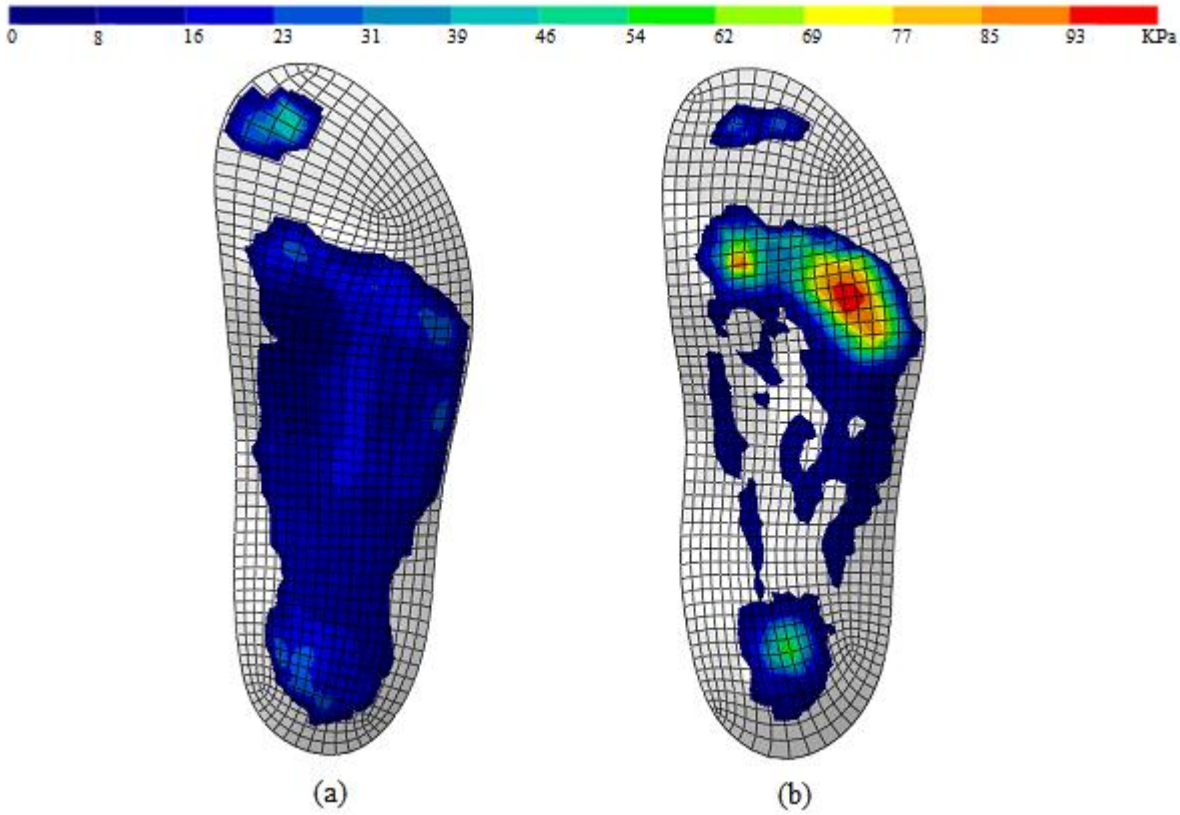

Figure 5.7: Plantar pressure distributions: a) on an FO developed with the proposed method, b) on an FO developed with a typical conventional method

The compression of the plantar soft tissues caused by contact with ground resulted in a FO design with poorer conformity to the plantar foot geometry than the proposed method, and consequently, higher peak plantar pressure (97% increase). The problem is more apparent in the forefoot where

greater tissue deformation resulted from contact with ground. Furthermore, the lack of a feedback step did not provide the opportunity to see high pressure areas and adjust the design accordingly.

5.3 Discussion

Carrying out the proposed method of FO development required a considerable amount of skilled computer labour. However, in contrast to highly subjective conventional methods, this labour has the potential to be fully automated. The computer labour was mostly in the form of work within CAD (Rhinoceros 3D) and FEA (Abaqus) software. Though the CAD operations were semi-automated with scripts, these scripts still had to be managed and manual work was still required for such operations as picking up the landmarks and designing the FO volumes. The FEA work included setting of loads, boundary conditions, and the soft tissue properties specific to the subject. The most time consuming part of the FEA work was the trial and error adjustment of boundary conditions while trying to achieve specific foot postures. Ideally, a real-time method of measuring these postures and correspondingly adjusting boundary conditions should be scripted for Abaqus.

Another source of manual computer labour was the repetitive importing and exporting of models between CAD (Rhinoceros 3D) and FEA (Abaqus). The most readily accessible solution is to automate both programs and devise a method for them to communicate and interact. Alternatively, a single program could be made responsible for both CAD and FEA work. Abaqus' CAD capabilities are limited and this would require a lot of development work. Rhinoceros can be expanded with the simulation plug-in, Scan & Solve (which forms a generalized FEA approach that eliminates meshing and has computational advantages), however it is a relatively new program and has yet to incorporate assemblies and contact modelling. Other software combinations such as Solid Works and Cosmos are possibilities. The most ideal solution would be to develop a complete software solution from the ground up for both the CAD and FEA processes.

FEA was selected for this project as it meets the modelling requirements as has been demonstrated and published on in the literature. However, there may be other methods that can achieve similar results at a lesser computational expense and should be considered for the problem. One possibility is surrogate FEA modelling as demonstrated by Trinidad [22]: a single FE model of a FO was run through a series of tests to predict arch deformation. The data could then be interpolated to determine FO arch deformation for a variety of loads. A similar but more sophisticated approach may be possible for the current application. Another possibility could be to build on the current methods

being developed for analysis of plantar pressure during the gait cycle; simplified modelling techniques such as the approximation of the soft tissues with equally spaced cross sections or spherical volumes [49] can be combined with rigid body models of the bones to rapidly determine plantar pressures. In addition to using a computationally efficient simulation model, harnessing greater computing power is also important. For commercial application of the proposed method, the execution of simulations on a powerful remote server should be considered.

The proposed method yielded a 49% decrease in peak plantar pressure when compared to a common conventional method. Other conventional modern and traditional methods may distort plantar soft tissue to a lesser extent. For example, traditional casting methods build the negative plaster cast about the patient's non-weight-bearing foot. However, the plaster does have some effect on the soft tissues it is in contact with and the practitioner affects the soft tissue in the process of correcting posture. The proposed method is the only known method that does not apply pressure to the plantar foot surface that allows for realistic control over the foot's posture. Furthermore, it is the only method that allows for the visualization of pressure distribution and the opportunity for optimization prior to fabrication of the FO.

Though not tested here, other metrics should also benefit from the proposed process. For example, the posture of the foot could be adjusted to reduce stress in the plantar fascia, and then the geometry adjusted incrementally to find a design that better achieves this. Other potential metrics include stresses in the soft tissues, positions of specific joints, stresses in bones, and FO stiffness via material combinations and thicknesses. Given the adaptation of the model to dynamic analysis, other metrics including joint articulation velocities could be considered.

A system operator could eventually develop the skill to be able to approximately achieve a desired criteria value after several attempts at adjusting the FO geometry manually. However, automated optimization routines could more accurately address several criteria simultaneously in a fewer number of steps all with less input required from the operator. Such automated optimization routines present great potential to the FO development process and are an important area for continuing research.

5.4 Summary

The proposed FO development process has been described and demonstrated in this chapter. Though the process requires considerable skilled computer labour, minimal subjective operator input was

required and thus there is potential for automating the system. The process was compared to a common modern FO development technique and proved to more effectively distribute plantar pressures. This was due to both the opportunity the proposed process provides for adjusting FO geometry after visualizing predicted plantar pressures and because the *foot geometry recording* step did not distort plantar soft tissue geometry. Use of the process for testing other metrics as well as implementing optimization routines is promising.

Chapter 6
Conclusion

The conclusions of this dissertation will now be presented on a chapter by chapter basis followed by a description of recommended improvements and advancements and other potential applications.

6.1 Conclusions

In chapter 2, a FE model of a foot was developed. Though many such models have been developed for the application of research use, the current model is intended for rapidly testing FO designs in a clinical setting and thus materials, mesh, and various model characteristics and settings were selected accordingly. The conclusions of the chapter are as follows:

- A comparison between simulated and experimental plantar pressure distributions on flat ground and a FO resulted in acceptable average plantar pressure errors of 2.2% and 5.0% of peak plantar pressure. Furthermore, the FO plantar pressure reductions experimentally shown were accurately reflected in the simulations.
- Solution times for the flat ground and FO loading tests were 29 and 32 minutes. Though this amount of time would be unacceptable for commercial use, it could be reduced through various improvements to the model and harnessing of greater computing power.
- The process used to develop the FE foot model required considerable skilled computer labour and thus could not be viably used for the purpose of developing FE foot models to be incorporated in the FO development process.

In chapter 3, a procedure was developed to rapidly create a simulation model by morphing the generic FE model from chapter 2 to the surface and anatomical landmarks of a specific foot acquired from structure light scan data. The procedure was tested and the conclusions are as follows:

- Acceptable average error in predicting bone geometry was achieved (2.53mm over 6 tests). Average model development time was 2 minutes and 17 seconds.
- Excessive element distortion was a problem for the morphed models. The models were made solvable by increasing soft tissue stiffness. Consequently, the resulting high plantar pressures

had to be scaled to be compared to the experimental results. The excessive distortion problem can be partially addressed through a single part mesh for the entire model.

- Average plantar pressure error between the scaled simulated plantar pressures and the experimental plantar pressure for the three tests was 3.2% of peak plantar pressure (only slightly greater than that of the original FE foot model: 2.2%). The method successfully developed patient specific FE foot models rapidly and automatically and thus is viable for use in the FO development process.

In chapter 4, methods were devised for designing and fabricating FOs. The methods replaced the traditional sculpting approach with a parametric design approach and manual fabrication steps with fully automated additive manufacturing. The methods successfully reduced the amount of subjective input required by lab technicians.

In chapter 5, the simulation techniques and FO design and fabrication methods were introduced into the FO development process and demonstrated for a single subject. The conclusions are as follows:

- The method allowed for exact control over the posture of the foot prior to designing a FO about the foot and for the testing of FO designs prior to fabrication.
- The proposed method proved superior to a conventional method as it resulted in a 49% lower peak plantar pressure.
- The primary deficiency for the process was the extensive skilled computer labour and computing time required. These deficiencies can be addressed by further automating the steps, improving the FE foot models, and making use of greater computing power.

The overall contribution of this dissertation was a novel process for developing FOs that incorporated simulation tools and advancements in FO design and fabrication. As hypothesized, the proposed process reduced the necessary subjective input required to produce a FO and improved the results by allowing for the validation of designs prior to fabrication.

6.2 Improvements and Advancements

The following are improvements and advancements to the results of this research that would benefit the implementation of a practical system:

- Improving the master (generic) model: Solution times for the current master FE foot model are likely too long for many applications. Though running the analysis on a faster computer, maybe even a powerful remote server, would be the obvious first step in reducing solution time, increasing computational efficiency would also be of benefit. A variety of methods could be used to increase computational efficiency, though perhaps the most important would be to convert the foot model into a single part with a single mesh. This is also likely to solve the problem of excessive distortion that caused the morphed models to run slow and sometimes fail. Accuracy could be improved by increasing model realism such as by modeling joint articulation via surface-to-surface sliding interactions rather than hinge and pin connections. System outputs in addition to plantar pressure and deformed geometry could be provided for by increasing model complexity. For example, modeling the bones as deformable solids rather than rigid shells can be done to allow for detecting high stress regions in the bones. For any given application, a compromise between model realism and computational expense must be made.
- Increasing patient specificity of the model: The master foot model was developed from a non-pathological foot and morphing it to a pathological foot may present some difficulties. For example, if the foot it is morphed to has a collapsed arch, this pathology may not be accurately represented in the morphed model. Similar problems exist for other pathologies such as Hallux rigidus or plantar fasciitis. To solve this problem, a library of foot models should be developed and an appropriate model should always serve as the generic model. Additionally, the tissue properties should be tuned to the specific foot to a greater extent for applications that warrant it. For example, soft tissue properties should be detected with an ultrasound probe device and attributed to the model and the plantar fascia stiffness may be tuned until the model exhibits the same changes upon weight-bearing as the physical foot as measured with a scanner. Finally, some applications may warrant the cost of an MRI. For these applications, the morphing algorithms should be adapted to morphing from bone landmarks to bone landmarks such that the application could at least benefit from the reduced costs associated with automating the assembly of the FE model.
- Optimizations: In chapter 5, it was demonstrated how the feedback loop of the proposed FO design steps could be used to manually go back and make changes to the postural control and FO design steps to achieve a different outcome. To turn this into an optimization routine, a

particular function should be noted in the validation step and fed back into the postural control and design steps to automatically guide changes made in these steps. Various functions that could be optimized include peak plantar pressure or stress, stress in the plantar fascia, and rearfoot and forefoot angles upon loading.

- Advancements in patient assessment: Step 1 (patient assessment) was left unaltered from traditional methods as described by Root et al. However, after advancing all of the other steps in the FO development process, it has become the step responsible for the majority of subjective input in the proposed process. The subjective component arises from poorly defined (planar) joint angles and positions being measured with simplistic tools and the corresponding dependence on practitioners' varying methods and skill. One possible beneficial advancement is to use more exactly defined landmarks, modern scanning tools, and the International Society of Biomechanics (ISB) recommended Joint Coordinate System (JCS). An even more scientific approach would be to assess the FE foot model rather than the physical foot. For example, the subtalar neutral joint position could be calculated as a function of contact position of adjacent articulating facets of the talus and calcaneus. A morphed FE foot model may not be accurate enough for this purpose. Instead, an actual MRI of the patient's foot could be used (morphing would still be useful for rapidly forming a meshed and assembled FE foot model). Currently, such a method is not feasible given the cost of MRIs, however, these are rapidly decreasing as the technology ages and foot only MRI machines become more popular. Before implementing these advancements, it would be more important to first reappraise Root et al.'s model and incorporate the more recent knowledge of potential FO benefits such as the ability to influence joint velocities during the stance phase of gait.

6.3 Other Applications

Other applications of the various developments in this dissertation are far reaching. They could be applied towards prostheses, surgical procedures, and in general, any research application of a simulation model that could be useful on a per patient basis but does not warrant the cost of conventional methods of developing a FE foot model. However, the most immediate alternative applications are shoe lasts and shoes and orthoses for other parts of the body, for example, the ankle foot orthosis and the spine orthosis:

- Custom shoe last and shoe design: The methods developed in this dissertation are relevant to custom shoe last design as follows. First, the morphing procedure can be applied to developing the geometry of a custom shoe last; an ideally fitting shoe last for a generic foot is morphed from the generic foot to a specific foot similar to how the bones were morphed. Second, the shoe last can be designed about a foot that is already posturaly adjusted and weight-bearing on the FO thereby eliminating much of the guess work. Finally, the simulation methods could be used to test last designs prior to fabrication or even standard shoe lasts in large scale shoe fitting studies.
- Ankle Foot Orthosis (AFO): An AFO is useful for stabilizing a dysfunctional, injured, or recovering ankle. Off the shelf AFOs are available, however, in many cases a custom AFO is warranted. Similar to FOs, traditional and modern methods exist for developing AFOs. Also similar to FOs, modern solutions have yet to take advantage of anatomical simulation models. In general, AFOs would gain from a similar approach as described in this dissertation including the ability to adjust posture prior to design, a parametric design approach, design validation prior to fabrication, and fabrication with additive manufacturing.
- Spine Orthosis: Though some practitioners are beginning to make the transition from traditional casting methods to modern digital methods, the transition is occurring far more slowly than with FOs. This is perhaps due to the smaller quantities associated with spine orthosis development as well as the comparably greater complexity and severity of conditions that warrant such devices. Furthermore, the devices are much larger and would be expensive to adapt to automated manufacturing methods such as CNC machining and additive manufacturing. However, modern methods do exist such as the solution by Vorum. Similar to the software for the FO, software for the spine orthosis are lacking realistic simulation techniques. Simulation techniques may be of even greater benefit to spine orthoses than FOs as physically controlling the posture of the body during scanning is extremely difficult and potentially painful for the patient. Furthermore, a validation step would prevent even more costly of reworks.

Bibliography

[1] C. A. Oatis, *Kinesiology: The Mechanics and Pathomechanics of Human Movement.* Baltimore: Lippincott Williams & Wilkins, 2009.

[2] G. Wu, S. Siegler, P. Allard, C. Kirtley, A. Leardini, D. Rosenbaum, M. Whittle, D. D. D'Lima, L. Cristofolini, H. Witte, O. Schmid and I. Stokes, "ISB Recommendation on Definitions of Joint Coordinate System of various Joints for the Reporting of Human Joint Motion--Part I: Ankle, Hip, and Spine," *Intern. Societ. of Biomec.,* 2002.

[3] M. L. Root, W. P. Orien and J. H. and Weed, "Normal and abnormal function of the foot," *Clinic. Biomec. Corp.,* vol. 2, pp. 478, 1977.

[4] M. L. Root, "Biomechanical examination of the foot," *Journal of the American Podiatry Association,* vol. 63, pp. 28, 1973.

[5] M. Root, J. Weed and W. Orien, "Neutral Position Casting Techniques," *Clinic. Biomec. Corp.,* 1971.

[6] J. W. Philps, *The Functional Foot Orthosis.* Edinburgh: Churchill Livingstone, 1995.

[7] A. K. L. Leung, J. C. Y. Cheng, A. F. T. Mak, "Orthotic design and foot impression procedures to control foot alignment," *Prosthet. Orthot. Int.,* vol. 28, pp. 254-262, 2004.

[8] A. K. L. Leung, J. C. Y. Cheng, A. F. T. Mak, "Orthotic design and foot impression procedures to control foot alignment," *Prosthet. Orthot. Int.,* vol. 28, pp. 254-262, 2004.

[9] W. C. C. Lee, C. K. L. Lee, A. K. L. Leung and S. W. Hutchins, "Is it important to position foot in subtalar joint neutral position during non-weight-bearing molding for foot orthoses?" *Journal of Rehabil. Resear. and Develop.,* vol. 49, pp. 459-66, 2012.

[10] E. Sobel and S. J. Levitz, "Reappraisal of the negative impression cast and the subtalar joint neutral position," *Journal Americ. Podiat. Medical. Associat.,* vol. 87, pp. 32-33, 1997.

[11] C. B. Blackwood, T. J. Yuen, B. J. Sangeorzan and W. R. Ledoux, "The midtarsal joint locking mechanism," *Foot Ankle Intern.,* vol. 26, pp. 1074-1080, 2005.

[12] N. Feldman and M. Roberts, "Orthotics: Worth the cost?" *F. I. R. M. Racing Newslet.,* 2010.

[13] N. A. Guldemond, P. Leffers, A. P. Sanders, H. Emmen, N. C. Schaper and G. H. I. M. Walenkamp, "Casting methods and plantar pressure - Effects of custom-made foot orthoses on dynamic plantar pressure distribution," *Journal Americ. Podiat. Medicine. Associat.,* vol. 96, pp. 9-18, 2006.

[14] S. Telfer, K. S. Gibson, K. Hennessy, M. P. Steultjens and J. Woodburn, "Computer-Aided Design of Customized Foot Orthoses: Reproducibility and Effect of Method Used to Obtain Foot Shape," *Archiv. Physic. Medicine. Rehabil.,* vol. 93, pp. 863-870, 2012.

[15] J. Foort, R. Spiers and M. Bannon, "Experimental fittings of sockets for below-knee amputees using computer aided design and manufacturing techniques," *Prosthet. Orthot. Intern.,* vol. 9, pp. 46-47, 1985.

[16] D. Jones, "Impact of advanced manufacturing technology on prosthetic and orthotic practice," *Journal Biomed. Engineer.,* vol. 10, 1988.

[17] B. Klasson, "Computer aided design, computer aided manufacture and other computer aids in prosthetics and orthotics," *Prosthet. Orthot. Intern.,* vol. 9, pp. 3-11, 1985.

[18] M. Jezersek and J. Mozina, "High-speed measurement of foot shape based on multiple-laser-plane triangulation," *Optical Engineer.,* vol. 48, pp. 113604-1-113604-8, 2009.

[19] S. Kosolapov, "Robust Algorithms Sequence for Structured Light 3D Scanner Adapted for Human Foot 3D Imaging," *Journal of Commun. and Comput.,* vol. 8, pp. 595-598, 2011.

[20] J. A. Rodriguez, "Computer vision of the foot sole based on laser metrology and algorithms of artificial intelligence," *Optical Engineer.,* vol. 48, pp. 123604-1-123604-14, 2009.

[21] S. E. Hussein, "An intelligent design for foot orthoses," *Key Eng Mat,* vol. 381-382, pp. 607-610, 2008.

[22] L. E. Trinidad, "Engineering modeling, analysis and optimal design of custom foot orthotic," *ProQues. Disser. and Theses,* 2011.

[23] Y. Hsu, Y. Gung, S. Shih, C. Feng, S. Wei, C. Yu and C. Chen, "Using an Optimization Approach to Design an Insole for Lowering Plantar Fascia Stress—A Finite Element Study," *Annals Biomed. Engeer.,* vol. 36, 2008.

[24] M. Arakawa, S. Miyake and S. Nakao, "Approximate multi-objective optimization of medical foot support: Case of 3D shape optimization," in *2009 American Society of Mechanical Engineers International Design Engineering Technical Conferences (IDETC/CIE 2009),* Omni San Diego Convention Center, San Diego, California, 2009.

[25] Jari, Javier, Kenny, Martin and Jim, "Embracing additive manufacture: implications for foot and ankle orthosis design," *BMC Muscul. Disord.,* vol. 13, pp. 84, 2012.

[26] J. H. P. Pallari, K. W. Dalgarno and J. Woodburn, "Mass customization of foot orthoses for rheumatoid arthritis using slective laser sinterin," *IEEE Transac. on Biomed. Engineer.,* vol. 57, pp. 1371(7)-1378, 2010.

[27] P. Houle, E. Beaulieu and Z. Liu, "Novel fully integrated computer system for custom footwear: From 3D digitization to manufacturing," in Electronic Imaging, San Jose, CA (USA), 2010.

[28] P. Crabtree, V. G. Dhokia, S. T. Newman and M. P. Ansell, "Manufacturing methodology for personalised symptom-specific sports insoles," *Robot. Comput. Integr. Manufac.*, vol. 25, pp. 972-979, 2009.

[29] Y. D. Gu, J. S. Li, M. J. Lake, Y. J. Zeng, X. J. Ren and Z. Y. Li, "Image-based midsole insert design and the material effects on heel plantar pressure distribution during simulated walking loads," *Comput. Method. Biomec. Biomed. Engineer.*, vol. 14, pp. 747-753, 2011.

[30] J. T. Cheung and M. Zhang, "Parametric design of pressure-relieving foot orthosis using statistics- based finite element method," *Medical Engeer. Physic.*, vol. 30, pp. 269-277, 2008.

[31] J. T. Cheung and M. Zhang, "A 3-dimensional finite element model of the human foot and ankle for insole design," *Archiv. Physic. Medical Rehabil.*, vol. 86, 2005.

[32] A. Erdemir, J. J. Saucerman, D. Lemmon, B. Loppnow, B. Turso, J. S. Ulbrecht and P. R. Cavanagh, "Local plantar pressure relief in therapeutic footwear: design guidelines from finite element models," *Journal Biomec.*, vol. 38, 2005.

[33] S. Goske, A. Erdemir, M. Petre, S. Budhabhatti and P. R. Cavanagh, "Reduction of plantar heel pressures: Insole design using finite element analysis," *Journal Biomec.*, vol. 39, pp. 2363-2370, 2006.

[34] D. Kelaher, G. A. Mirka and K. Q. Dudziak, "Effects of semi-rigid arch-support orthotics: an investigation with potential ergonomic implications," *Applied Ergonom.*, vol. 31, 2000.

[35] B. Tsung, M. Zhang, A. Mak and M. Wong, "Effectiveness of insoles on plantar pressure redistribution," 2004.

[36] S. W. Ki, A. K. L. Leung and A. N. M. Li, "Comparison of plantar pressure distribution patterns between foot orthoses provided by the CAD-CAM and foam impression methods," *Prosth. Orthot. Intern.*, vol. 32, pp. 356-362, 09, 2008.

[37] W. CHOW and E. ODELL, "Deformations and Stresses in Soft Body Tissues of a Sitting Person," *Journal Biomec. Engeer. Transac. ASME*, vol. 100, pp. 79-87, 1978.

[38] R. Crowninshield and S. Nakamura, "An Analysis of Soft-Tissue Loading in the Foot," 1981.

[39] K. M. Patil, L. H. Braak and A. Huson, "Stresses in a simplified two dimensional model of a normal foot — A preliminary analysis," *Mechan. Resear. Commun.*, vol. 20, 1993.

[40] K. M. Patil, L. H. Braak and A. Huson, "Analysis of stresses in two-dimensional models of normal and neuropathic feet," *Medical Biolog. Engeer. Comput.*, vol. 34, pp. 280-284, 1996.

[41] S. Jacob, K. M. Patil, L. H. Braak and A. Huson, "Stresses in a 3D two arch model of a normal human foot," *Mechan. Resear. Commun.*, vol. 23, 1996.

[42] J. T. Cheung, M. Zhang, A. K. Leung and Y. Fan, "Three-dimensional finite element analysis of the foot during standing—a material sensitivity study," *Journal Biomec.*, vol. 38, pp. 1045-1054, 2005.

[43] S. P. Budhabhatti, A. Erdemir, M. Petre, J. Sferra, B. Donley and P. R. Cavanagh, "Finite element modeling of the first ray of the foot: a tool for the design of interventions," *Transac. of the ASME. Journal of Biomec. Engineer.*, vol. 129, pp. 750-756, 2007.

[44] Y. M. Tang and K. C. Hui, "The effect of tendons on foot skin deformation," *Comput. -Aided Design*, vol. 39, 2007.

[45] N. Tzur, E. Weisz, Y. Hirsch-Falk and A. Gefen, "Role of EVA viscoelastic properties in the protective performance of a sport shoe: Computational studies," *Biomed. Mater. Engeer.*, vol. 16, pp. 289-299, 2006.

[46] R. Rizza, X. Liu, J. Thometz, R. Lyon and C. Tassone, "A New Method In The Design Of A Dynamic Pedorthosis For Children With Residual Clubfoot," *Journal of Medical Devices*, vol. 4, 2010.

[47] J. T. Cheung, M. Zhang and K. An, "Effect of Achilles tendon loading on plantar fascia tension in the standing foot," *Clinical Biomec.*, vol. 21, pp. 194-203, 2006.

[48] L. Wu, "Nonlinear finite element analysis for musculoskeletal biomechanics of medial and lateral plantar longitudinal arch of Virtual Chinese Human after plantar ligamentous structure failures," *Clinical Biomec.*, vol. 22, pp. 221-229, 2007.

[49] H. C. ler, N. Berme and S. R. Simon, "A viscoelastic sphere model for the representation of plantar soft tissue during simulations," *Journal Biomec.*, vol. 31, 1998.

[50] A. Gefen, "Plantar soft tissue loading under the medial metatarsals in the standing diabetic foot," *Medical Engeer. Physic.*, vol. 25, pp. 491-499, 2003.

[51] R. Actis, L. Ventura, K. Smith, P. Commean, D. Lott, T. Pilgram and M. Mueller, "Numerical simulation of the plantar pressure distribution in the diabetic foot during the push-off stance," 2006.

[52] G. Yarnitzky, Z. Yizhar and A. Gefen, "Real-time subject-specific monitoring of internal deformations and stresses in the soft tissues of the foot: A new approach in gait analysis," *Journal Biomec.*, vol. 39, pp. 2673-2689, 2006.

[53] A. Natali, A. Forestiero, E. Carniel, P. Pavan and C. Dal Zovo, "Investigation of foot plantar pressure: experimental and numerical analysis," *Medical. Biolog. Engeer. Comput.*, vol. 48, pp. 1167-1174, 2010.

[54] Y. Gu, J. Li, X. Ren, M. J. Lake and Y. Zeng, "Heel skin stiffness effect on the hind foot biomechanics during heel strike," *Skin Resear. Technol.*, vol. 16, pp. 291-296, 2010.

[55] Chen, Taeyong Lee, P. V. Lee, Jin Woo Lee and Sung-Jae Lee, "Effects of internal stress concentrations in plantar soft-tissue-A preliminary three-dimensional finite element analysis," *Medical Engeer. Physic.*, vol. 32, pp. 324-331, 2010.

[56] A. Erdemir, M. L. Viveiros, J. S. Ulbrecht and P. R. Cavanagh, "An inverse finite-element model of heel-pad indentation," *Journal Biomec.*, vol. 39, pp. 1279-1286, 2006.

[57] H. Y. K. Cheng, C. L. Lin, H. W. Wang and S. W. Chou, "Finite element analysis of plantar fascia under stretch-The relative contribution of windlass mechanism and Achilles tendon force," *Journal Biomec.*, vol. 41, pp. 1937-1944, 2008.

[58] Y. D. Gu, X. J. Ren, J. S. Li, M. J. Lake, Q. Y. Zhang and Y. J. Zeng, "Computer simulation of stress distribution in the metatarsals at different inversion landing angles using the finite element method," 2010.

[59] A. Gonzalez, J. Bayod, J. C. Prados-Frutos, M. Losa-Iglesias, K. T. Jules, R. B. de Bengoa-Vallejo and M. Doblare, "Finite-element simulation of flexor digitorum longus or flexor digitorum brevis tendon transfer for the treatment of claw toe deformity," *Journal Biomec.*, vol. 42, pp. 1697-1704, 2009.

[60] A. Gefen, "Stress analysis of the standing foot following surgical plantar fascia release," *Journal Biomec.*, vol. 35, 2002.

[61] K. Tao, D. Wang, C. Wang, X. Wang, A. Liu, C. J. Nester and D. Howard, "An In Vivo Experimental Validation of a Computational Model of Human Foot," *Journal of Bionic Engineer.*, vol. 6, pp. 387-397, 2009.

[62] P. J. Antunes, G. R. Dias, A. T. Coelho, F. Rebelo and T. Pereira, "Nonlinear 3D foot FEA modelling from CT scan medical images," in *VIPIMAGE 2007 - 1st ECCOMAS Thematic Conference on Computational Vision and Medical Image Processing*, 2008, pp. 135-142.

[63] D. D. Anderson, J. K. Goldsworthy, W. Li, M. James Rudert, Y. Tochigi and T. D. Brown, "Physical validation of a patient-specific contact finite element model of the ankle," *Journal Biomec.*, vol. 40, pp. 1662-1669, 2007.

[64] P. Sun, S. Shih, Y. Chen, Y. Hsu, R. Yang and C. Chen, "Biomechanical analysis of foot with different foot arch heights: a finite element analysis," *Comput. Methods Biomec. Biomed. Engineer.*, vol. 15, pp. 563-569, 2012.

[65] W. C. H. Parr, H. J. Chatterjee and C. Soligo, "Calculating the axes of rotation for the subtalar and talocrural joints using 3D bone reconstructions," *Journal Biomec.*, vol. 45, pp. 1103-1107, 2012.

[66] J. L. Tweed, J. A. Campbell, R. J. Thompson and M. J. Curran, "The function of the midtarsal joint: a review of the literature." *Foot,* vol. 18, pp. 106-12, 2008.

[67] C. Nester, P. Bowker and P. Bowden, "Kinematics of the midtarsal joint during standing leg rotation," *Journal American Podiat. Medical Associat.,* vol. 92, pp. 77-81, 2002.

[68] G. R. Fritz and D. Prieskorn, "First Metatarsocuneiform Motion - a Radiographic and Statistical-Analysis," *Foot & Ankle Intern.l,* vol. 16, pp. 117-123, 1995.

[69] W. M. Glasoe, M. K. Allen and J. Yack, "Measurement of dorsal mobility in the first ray: Elimination of fat pad compression as a variable," *Foot & Ankle Intern.,* vol. 19, pp. 542-546, 1998.

[70] S. C. Tadepalli, A. Erdemir and P. R. Cavanagh, "Comparison of hexahedral and tetrahedral elements in finite element analysis of the foot and footwear," *Journal Biomec.,* vol. 44, pp. 2337-2343, 2011.

[71] A. Simkin, "Structural Analysis of the Human Foot in Standing Posture," 1982.

[72] S. Siegler, J. Block and C. D. Schneck, "The Mechanical Characteristics of the Collateral Ligaments of the Human Ankle Joint," *Foot Ankle,* vol. 8, pp. 234-242, 1988.

[73] D. G. Wright and D. C. Rennels, "A Study of the Elastic Properties of Plantar Fascia," *Journal of Bone and Joint Surgery-American,* vol. 46, pp. 482-492, 1964.

[74] Y. P. Y. Zheng, Y. K. Y. Choi, K. K. Wong, S. S. Chan and A. F. A. Mak, "Biomechanical assessment of plantar foot tissue in diabetic patients using an ultrasound indentation system," *Ultras. Medical. Biolog.,* vol. 26, pp. 451-456, 2000.

[75] A. A. Gefen, M. M. Megido-Ravid and Y. Y. Itzchak, "In vivo biomechanical behavior of the human heel pad during the stance phase of gait," *Journal Biomec.,* vol. 34, pp. 1661-1665, 2001.

[76] J. W. J. Klaesner, M. K. M. Hastings, D. D. Zou, C. C. Lewis and M. J. M. Mueller, "Plantar tissue stiffness in patients with diabetes mellitus and peripheral neuropathy," *Archiv. Physic. Medicine. Rehabil.,* vol. 83, pp. 1796-1801, 2002.

[77] S. J. Lochner, J. P. Huissoon and S. S. Bedi, "Development of a patient-specific anatomical foot model from structured light scan data," *Comput. Method. Biomec. Biomed. Engineer.,* 2012.

[78] I. A. I. Sigal, H. H. Yang, M. D. M. Roberts and J. C. J. Downs, "Morphing methods to parameterize specimen-specific finite element model geometries." *Journal Biomec.,* vol. 43, pp. 254-262, 2010.

[79] B. B. Couteau, Y. Y. Payan and S. S. Lavallée, "The mesh-matching algorithm: an automatic 3D mesh generator for finite element structures." *Journal Biomec.,* vol. 33, pp. 1005-1009, 2000.

[80] J. Koikkalainen and J. Lotjonen, "Reconstruction of 3-D head geometry from digitized point sets: an evaluation study," *IEEE Transactions on Information Technology in Biomedicine,* vol. 8, pp. 377-386, 2004.

[81] T. W. Sederberg and S. R. Parry, "Free-form deformation of solid geometric models," *ACM SIGGRAPH Computer Graphics,* vol. 20, pp. 151-160, 1986.

[82] D. McFadden and E. Shubel, "Relative lengths of fingers and toes in human males and females," *Horm. Behav.,* vol. 42, pp. 492-500, 2002.

[83] S. Telfer and J. Woodburn, "The use of 3D surface scanning for the measurement and assessment of the human foot," *Journal of Foot and Ankle Resear.,* vol. 3, pp. 19, 2010.

[84] S. J. Lochner, J. P. Huissoon and S. S. Bedi, "Parametric design of Custom foot orthotic model," *Computer-Aided Design and Applications,* vol. 9, pp. 1-11, 2012.

[85] S. Sun, Y. Chou and C. Sue, "Classification and mass production technique for three-quarter shoe insoles using non-weight-bearing plantar shapes," *Applied Ergonic.,* vol. 40, pp. 630-635, 2009.

[86] C. P. Witana, S. Xiong, J. Zhao and R. S. Goonetilleke, "Foot measurements from three-dimensional scans: A comparison and evaluation of different methods," *Intern. Journal Indust. Ergonom.,* vol. 36, 2006.